MESON PHOTOPRODUCTION

Chairman	A. Alikhanyan
Rapporteur	K. Lübelsmeyer
Discussion leaders	G. Vartapetyan
	S. Ting
Secretaries	P. Baranov
	E. Leikin
	V. Zamiralov
	G. Melkumov

MESON PHOTOPRODUCTION

K. Lübelsmeyer

Since there have been more than fifty papers on meson photoproduction contributed to this conference, there is no chance to give a detailed discussion of every experiment. I am therefore going to try to give a summary of the essential new results. Moreover I restrict myself to meson photoproduction experiments above the *s*-channel resonance region and will regretfully give only a tabulated summary of the very nice work in the region of the resonances.

If one examines the various photoproduction processes one realises immediately, that there is a large similarity obvious between photoproduction of pseudoscalar mesons ($J^P = 0^-$; π, η, K) and inelastic hadronic reactions as for instance $\pi^- p \to \pi^0 n$, $\pi^- p \to \eta n$, $\pi^- p \to \rho^0 n$ at one side and photoproduction of vector mesons ($J^P = 1^-$; ρ^0, ω, Φ) and elastic hadronic reactions, which show a dominant diffractive behaviour. This can be understood assuming, that the photons behave hadron like. The formulation of this assumption is contained in the vector dominance model (VDM), where the photon is supposed to be a superposition of the known vector mesons ρ^0, ω and Φ, which carry the same quantum numbers $J^P = 1^-$ as the photon. Within this idea, the photoproduction reactions have appeared to be a very suitable additional tool to study hadron dynamics.

My talk will be divided into two parts:

1) pseudoscalar photoproduction and
2) vector meson photoproduction and related topics as total photon cross sections and Compton scattering.

1. Pseudoscalar Meson Photoproduction

1.1. NEUTRAL π AND η PHOTOPRODUCTION

The previous data on π^0 photoproduction of Richter's group at SLAC [1] for photon energies $k = 6$, 9, 12 and 15 *GeV* have been extended down to momentum transfers squared $|t|$ of 0.1 GeV^2 using a low temperature

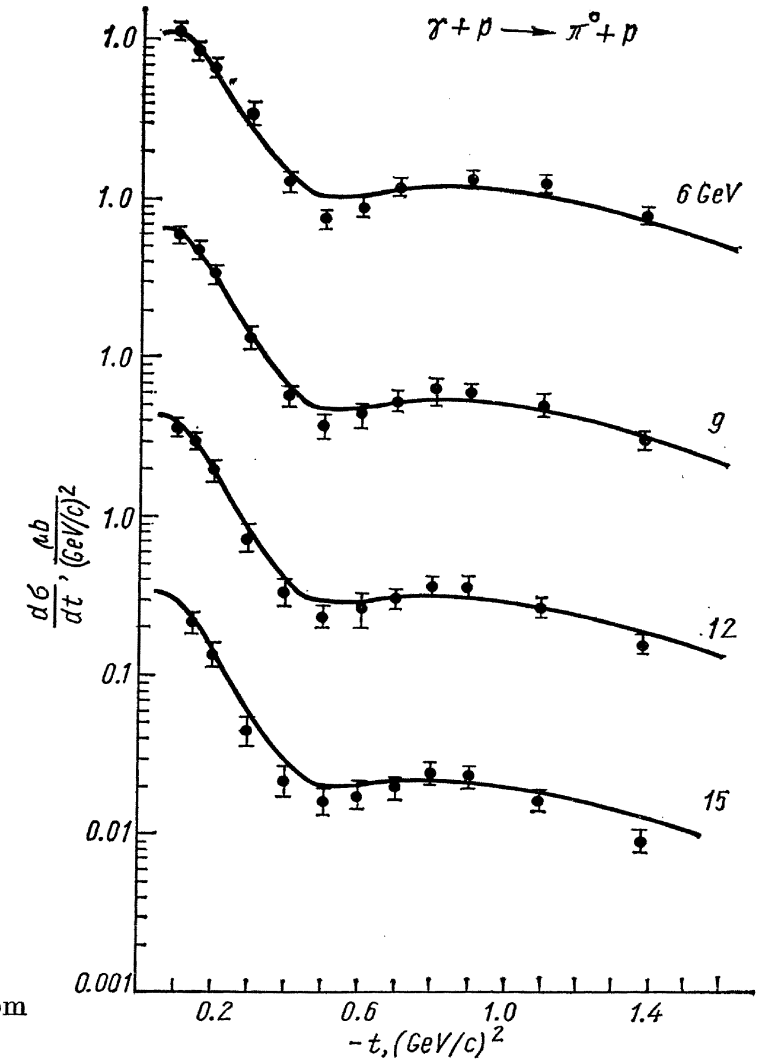

Fig. 1. The curves are obtained from a Regge-cut fit of ref. [4].

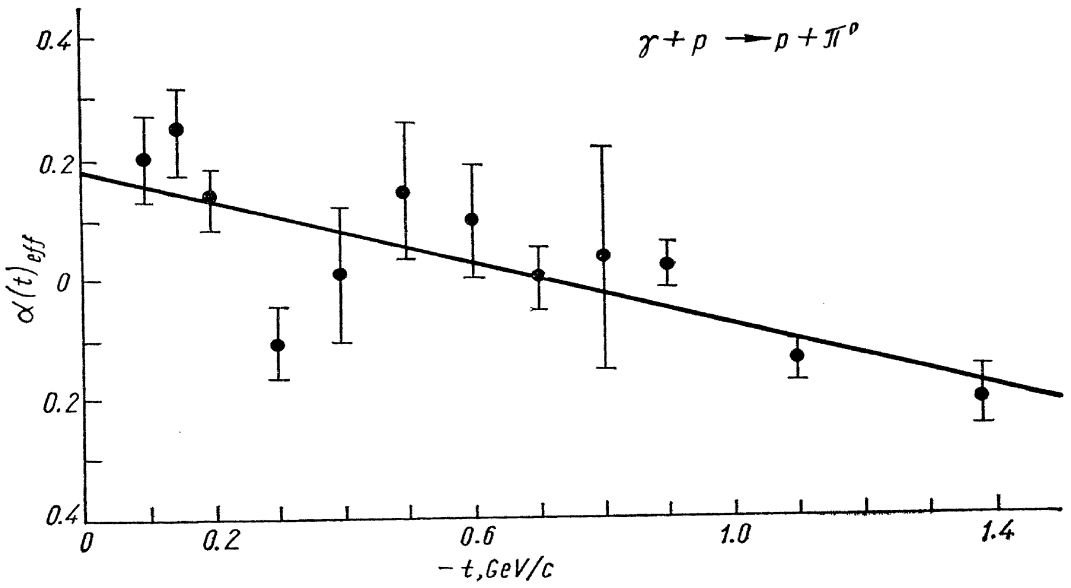

Fig. 2. The data are from ref. [2].

hydrogen gas target[2]. The process was identified by observing the recoil proton in the SLAC 1.6 *GeV/c* spectrometer. The data are shown in fig. 1. After a fall off from $|t| = 0.1$ to 0.4 GeV^2 the distributions show a dip around $|t| = 0.5$ GeV^2, which does not change much with increasing energy. These differences from ref. 1 are mainly due to Compton corrections, for which only estimates were available previously.

The s dependence (s square of total centre-of-mass energy) of the data at fixed momentum transfer can be expressed in terms of an effective $\alpha_{\text{eff}}(t)$, by fitting the cross section to the form

$$\frac{d\sigma}{dt} = f(t)(s - M^2)^{2\alpha_{\text{eff}}(t)-2}. \qquad (1)$$

The values of $\alpha_{\text{eff}}(t)$ obtained are shown in fig. 2, yielding $\alpha_{\text{eff}}(t) = 0.18 + 0.26 \cdot t$. For small values of $|t|$, $\alpha_{\text{eff}}(t)$ is different from zero, thus giving no evidence for the presence of fixed poles in the production amplitudes. New measurements of the differential cross section of η photoproduction have been contributed to this conference by the Ritson group at SLAC [3] and our Bonn group at DESY [4]. Preliminary results of both experiments have been reported at the Daresbury Conference [5]. From the SLAC group there are now data available in the momentum transfer range from 0.3 to 1.4 GeV^2 at incident photon energies around 6 *GeV* and 9 *GeV*. The process was observed by detecting the recoil proton in the SLAC 1.6 *GeV/c* spectrometer. This method limits the smallest $|t|$ value to 0.3 GeV^2. In the Bonn experiment the process was identified by detecting the η meson through its two photon decay $\left(B = \frac{\Gamma(\eta \to \gamma\gamma)}{\Gamma(\eta \to \text{all})} = 0.375\right)$ [6] in an arrangement of 14 total absorbing lead glass Cerenkov-counters. This method allowed us to measure the η photoproduction in the momentum transfer range from zero to 1.4 GeV^2 at 13 different $|t|$— values simultaneously. The experiment was carried out at mean photon energies of 4 and 6 *GeV*.

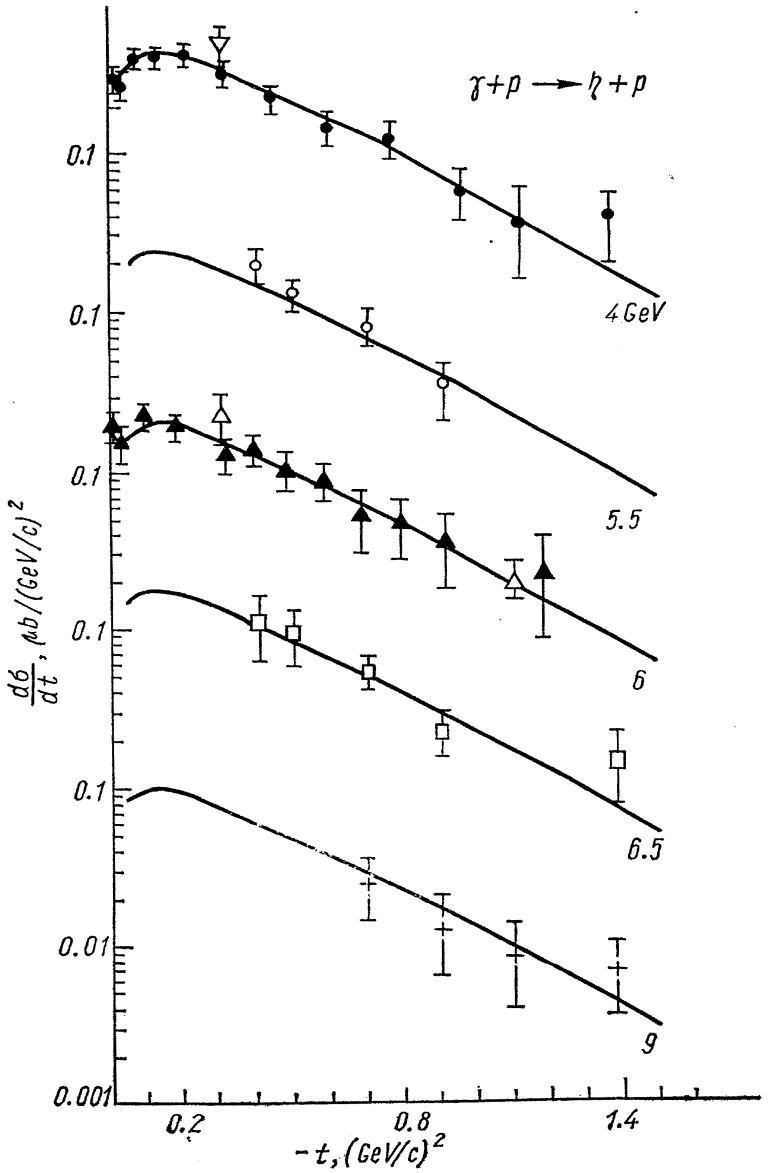

Fig. 3. The curves are obtained from a Regge-cut fit of ref. [4].

The data of both experiments are shown in fig. 3. The Bonn data show a slight maximum around $|t| = 0.15$ GeV^2, a decrease towards the forward direction and again an increase in the extreme forward direction. This

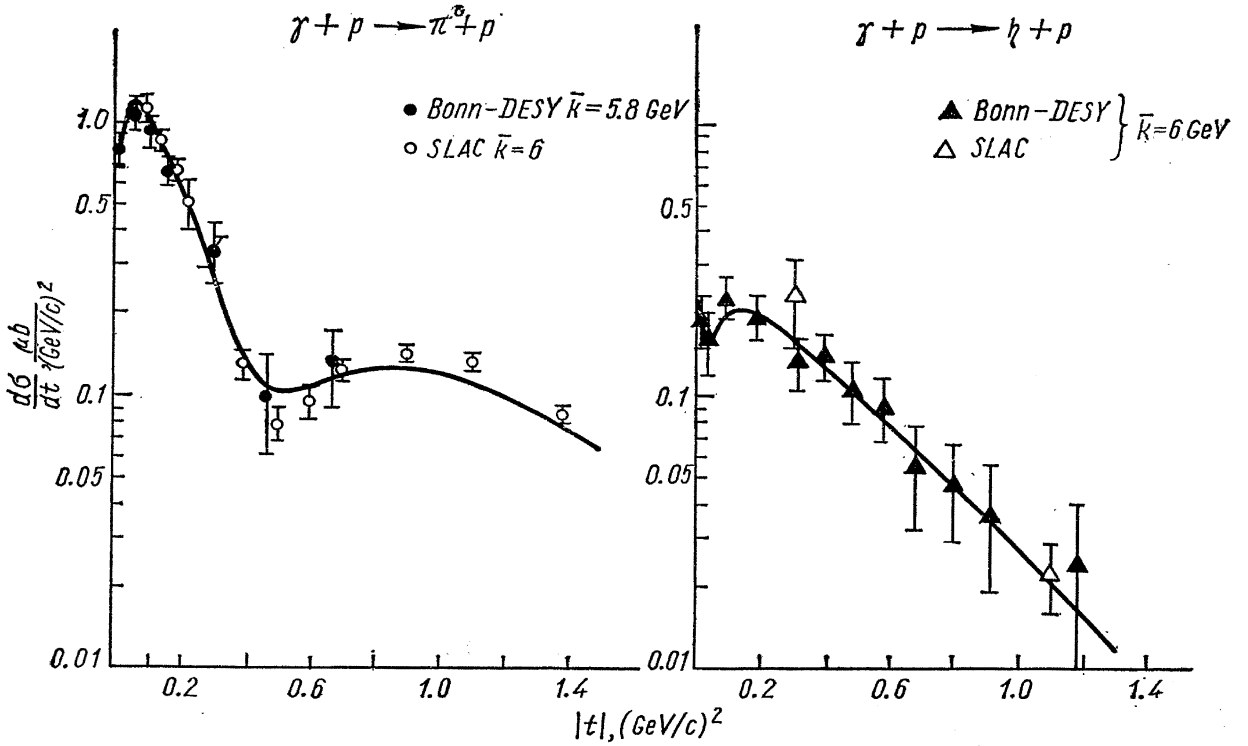

Fig. 4. The data are from refs. [2, 16, 3] and [4]. The solid lines are Regge-cut fits of ref. [4].

increase, which is due to the Primakoff-effect, becomes more pronounced at 6 *GeV*, accounting for about 30% ($\Gamma_{\eta\to\gamma\gamma} = 1$ *keV* [6, 7]) of the measured cross section at $\theta_\eta \sim 0°$. After the slight maximum at $|t| = 0.15$ *GeV*^{2} both data sets, which agree remarkable, show a completely smooth fall off out to 1.4 *GeV*^{2}, showing no indication of a dip arount $|t| = 0.5$ *GeV*^{2} in contrast to neutral π photoproduction. The *s* dependence at small *t* requires as in the case of the π^0 an effective α_{eff} (0) around 0.2.

Various versions of strong absorption Regge-cut models are able to describe the π^0 and η photoproduction data. One category of these models [8—12] (for older references see ref. 5) explain the dip in π^0 photoproduction by wrong signature nonsense factors contained in the helicity amplitudes, while in the case of η photoproduction this zero is filled up by a large cut contribution. The amplitudes of the second category of these models [13—15] do not vanish at these nonsense points and the dip in the case of the π^0 is obtained by a destructive interference of Regge-pole and cut contributions. At the moment the

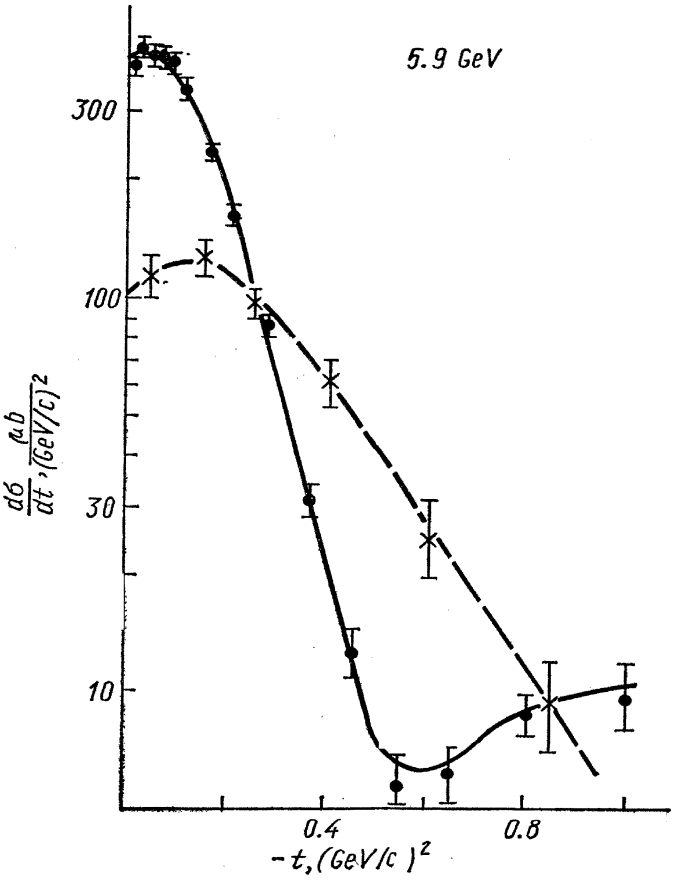

Fig. 5. The data are from refs. [18, 19] and [20]. The solid ($\pi^- p \to \pi^0 n$) and dashed ($\pi^- p \to \eta n$) lines are Regge-cut model fits.

experiments including data on neutrons and with polarized photons [5] do not favour one of the two categories.

Besides these Regge-cut models other peripheral models [17] have been proposed, which are able to explain the cross sections and the accurence or nonaccurence of dips.

The curves shown in fig. 1 and 3 show a fit, which we have applied to the data of refs. [2, 16, 3] and [4], using a modified version of the simple model, originally proposed by A. Capella and J. Tran Thanh Van [8]. The amplitudes contain reggeized ρ and ω exchange and the corresponding Pomeranchuk cuts and in addition B (1235 *MeV*, $J^P = 1^+$) exchange. The fits reproduce the π^0 data well down to 4 *GeV* and the η data, filling the dip by a large cut contribution.

Independent of any special model, which will be able to describe the data, the comparison of the two photoproduction reactions $\gamma + p \to \pi^0 + p$ and $\gamma + p \to \eta + p$ and the two charge exchange reactions $\pi^- + p \to \pi^0 + n$ [18, 19] and $\pi^- + p \to \eta + n$ [20] in fig. 4 and 5 establishes the close similarity between photoproduction processes of pseudoscalar mesons and inelastic hadronic processes.

1.2. CHARGED PION PHOTOPRODUCTION

Via the vector dominance model (VDM) the photoproduction of charged pions is closely related to the reactions $\pi^- + p \to V^0 + n$ by time reversal and iso invariance, where V^0 stands for the known vector-mesons ρ^0, ω and Φ. Neglecting the small Φ contribution, the sum of photoproduction cross section on protons and neutrons has the advantage, that the interference term between the ρ^0 and ω contributions cancels [5]. We obtain then the VDM relation:

$$\frac{1}{2}\left[\frac{d\sigma}{dt}(\gamma p \to \pi^+ n) + \frac{d\sigma}{dt}(\gamma n \to \pi^- p)\right] = \frac{\alpha\pi}{\gamma_\rho^2}\left[X_{11}^{\rho^0} + \xi X_{1-1}^{\rho^0}\right]\frac{d\sigma}{dt}(\pi^- p \to \rho^0 n) + \\ + \frac{\alpha\pi}{\gamma_\omega^2}\left[X_{11}^{\omega} + \xi X_{1-1}^{\omega}\right]\frac{d\sigma}{dt}(\pi^- p \to \omega n). \qquad (2)$$

Here $\gamma_\rho^2/4$ and $\gamma_\omega^2/4\pi$ are the ρ-photon and ω-photon coupling constants. X_{11} and X_{1-1} are the density matrix elements in the helicity frame and ξ is the polarization of the photon ($\xi = +1$ transverse, $\xi = -1$ parallel to production plane). Neglecting also the ω contribution in equ. (2) (only a few per cent effect), the photoproduction cross sections can be compared with the process $\pi^- + p \to \rho^0 + n$.

The reaction $\pi^- + p \to \pi^+\pi^- n$ in the region of the ρ meson has been measured at SLAC (21) with a wire spark chamber spectrometer using a 15 *GeV/c* pion beam. The dipion decay angular distributions have been fitted in terms of S and P waves obtaining $\frac{d\sigma}{dt}$ and the density matrix elements in the helicity frame. From the analysis it turned out, that the density matrix elements connected with the S-wave do not vanish, so that the dipion system may not be described by a pure P wave (i. e. pure ρ^0). This experiment determines only $X_{11} + \frac{1}{3}X_{ss}$, having no satisfactory possibility to measure each quantity separately. However there must be a number of Schwartz inequalities be satisfied, which allow the determination of an upper limit of X_{11}.

In fig. 6 a comparison of the upper limits on $2 \cdot X_{11}^{\rho^0} \cdot \frac{d\sigma}{dt}(\pi^- p \to \rho^0 n)$ and the photoproduction data of charged pions [22] according to equ. (2) (neglecting the ω contribution) using $\gamma_\rho^2/4\pi = 0.52$ is shown. The photoproduction data are

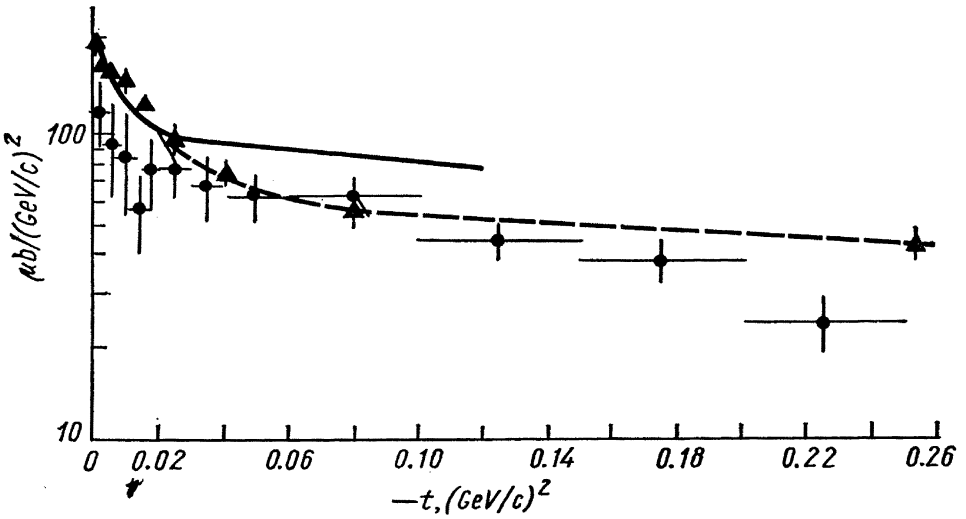

Fig. 6. $\pi^- p \to \rho^0 n$ at 15 *GeV*. ● — upper limit for $2X_{11}\frac{d\sigma}{dt}$; ▲ — VDM prediction from $\gamma N \to \pi^{\pm} N$ (– – – – – to guide the eye); ——— — prediction of Cho — Sakurai. The photoproduction data are $(1 + R)\,\frac{\gamma_\rho^2}{\pi\alpha}\cdot\frac{d\sigma}{dt}(\gamma p \to \to \pi^+ n)$ where $R = \frac{d\sigma(\gamma n \to \pi^- p)}{d\sigma(\gamma p \to \pi^+ n)}$. These data have been scaled by the factor $(s - M_N^2)^{-2}$.

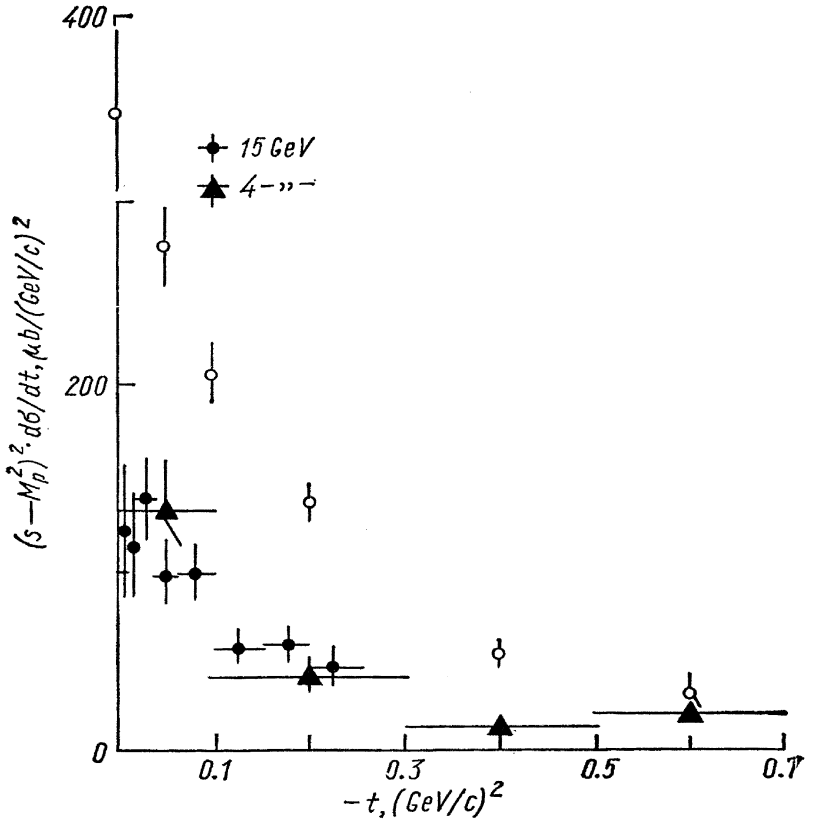

Fig. 7. A value of $\gamma_\rho^2/4\pi = 0.52$ was used.

roughly 50% higher at small momentum transfers, while at larger $|t|$ values the agreement gets better. The VDM prediction of the Cho — Sakurai model [23] agrees well with the photoproduction data at small $|t|$ values.

It has been pointed out by several authors that the VDM prediction for photoproduction with polarized photons perpendicular to the production plane

$$\frac{1}{2}\left[\frac{d\sigma}{dt_\perp}(\gamma p \to \pi^+ n) + \frac{d\sigma}{dt_\perp}(\gamma n \to \pi^- p)\right] = \frac{\alpha\pi}{\gamma_\rho^2}[X_{11}^{\rho^0} + X_{1-1}^{\rho^0}]\frac{d\sigma}{dt}(\pi^- p \to \rho^0 n) \quad (3)$$

is independent of certain ambiguities of the choice of the reference frame. Fig. 7 shows the photoproduction data [5] (open circles) and the upper limits on $\pi\alpha/\gamma_\rho^2 \cdot (X_{11}^{\rho^0} + X_{1-1}^{\rho^0})\ \frac{d\sigma}{dt}(\pi^- p \to \rho^0 n)$. The photoproduction data are higher by a factor 2 to 3, where a precise knowledge of the S wave contribution would make this disagreement stronger.

Since the new 15 *GeV* data agree with those of ref. 24 at 4 *GeV*, the $(s - M_p^2)^{-2}$ scaling seems not to be the source of the discrepancy. Furthermore it has been suggested [25] that higher partial waves are needed to fit the decay angular distributions. From this experiment there is no compelling evidence for including D waves or even higher partial waves in the fits. So we can conclude, that the discrepancies in VDM relations concerning pseudoscalar meson photoproduction are still present.

At SLAC the first photoproduction experiment using a polarized proton target has been carried out [26]. The reaction $\gamma + p \to \pi^+ + n$ was measured at mean incident photon energies of 5 and 16 *GeV* in the momentum transfer range $0.02 < |t| < 1\ GeV^2$ with the polarization of the target proton pointing in the direction $+\vec{n}$ (up) and $-\vec{n}$ (down) where $\vec{n}$ is the normal to the production plane. The target was a butanol target with a typical polarization of 20%. The process was observed by detecting the π^+ mesons in the SLAC 20 *GeV/c* spectrometer.

The data on the asymmetry are shown in fig. 8. In addition to the indicated statistical errors, there is to be applied to all the data a systematic error of 12%.

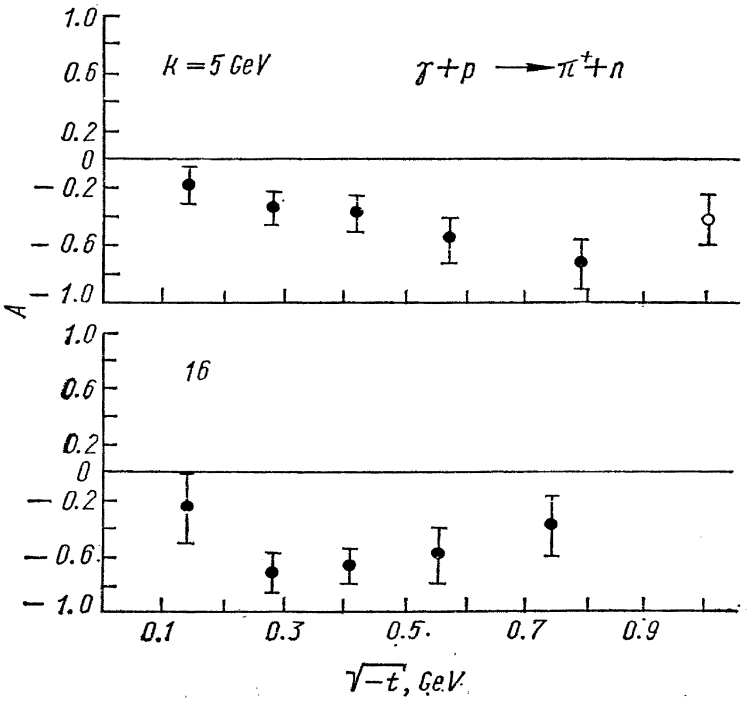

Fig. 8. Asymmetry A in $\gamma p \to \pi^+ n$ with a polarized target from ref. [26]. Errors shown are statistically only.

The main feature of the data is a large negative asymmetry at both energies out to the largest momentum transfers. Especially at 5 *GeV* the t distribution is quite structureless for $\sqrt{-t} < 0.8\ GeV$.

The asymmetry $A(t)$ can be expressed in terms of s-channel helicity amplitudes in the following way

$$A(t) = \frac{\frac{d\sigma}{dt\uparrow} - \frac{d\sigma}{dt\downarrow}}{\frac{d\sigma}{dt\uparrow} + \frac{d\sigma}{dt\downarrow}} = -\frac{2\,\mathrm{Im}\,(h_+^* \varphi_+ + h_-^* \varphi_-)}{|h_+|^2 + |h_-|^2 + |\varphi_+|^2 + |\varphi_-|^2}, \quad (4)$$

where the denominator is simply $d\sigma/dt$. h_+ and h_- are the s channel helicity non flip and φ_+ and φ_- are s channel helicity flip amplitudes.

In the high energy limit the amplitudes with the index + obtain only contributions from natural parity t channel exchange, while the amplitudes with the index — obtain only contributions from unnatural parity t channel exchange. From equ. 4 it is evident, that an asymmetry A (t) different from zero can only be obtained by an interference of at least two amplitudes of the same naturality, which are out of phase. From experiments with polarized photons [5] we know, that the unnatural parity contributions are small. Thus in order to reproduce the observed large asymmetry, a model must have appreciable h_+ and φ_+ amplitudes with different phases.

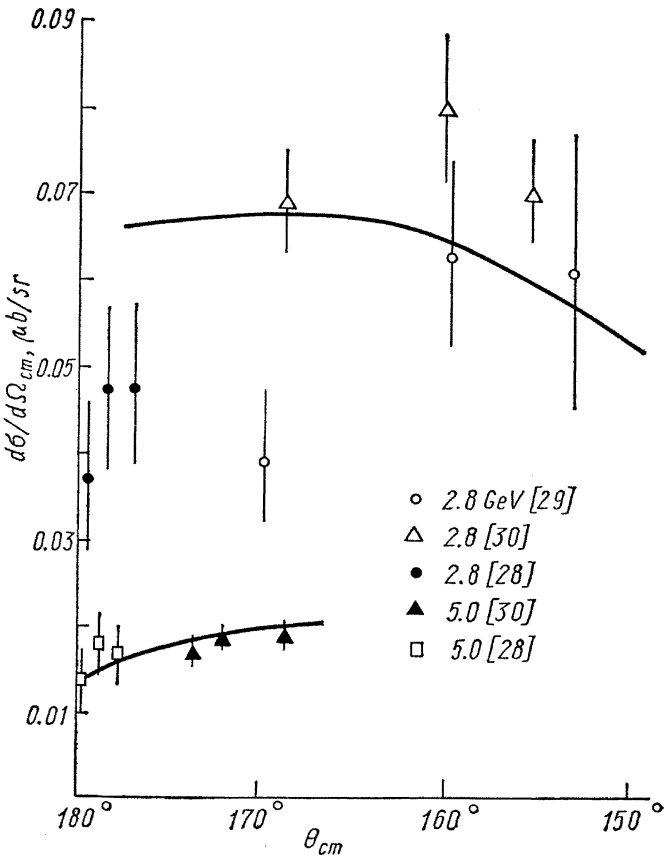

Fig. 9.

Various theoretical models based on Regge poles with absorption cuts (as mentioned in ref. 5 and section 1.1), electric Born approximation with and without absorption and phenomenological fixed poles have been applied to the differential cross section data and the data with polarized photons. These models are in principle also able to explain the asymmetry data (the ρ and A_2 exchange and the ρ, A_2 and π cuts contribute to natural parity amplitudes [5]. At the moment there exist only predictions based on an absorptive Regge cut model by Jackson and Quigg [27]. This and the other models mentioned are quite flexible, so that they are able to reproduce a wide range of asymmetries. The hope is, that the ambiguity inherent in these models can be reduced by these and future asymmetry data.

From Cornell new data on positive pion photoproduction in the backward direction have been contributed to this conference [28]. They have measured the reaction $\gamma + p \to \pi^+ + n$ for incident gamma ray energies from 0.7 to 8 *GeV* and π^+ c. m. angles from roughly 177° to 180°. This extreme backward direction was not covered by previous experiments at CEA [29] and SLAC [30]. The positive pions were momentum analyzed using a magnetic spectrometer and detected with scintillation counters and wire spark chambers. Fig. 9 shows the c. m. angular distributions at 2.8 and 5.0 *GeV* from this experiment together with the CEA (ref. [29]) and SLAC (ref. 30) data. From the SLAC data [30] there was already some evidence, that the cross section dips in the extreme backward direction. This is nicely confirmed by the new Cornell data. The solid curves are the Regge pole predictions of Barger and Weiler [31], involving N_α, N_γ and Δ_δ trajectories. The 5 *GeV* data, both from Cornell and SLAC are well reproduced, while the fit at 2.8 *GeV* is not good, when the Cornell data are included.

1.3. $\pi\Delta$-PHOTOPRODUCTION

Previous photoproduction experiments have studied the reactions $\gamma + p \to \pi^- + \Delta^{++}$ using bubble chambers [32, 33] and the SLAC-spectrometer [34]. For photon energies k above 2 *GeV* the differential cross section

$\frac{d\sigma}{dt}$ shows an energy dependence close to $1/k^2$ in common with various other pseudoscalar photoproduction processes. Such an energy dependence would be expected, if the process is dominated by one pion exchange (OPE), but OPE leads to zero cross section in the forward direction, in contrast to the experiment [34]. These difficulties are overcome by a gauge invariant extension (GIOPE) of the OPE model proposed by Stichel and Scholz [35].

To provide a further check of this model, the reaction $\gamma p \to \pi^- \Delta^{++}$ has been measured at SLAC [36], exposing the 82″ bubble-chamber to a linearly polarized photon beam of 2.8 and 4.7 *GeV*. This photon beam is obtained by backscattering ruby laser light from the 20 *GeV* electron beam. The 180° scattered photons have multi-*GeV* energies and are fairly monoenergetic. By collimating both the electron and the backscattered photon beam to less than 10^{-5} radians the width at half maximum of the photon energy spectrum is $\pm$ 2.6% and $\pm$ 3.3% at 2.8 and 4.7 *GeV*, respectively. Furthermore the high energetic photons maintain the polarization of the incident visible light, resulting in a 94% resp. 92% linear polarization for the two energies mentioned. (For more details of this technique see ref. [37].)

The $\Delta^{++} \to p\pi^+$ angular distributions have been analyzed in terms of the Δ spin density matrix element in the Gottfried — Jackson frame. For pure π exchange the density matrix element X^1_{11} is equal to — 0.5 and all other matrix elements are 0. This would lead to a polarization asymmetry

$$\Sigma = -2(X^1_{33} + X^1_{11}) = 1 \qquad (5)$$

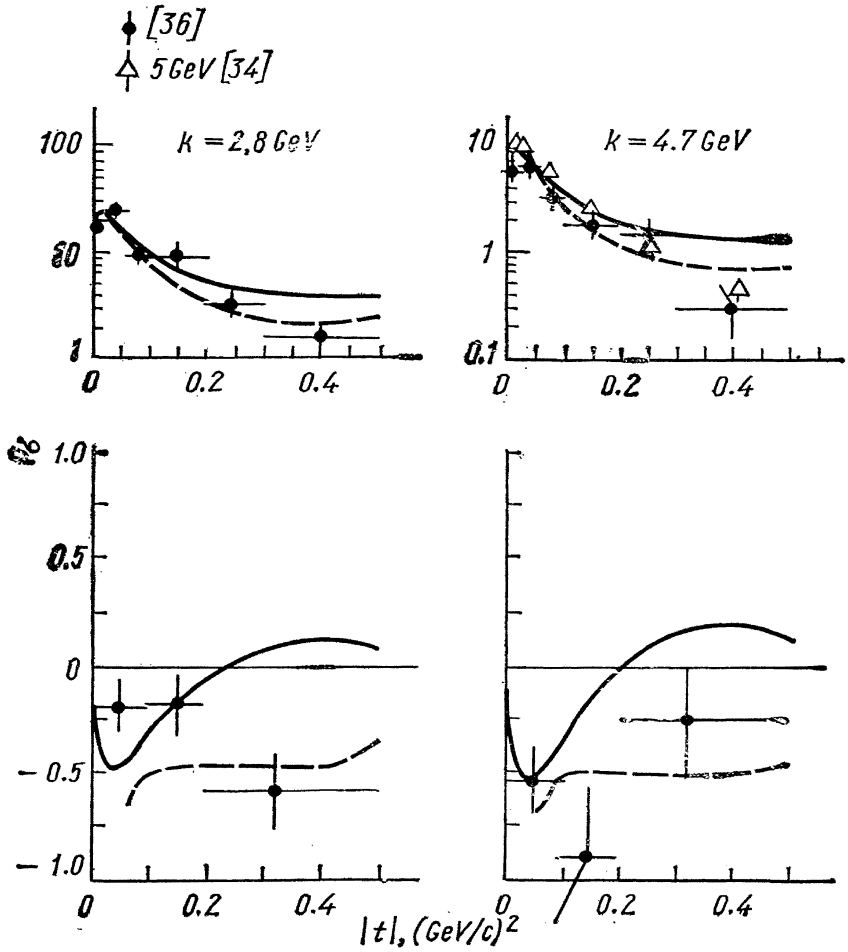

Fig. 10.

where Σ is defined as

$$\Sigma = \frac{1}{P_\gamma} \cdot \frac{W(\varphi = 0) - W(\varphi = \pi/2)}{W(\varphi = 0) + W(\varphi = \pi/2)}. \tag{6}$$

P_γ is the degree of linear polarization and $W(\varphi)$ is the decay angular distribution integrated over θ and φ. φ is the angle between the electric vector ε of the photon and the production plane. A related quantity is the parity asymmetry P_σ, defined in terms of the cross sections for natural and unnatural parity exchange in the t channel, σ^+ and σ^-:

$$P_\sigma = \frac{\sigma^+ - \sigma^-}{\sigma^+ + \sigma^-}. \tag{7}$$

At high energies the π contributes only to σ^-, so that $P_\sigma = -1$ for pure π exchange. Generally, the following expression for P_σ holds in the high energy limit:

$$P_\sigma = 2 \cdot (X^1_{33} + X^1_{11}) = -\Sigma. \tag{8}$$

The top graph of fig. 10 shows the differential cross section $\frac{d\sigma}{dt}$ for $\pi^-\Delta^{++}$ production together with the data of ref. (34) at 5 *GeV*, which are slightly higher. (Using the same parametrization for $\Gamma(M)$ of the Δ as in ref. (34) the authors find values of $\frac{d\sigma}{dt}$ 20% larger than the quoted ones.) The lower graph shows the parity asymmetry P_σ. In the momentum transfer range $0.05 < |t| < 0.3$ *GeV*^{2} P_σ is quite different from -1. Averaging the values on P_σ for $|t| < 0.5$ *GeV*^{2} leads to $\bar{P}_\sigma = -0.27 \pm 0.12$ for 2.8 *GeV* and $\bar{P}_\sigma = -0.53 \pm 0.15$ for 4.7 *GeV*. This indicates the presence of other production mechanism besides π exchange. The solid lines in fig. 10 are predictions of the gauge invariant OPE model with the absorption parameter $C_{in} = C_{out} = C = 0.8$. For comparison the dashed lines give the predictions for $C = 1$. For $|t| < 0.3$ *GeV*^{2} the cross section data are rather well reproduced, but at larger $|t|$ too much Δ^{++} is predicted. The parity asymmetry parameter P_σ is reproduced fairly well only for $|t| < 0.1$ *GeV*^{2}.

1.4. PSEUDOSCALAR MESON PHOTOPRODUCTION IN THE RESONANCE REGION

The photoproduction work in the resonance region below 2 *GeV* submitted to this conference is summarized in table 1. For a complete coverage of the recent photoproduction data the reviews of G. v. Holtey [38] (First resonance region) and H. Fischer [39] (Intermediate energy region) are highly recommended. The strong interest in this energy region where the production mechanism is dominated by a channel resonances, has mainly two reasons:

1) comparison with detailed theories (dispersion relations, current algebra) is possible and

2) in the frame work of F. E. S. R. most accurate data in this region are desirable to predict the high energy behaviour.

Fig. 11 may serve to demonstrate, what degree of precision has been reached in the first resonance region.

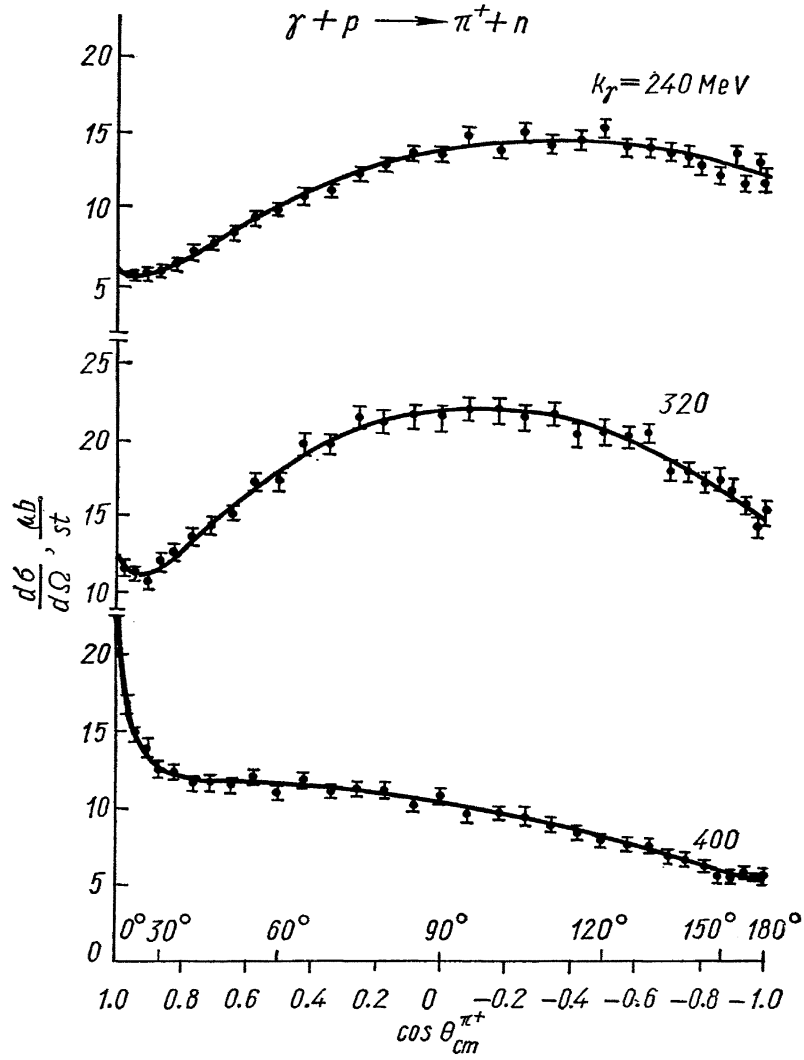

Fig. 11. Solid line: polynomial fit to all experimental points (ref. [49]).

Table 1

Reaction	Photon Energy [GeV]	θ_{cm}	Quantity measured	Institute
$\gamma p \to K^+ \Lambda$	1.3	6° — 90°	cross section	Bonn [40]
$\gamma p \to K^+ \Sigma^0$	1.45			
$\gamma p \to K^+ \Lambda$	1—2	90° — 135°	cross section	Orsay [41]
$\gamma p \to K^+ \Sigma^0$				
$\gamma n \to \pi^- p$ (Li, C)	0.55—0.84	90°	$P \uparrow$	Kharkov (42]
$\gamma n \to \pi^- p$ (D_2)	.5—0.7	90°	$P \uparrow$	Frascati [43]
$\gamma p \to \pi^0 p$	0.4—1.2	40° — 150°	$P \uparrow$	Bonn [44]
Polarized photons:				
$\gamma p \to \pi^0 p$	0.25—0.6	90°	asymmetry	Kharkov [45]
$\gamma p \to \pi^0 p$	0.28—0.6	90°		Frascati [46]
$\gamma p \to \pi^+ n$	~0.35	110° — 140°		Tomsk [47]
$\gamma p \to \pi^0 p$	0.34—0.42	10° — 70°	cross section	Bonn [48]
$\gamma p \to \pi^+ n$	0.22—0.425	15° — 180°	cross section	Bonn [49]
$\gamma p \to \pi^+ n$	0.6—1.3	180°	cross section	Bonn [50]
$\gamma p \to \pi^+ n$	0.3—1.2	180°	cross section	Tokyo [51]
$\gamma p \to \eta p$	0.8—1.1	90°	$P \uparrow$	Caltech [52]
$\gamma p \to \gamma p$ (Compton-Scattering)	0.2—0.45	50° — 130°	cross section	Bonn [131]

2. Vector-Meson Photoproduction

2.1. ρ^0-PHOTOPRODUCTION ON HYDROGEN

Considerable data on ρ^0-meson photoproduction has appeared during the two last years, which has been summarized in the review talk of Prof. Silverman [53] at the Liverpool photon and electron conference in 1969. More recent summaries can be found in the proceeding of the «Daresbury Study Weekend in Vector Meson Photoproduction (June 1970)» [54a] and in a lecture of Prof. D. W. G. S. Leith given at the Scottish Universities Summer School (July 1970) [54b].

To the Kiev conference the results of two new experiments from Cornell [55] and from the DESY — MIT group [56] have been contributed. In both experiments only the $\pi^+\pi^-$ pairs are detected in a double arm spectrometer, while the recoil proton is not observed.

This way there are no additional kinematical constraints left, to separate inelastically produced $\pi^+\pi^-$ pairs from elastically produced ones. This fact and the unknown form of a nonresonant background together with the lack of a theory for wide resonances make the analysis of the reaction $\gamma + p \to p + \pi^+ + \pi^-$ in terms of ρ production complicated. The DESY — MIT group has analysed their data by fitting the experimental data, given as $\pi\pi$ cross sections $\frac{d\sigma}{d\Omega dm}$ (m mass of $\pi\pi$ system), to the following equations:

$$\frac{d\sigma}{d\Omega dm} = C \cdot g(p) \cdot 2mR(m) + BG(p, m) \tag{9}$$

where

$$9(p) = p^2\left(1 + \frac{R}{p}\right)^2 \tag{10}$$

takes into account the decrease of the cross section with energy. $BG(p, m)$ is a polynomial background function in p and m, responsible for part of the nonresonant and the inelastic $\pi\pi$ production. For the ρ shape $R(m)$ different hypotheses have been made:

1) Relativistic P-wave Jackson form [57] with Ross — Stodolsky-term [58].

2) No Ross — Stodolsky-term but instead an interference term [59]

$$I(m) = \frac{A}{m2} \cdot \frac{m^2 - m_\rho^2}{(m_\rho^2 - m^2)^2 + m_\rho^2 \Gamma_\rho^2(m)} \cdot^{*} \tag{11}$$

3) Both Ross — Stodolsky factor and $I(m)$.

The values of $\left.\frac{d\sigma}{dt}\right|_{t=0}$ obtained from the three fits are shown in fig. 12. Within the errors which include uncertainties due to background subtraction the cross sections obtained from the three hypotheses agree with each other. In this paper [56] also the energy dependence of $\left.\frac{d\sigma}{dt}\right|_{t=0}$ was studied. For the three hypotheses for the ρ shape the authors found

$$1)\ \left.\frac{d\sigma}{dt}\right|_{t=0} \sim \left(1 + \frac{1.0 \pm 0.3}{p}\right)^2 \tag{12}$$

$$2)\ \left.\frac{d\sigma}{dt}\right|_{t=0} \sim \left(1 + \frac{1.3 \pm 0.3}{p}\right)^2 \tag{13}$$

$$3)\ \left.\frac{d\sigma}{dt}\right|_{t=0} \sim \left(1 + \frac{1.0 \pm 0.4}{p}\right)^2 \tag{14}$$

* This function represents an interference of the ρ^0 amplitude with part of the background, where the nonresonant $\pi\pi$ pairs are diffractively produced off the nucleon (Drell type mechanism).

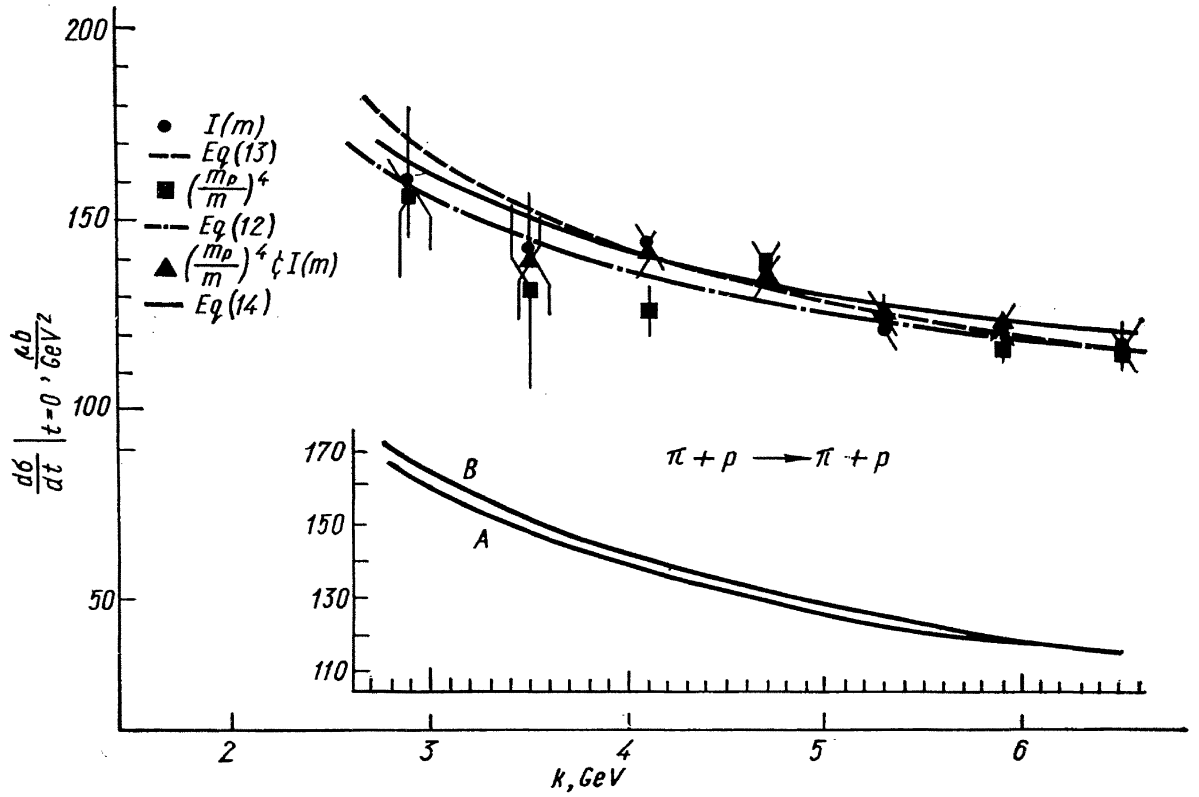

Fig. 12.

which are shown in fig. 12. This energy dependence of the photoproduction cross section can be compared with that of elastic $\pi^+ p$ and $\pi^- p$ scattering via the VDM and a broken SU (3) quark model [60] by (assuming ρ^0 dominance)

$$\frac{d\sigma}{dt}^{\text{Photo}}(t) = \frac{\alpha\pi}{4\gamma_\rho^2}(1+\beta_\rho^2)\left[\sqrt{\frac{d\sigma}{dt}(\pi^+p)/(1+\beta_+^2)} + \sqrt{\frac{d\sigma}{dt}(\pi^-p)/(1+\beta_-^2)}\right]^2 \quad (15)$$

where β_ρ, β_+ and β_- are the ratios of the real to imaginary parts of the ρp, $\pi^+ p$ and $\pi^- p$ elastic amplitudes, respectively. In the same energy region from 3 to 7 GeV the $\pi^\pm p$ cross section is found to be (61) (see fig. 12)

$$\begin{aligned} &\frac{d\sigma}{dt}(\pi^+p)\Big|_{t=0} \sim \left(1+\frac{1.1}{p}\right)^2 \quad (A) \\ &\frac{d\sigma}{dt}(\pi^-p)\Big|_{t=0} \sim \left(1+\frac{1.2}{p}\right)^2 \quad (B) \end{aligned} \quad (16)$$

showing the close similarity between the ρ photoproduction data and the $\pi^\pm p$ data via equ. (15). In fact the SLAC group F [1] obtained a good fit to their photoproduction data by inserting πp scattering data as a fixed parameter. Expressed in this form, the SLAC data has the energy dependence

$$\frac{d\sigma}{dt}\Big|_{t=0} \sim \left(1+\frac{1.3}{p}\right)^2. \quad (17)$$

From these two experiments one can conclude, that between 3 and 18 GeV there is a strong similarity between forward ρ photoproduction and elastic πp scattering. Furthermore the VDM and the quark model (equ. 15) seem to give a good description.

In the Cornell experiment [55] the dipion mass distribution is analyzed in terms of a relativistic P-wave Jackson form [57] and a Drell type non-resonant $\pi\pi$-background including the interference term [59] between both

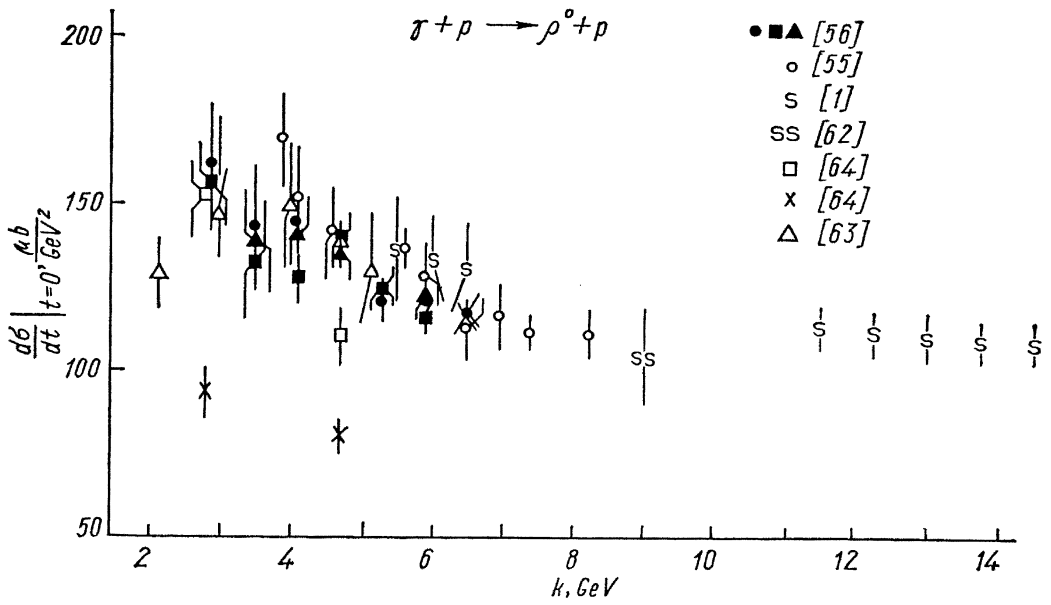

Fig. 13.

production mechanisms. No orbitrary background function is included. The energy dependence of $\frac{d\sigma}{dt}\Big|_{t=0}$ is accounted for by a factor $\left(1 + \frac{1.3}{p}\right)^2$. The data on $\frac{d\sigma}{dt}\Big|_{t=0}$ are shown in fig. 13 together with the DESY — MIT data and other recent data. Around 4 *GeV* the Cornell data seem to be somewhat higher. The authors emphasize, that these data represent measurements mainly at the peak of the ρ^0 mass shape. Since detailed mass spectra have not been measured at large t, it is possible that the t-dependence of the Drell type amplitude and interference term may affect these results (see below). I have also included a new point at 9 *GeV*, which was contributed by the SLAC group $B + C$ [62]. In the analysis a Drell — Söding type background was used.

Three experiments at SLAC [64] (further quoted as SBT-collaboration), DESY [65] and Cornell [66] have been carried out using a linearly polarized photon beam to produce ρ^0 mesons. This techniques allows one in a very elegant way to study the production mechanism in detail. Before I come to this point, I like to discuss first the results on $\frac{d\sigma}{dt}(t)$ of the SBT experiment [64].

The process $\gamma p \to \pi^+\pi^- p$ was studied in the SLAC 82-*inch* HBC using a linearly polarized photon beam of 2.8 and 4.7 *GeV* (see section 1.3). Since in the HBC the recoil proton can also be detected, elastically produced $\pi^+\pi^-$ pairs can be selected. Also in this experiments several assumptions about the ρ shape have been tested:

1) A relativistic P-wave Jackson form multiplied by a modified Ross — Stodolsky [58] factor $\left(\frac{m_\rho}{m}\right)^{n(t)}$. Maximum likelihood fits have been made for each event allowing for ρ^0 and Δ^{++} (1236) production and a phase space term and fitting these contributions together with the parameter $n\,(t)$. The fits describe the $\pi^+\pi^-$ mass spectra well and the values [64] for $n\,(t)$ are shown in fig. 14. In contrast to the prediction of Ross — Stodolsky [58], namely $n\,(t = 0) = 4$, the parameter is ~ 5 near $t = 0$ and drops to zero around $t = 0.5$ *GeV*^{2}. However it should be mentioned, that in evaluating the cross section $\frac{d\sigma}{dt}\Big|_{t=0}$ this has little influence in comparison with putting $n\,(t = 0) = 4$.

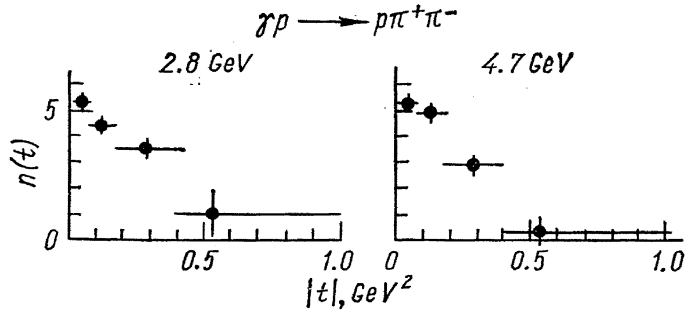

Fig. 14.

2) From an analysis of the ρ angular decay distributions the contribution of the *s*-channel c.m. helicity — conserving *P*-wave ππ-contribution (π (*t*)) could be determined. It is remarkable, that in the ρ mass region this contribution accounts for almost all the ππ-events and shows the same skewing on the experimental mass distribution.

3) Since the moment γ_4^0 shows a distinctive interference pattern in the ρ region, which can be interpreted as an interference between the ρ^0 and nonresonant $\pi^+\pi^-$ pairs (Drell-type production), a further comparison of the data was made with the Söding model [59]. The results are shown in table 2 [67] and fig. 15 [64].

Within the errors the first three assumptions lead to the same results. The cross sections obtained with the Söding model are considerably lower; although this hypothesis fits the data well. A comparison of all recent data on $\left.\frac{d\sigma}{dt}\right|_{t=0}$ is

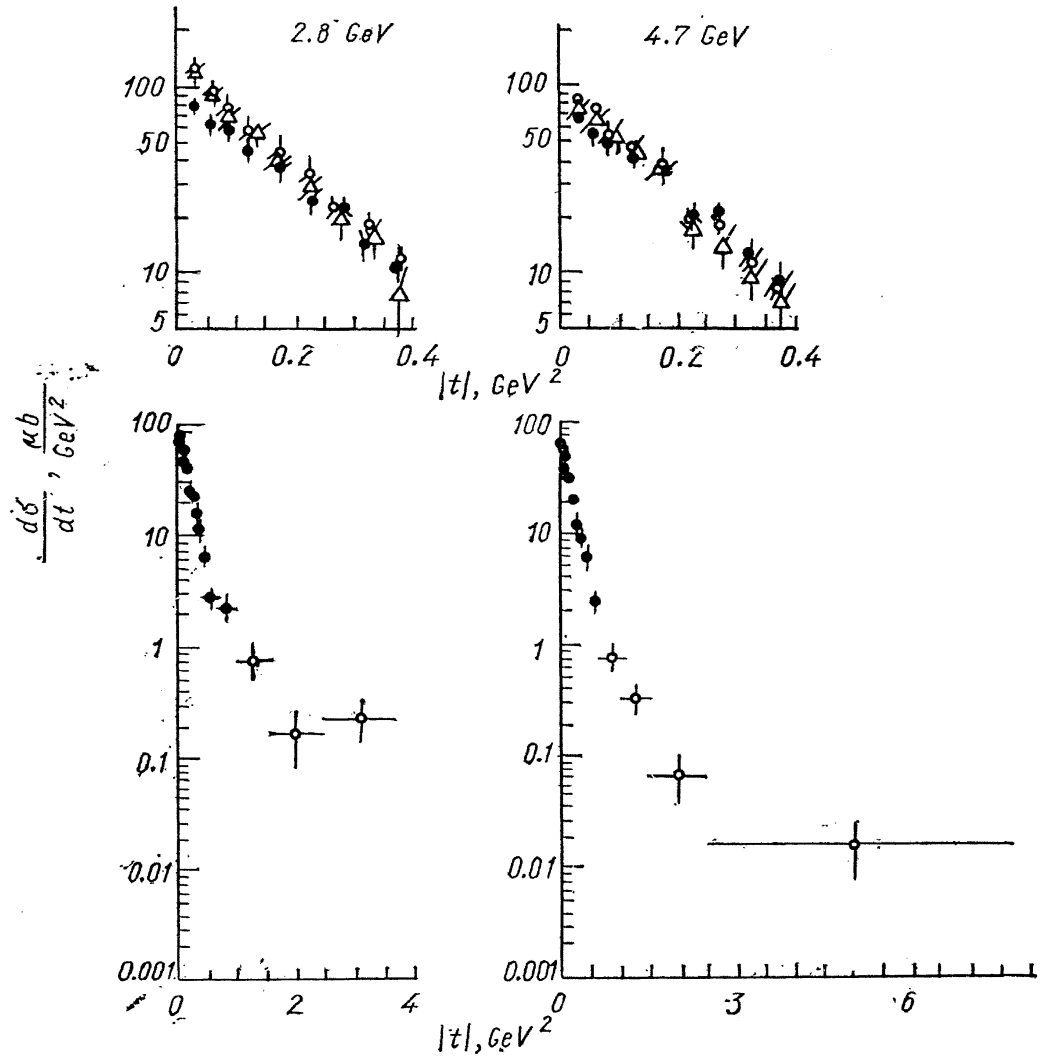

Fig. 15. $\gamma p \to \rho^0 p$. △ — *p*-wave intensity; ○ — with $(M_\rho/M_{\pi\pi})^{n(t)}$; ● — Söding model.

Table 2

$$\left.\frac{d\sigma}{dt}\right|_{t=0} (\gamma p \to \rho^0 p) \left[\frac{\mu b}{GeV^2}\right]$$

ρ-shape	$(m_\rho/m)^4$	$(m_\rho/m)^{n(t)}$	π (t)	Drell — Söding
$k = 2.8$ *GeV*	153±10	143±10	144±13	93±7
$k = 4.7$ *GeV*	110±8	108±6	102±8	80±5

$$\sigma_{tot} (\gamma p \to \rho^0 p) [\mu b]$$

ρ-shape	$[m_\rho/m)^4$	$(m_\rho/m)^{n(t)}$	π (t)	Drell — Söding
$k = 2.8$ *GeV*	21.4±0.6	20.9±1.0	18.9±1.1	16.4±1.0
$k = 4.7$ *GeV*	15.5±0.4	15.8±0.8	13.5±1.0	14.4±0.7

Table 3

$$\left.\frac{d\sigma}{dt}\right|_{t=0} \left[\frac{\mu b}{GeV^2}\right] \gamma + p \to \rho^0 + p$$

k [*GeV*]	Jackson [57]	$(m_\rho/m)^4$	I (m)	$(m_\rho/m)^4 + I(m)$	Drell — Söding	Ref.
2.15		129±11.3				DESY — HBC [63]
2.8		153±10			93±7	SLAC — HBC [64]
2.9		156±18	161±18	156±12		DESY — MIT [56]
3.0		147±13.0				DESY — HBC [63]
3.5		132±27	142±18	139±15		DESY — MIT [56]
3.9					169±14	Cornell [55]
4.0		149±18.5				DESY — HBC [63]
4.1					151±14	Cornell [55]
4.1		127±7	144±9	141±9		DFSY — MIT [56]
4.6					141±13	Cornell [55]
4.7		110±8			80±5	SLAC — HBC [64]
4.7		139±7	138±7	135±7		DESY — MIT [56]
5.15		130±16.2				DESY — HBC [63]
5,3		125±6	120±6	126±6		DESY — MIT [56]
5.5	136±17					SLAC — F [1]
5.6					136±6	Cornell [55]
5.9		116±4	121±4	124±4		DESY — MIT [56]
5.9					128±9	Cornell [55]
6.0	133±14					SLAC — F [1]
6.5		116±5	116±5	116±5		DESY — MIT [56]
6.5					112±9	Cornell [55]
6.5	131±13					SLAC — F [1]
6.95					116±10	Cornell [55]
7.4					111±4.5	Cornell [55]
8.25					111±7	Cornell [55]
9.0					104±14	SLAC B + C [62]
11.5	113±7					SLAC F [1]
12.25	112±7					»
13.0	110±7					»
13.75	109±6					»
14.5	108±7					»
15.25	107±7					»
16.0	106±7					»
16.9	105±6					»
17.8	105±6					»

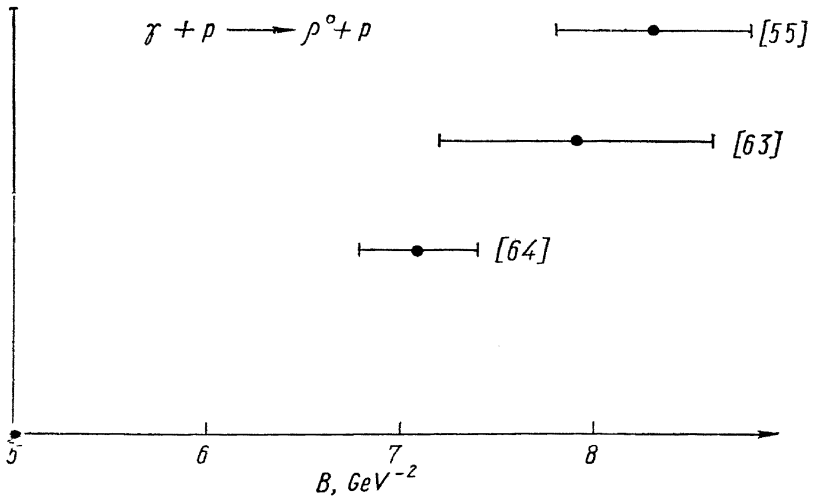

Fig. 16.

given in fig. 13 and table 3. All data agree within quite a broad band, which has a width of the order of ±10%, besides the SLAC data [64] analyzed with the Söding model. These two cross sections at 2.8 and 4.7 *GeV* are about 55 $\mu b/GeV^2$ lower than the other experiments. The authors mention, that a correction for double counting effect would raise the cross section by more than 10 $\mu b/GeV^2$. Fitting the t dependence of the ρ cross section to the form $\frac{d\sigma}{dt} = Ae^{Bt}$, the slope parameter B is around 8 GeV^{-2} for all experiments and energies of ~ 5 *GeV* besides the SBT — HBC point (analyzed with the Söding model), which gives $B = 5.5 \pm 0.3$ GeV^{-2}. Some values for B are summarized in fig. 16. Via the VDM and the optical theorem the forward ρ^0 photoproduction cross section can be related to the total $\gamma - p$ hadronic cross section $\sigma(\gamma p)$ and the total $\rho - N$ cross section $\sigma(\rho N)$. This will be discussed in section 2.9.

2.2. PRODUCTION MECHANISM IN ρ^0 PHOTOPRODUCTION

Comparing the energy dependence of forward photoproduced ρ^0 mesons with that of elastically scattered $\pi^\pm$ mesons on protons, we have found a close similarity indicating, that forward ρ^0 photoproduction proceeds also dominantly by diffraction. To study this typical feature of strong interaction dynamics in more detail, the ρ^0 decay angular distributions photoproduced by linearly polarized photons have been investigated at SLAC [64] (SBT — collaboration), DESY [65] and Cornell [66]. At DESY and Cornell the linearly polarized photon beam was produced on a diamand crystal. A spectrometer and spark chamber set up was used to identify the π^+ and π^- mesons as well as the recoil proton. At SLAC the Compton backscattered light of a ruby laser (see section 1.3) together with the 82″ bubble chamber was used.

The decay angular distribution can be expressed in terms of the ρ^0 density matrix elements. Splitting these matrix elements according to the density matrix of the incoming linearly polarized photon, one obtains

$$X_{\lambda'_\rho \lambda_\rho} = [X^0 - P_\gamma (X^1 \cos 2\varphi + X^2 \sin 2\varphi)]_{\lambda'_\rho \lambda_\rho}. \tag{18}$$

Here P_γ is the degree of linear polarization of the photon and φ the angle between the photon electric polarization vector ε and the production plane. Expressed in terms of bilinear combinations of ***s*-channel** helicity amplitudes, the ρ^0 density matrix elements are [68]

$$\begin{aligned}
X^0_{\lambda'_\rho \lambda_\rho} &\sim \sum_{\lambda_\gamma, \lambda_{N'}, \lambda_N} T^*_{\lambda'_\rho \lambda_{N'}, \lambda_\gamma \lambda_N} T_{\lambda_\rho \lambda_{N'}, \lambda_\gamma \lambda_N}; \\
X^1_{\lambda'_\rho \lambda_\rho} &\sim \sum_{\lambda_\gamma, \lambda_{N'}, \lambda_N} T^*_{\lambda'_\rho \lambda_{N'}, \lambda_\gamma \lambda_N} T_{\lambda_\rho \lambda_{N'}, -\lambda_\gamma \lambda_N}; \\
X^2_{\lambda'_\rho \lambda_\rho} &\sim -i \sum_{\lambda_\gamma, \lambda_{N'}, \lambda_N \lambda_\gamma} T^*_{\lambda'_\rho \lambda_{N'}, \lambda_\gamma \lambda_N} T_{\lambda_\rho \lambda_{N'}, -\lambda_\gamma \lambda_N}.
\end{aligned} \tag{19}$$

Assuming the helicity to be **conserved in the** *s*-**channel**, the helicity amplitudes have the simple structure

$$T_{\lambda_\rho \lambda_{N'}, \lambda_\gamma \lambda_N} = t_{\lambda_\gamma \lambda_N} \delta_{\lambda_{N'} \lambda_N} \delta_{\lambda_\rho \lambda_\gamma}. \tag{20}$$

This leads with the correct normalization to the density matrix elements (using equ. (19))

$$\begin{aligned} X^0_{11} &= X^0_{-1-1} = 0{,}5; \quad X^0_{00} = 0 \\ X^1_{1-1} &= X^1_{-11} = a \\ X^2_{1-1} &= -X^2_{-11} = -ia \end{aligned} \tag{21}$$

with the constant a real ($-0{,}5 \leqslant a \leqslant 0{,}5$) and all other elements (helicity flip contributions) being equal to zero.

The decay angular distribution of the ρ^0 meson W ($\cos\theta$, φ, Φ), where θ and φ are the polar and azimuthal angles of the π^+ in the ρ^0 rest frame, takes then the simple form

$$W(\cos\theta, \psi) = \frac{3}{8\pi} \sin^2\theta (1 + 2P_\gamma a \cos 2\psi) \tag{22}$$

where the angle $\psi = \varphi - \Phi$ is in the forward direction the angle between the photon polarization ε and the ρ^0 decay planes.

The SLAC measurements [64] were carried out at photon energies of 2.8 and 4.7 *GeV* and fixed polarization direction. Fig. 17 shows the distributions of the polar angle θ and the angle ψ in the helicity system for events in the ρ^0 mass region with $|t| < 0.4$ *GeV*^{2}, where t is the square of the four-momentum transfer between the incoming and outgoing proton. The $\cos\theta$ distributions are proportional to $\sin^2\theta$ in agreement with equ. (22), i. e., the ρ^0 mesons are produced with c. m. s. helicity ± 1. Moreover the ψ distributions are proportional to $\cos^2\psi$, which corresponds to $a = 0.5$ in equs. (22) and (21) showing that the ρ^0 is almost completely linearly polarized as the photon (P_γ is close to 1, see section 1.3).

Fig. 18 shows the density matrix elements X^0_{00} and X^1_{1-1} in the **helicity system** for $|t| < 0.4$ *GeV*^{2}. In the ρ^0 mass region X^0_{00} is zero within the errors. Furthermore all other helicity flip contributions are also zero within the errors showing in agreement with equs. (21), that the ρ^0 production mechanism conserves *s*-channel c. m. s. helicity. In the Gottfried — Jackson and Adair system the density matrix elements vary rapidly with t. This excludes t-channel helicity conservation and the hypothesis of spin independence in the total c. m. system for ρ^0 production. The density matrices can be used for further investigations of the **pro-**

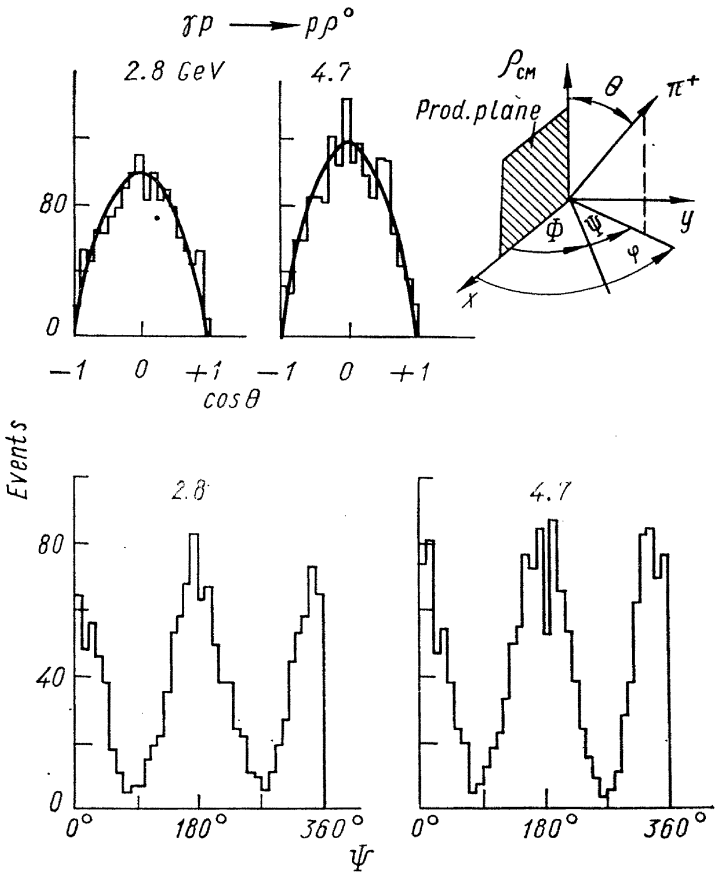

Fig. 17.

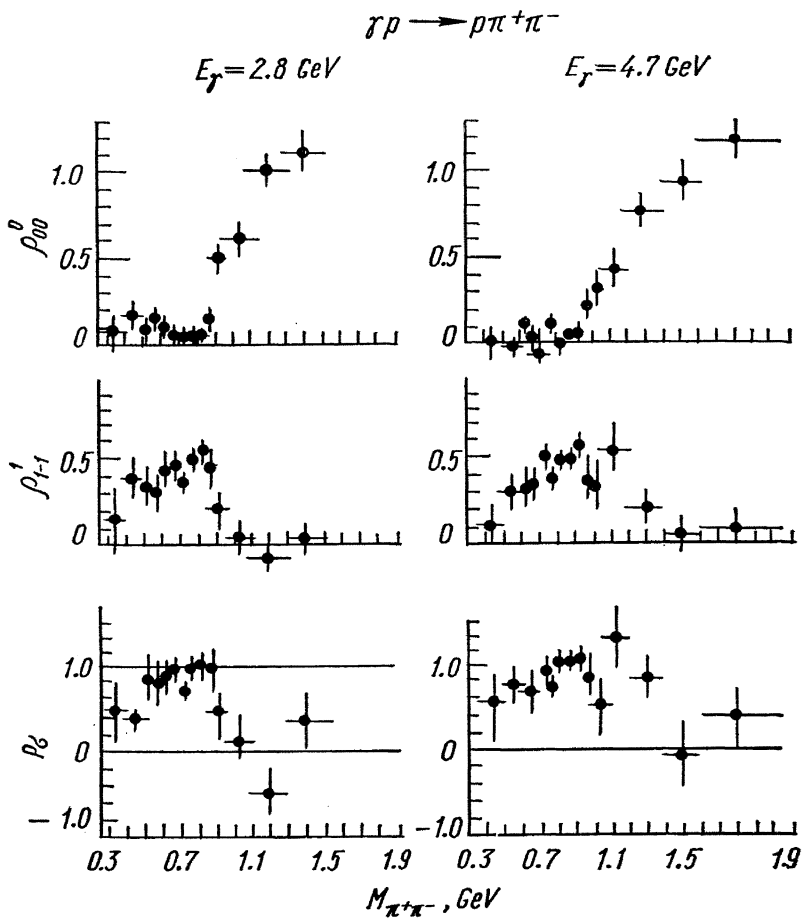

Fig. 18.

duction mechanism. For example the contributions σ^+ and σ^- from natural ($\eta_p = (-1)^J$) and unnatural ($\eta_p = -(-1)^J$) parity exchanges in the t-channel can be obtained from

$$P_\sigma = \frac{\sigma^+ - \sigma^-}{\sigma^+ + \sigma^+} \qquad (23)$$

which to leading order in energy is given by

$$P_\sigma = 2X^1_{1-1} - X^1_{00}. \qquad (24)$$

From fig. 18 we see, that in the ρ^0 mass region X^1_{1-1} is equal to 0. 5 within the errors (in agreement with the $\cos^2\psi$ distribution, fig. 17) and P_σ equal to 1, showing that ρ^0 production is completely dominated by **natural** parity exchange. Averaging P_σ over the range $|t| < 1$ GeV^2 the contribution from **unnatural** parity exchange is $3.1 \pm 2.2\%$ at 2.8 *GeV* and $-1.1 \pm 1.9\%$ at 4.7 *GeV*.

The DESY [65] and Cornell [66] experiments were done with spectrometers of limited acceptance. The symmetric decay $\rho^0 \to \pi^+\pi^-$ was observed for decay planes near a direction $\vec{n}_H$ normal ($\theta = \pi/2$, $\varphi = \pi/2$) to the horizontal sym-

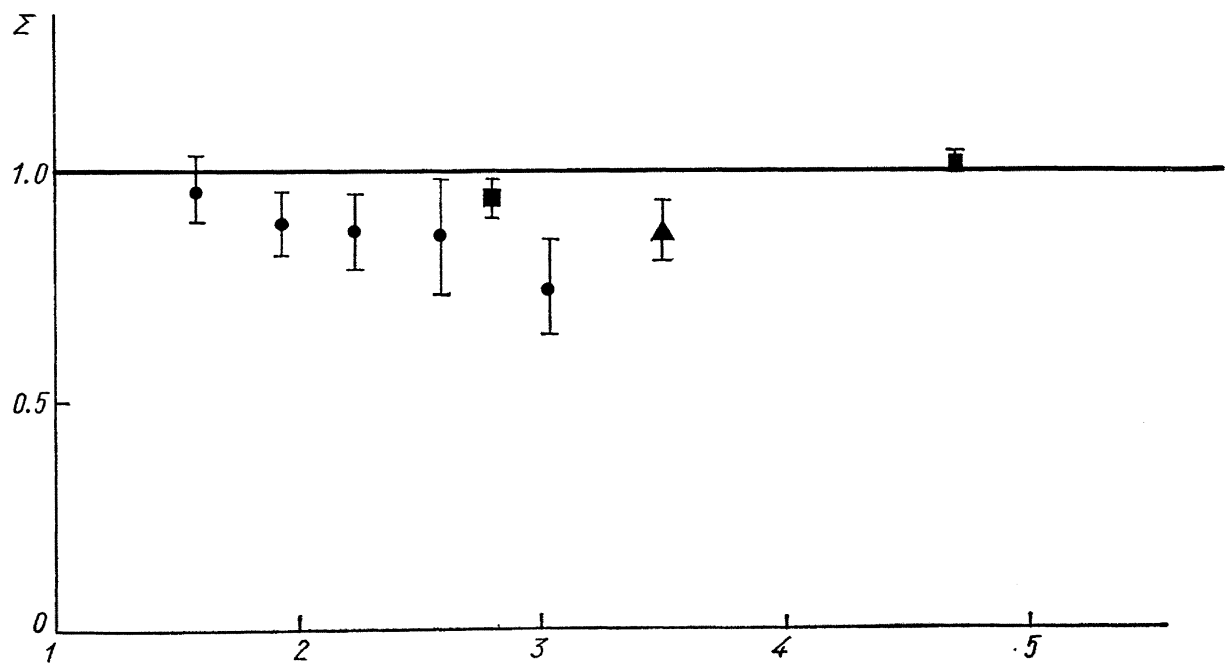

Fig. 19. $\gamma p \to \rho^0 p$; ■ — SLAC [64], $|t| < 1$ $GeV/c)^2$; ● — DESY [65], $|t| < 0.4$ $(GeV/c)^2$; ▲ — Cornell [66].

metry (production) plane. The counting rates $\sigma_{\parallel}$ were obtained when the linear photon polarization ε was directed parallel to $\vec{n}_N$ and $\sigma_{\perp}$ for an orientation perpendicular to it. The asymmetry ratio Σ is then given

$$\Sigma = \frac{\sigma_{\parallel} - \sigma_{\perp}}{\sigma_{\parallel} + \sigma_{\perp}} = \frac{X^1_{11} + X^1_{1-1}}{X^0_{11} + X^0_{1-1}}. \tag{25}$$

For a *s*-channel helicity conserving production mechanism dominated by natural parity exchange Σ should be close to $+1$. In fig. 19 the results of the three experiments on Σ are summarized. The values stay close to 1 down to 1.6 *GeV*, showing no influence of *s*-channel resonances. This is in agreement with calculations of Schildknecht and Schrempp [69], who predict a change of Σ smaller than 5% for Δ (1950) and smaller than 2% for Δ (2420), as long as they are coupled by magnetic multipole transitions only, like the Δ (1236) resonance.

In summary ρ^0 photoproduction conserves helicity in the *s*-channel c. m. system up to $|t| = 0.4$ *GeV*^{2} and proceeds almost completely through natural parity exchange.

2.3. ρ^0 PHOTOPRODUCTION ON COMPOSITE SYSTEMS

2.3.1. ρ^0 PHOTOPRODUCTION ON DEUTERIUM

The investigation of the reaction $\gamma + d \to \rho^0 + X^0$ where X^0 is eather the deuteron nucleus (coherent production) or the unbound *pn*-system (incoherent production) allows by comparison with the hydrogen data a test of the hypothesis, that the production mechanism is diffractive. Assuming pure diffraction the ratio for the $t = 0$ cross sections is predicted to be [53]

$$R_{D_H,th} = \frac{\frac{d\sigma}{dt}(D,\ t=0)}{\frac{d\sigma}{dt}(H,\ t=0)} = 3.64. \tag{26}$$

This ratio is not 4 because of the Glauber corrections. Fig. 20 shows the energy dependence of the ratio R_{D_H} obtained in the Cornell experiment [55]. Below 6 *GeV* the ratio is lower than the Glauber prediction (straight line) while for energies above 6 *GeV* the data are consistent with the theory. The SLAC experiment [62] at 9 *GeV* gives a ratio of $R_{D_H} = 3.5 \pm 0.3$ consistent with theory and the Cornell data.

The discrepancy of R_{D_H} from the predicted value below 6 *GeV* can be used to speculate about the presence of $I = 1$ isospin *t*-channel exchange in the nucleon amplitudes [55].

The Ritson group at SLAC has contributed a new experiment on coherent ρ^0 production off deuterons [70]. They have measured angular distribution

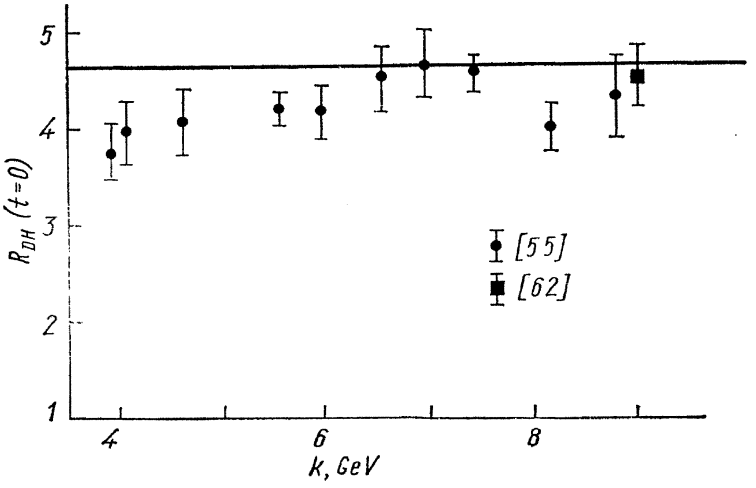

Fig. 20.

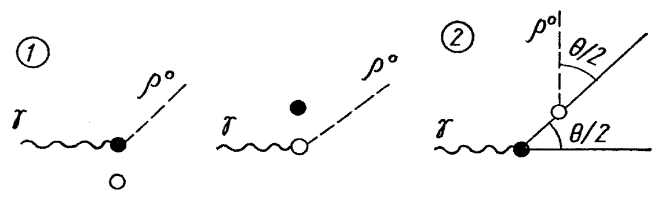

Fig. 21. 1: small $|t|$, single scattering;

$$\frac{d\sigma}{dt} \sim \frac{\sigma_{\rho N}^2}{\gamma_\rho^2} f_N^2(t)\, F_D^2(t) \quad \downarrow e^{8t} \quad \downarrow e^{30t}$$

2: $|t| > 0.6$ $(GeV/c)^2$, double scattering;

$$\frac{d\sigma}{dt} \sim \frac{\sigma_{\rho N}^4}{\gamma_\rho^2} f_N^4\left(\frac{t}{4}\right)\left\langle \frac{1}{r^2} \right\rangle \quad \downarrow e^{4t}$$

of the reaction $\gamma + d \to \rho^0 + d$ at 6, 12 and 18 *GeV* in the momentum transfer range $|t|$ from 0.15 to 1.4 GeV^2. The recoil deuteron was detected in the SLAC 1.6 *GeV/c* spectrometer using a chopped beam time-of-flight technique. This experiment was planned at a time, where there was a lot of confusion in determining the total ρ-nucleon cross section $\sigma_{\rho N}$ and the γ — ρ coupling constant $\gamma_\rho^2/4\pi$ from ρ^0 photoproduction experiments off complex nuclei (c.f. section 2.3.2)

This new method avoids difficulties with nuclear size and real parts which beset the determination of $\sigma_{\rho N}$ and $\gamma_\rho^2/4\pi$ from complex nuclei. The idea of this experiment is, that at large $|t| > 0.6$ GeV^2 the requirement that the **deuteron remains bound** causes the process to be dominated by a two step process. The ρ^0 is produced on one nucleon and scatters on the other, giving approximately equal recoil to both nucleons. At small t-values the process is dominated by single scattering. Since the deuteron has isospin $I = 0$ only the isovector part of the photon contributes, which means ρ dominance in the framework of the VDM. Fig. 21 shows a raw sketch of the situation. At small $|t|$ values the cross section is proportional to $\sigma_{\rho N}^2/\gamma_\rho^2$ and has a steep fall-off with $|t|$ according mainly to the deuteron formfactor. At large $|t| > 0.6$ GeV^2 the cross section is dominated by the double scattering contribution, which is proportional to $\sigma_{\rho N}^4/\gamma_\rho^2$ and has a $|t|$ dependence of approximately e^{4t}. Since the cross sec-

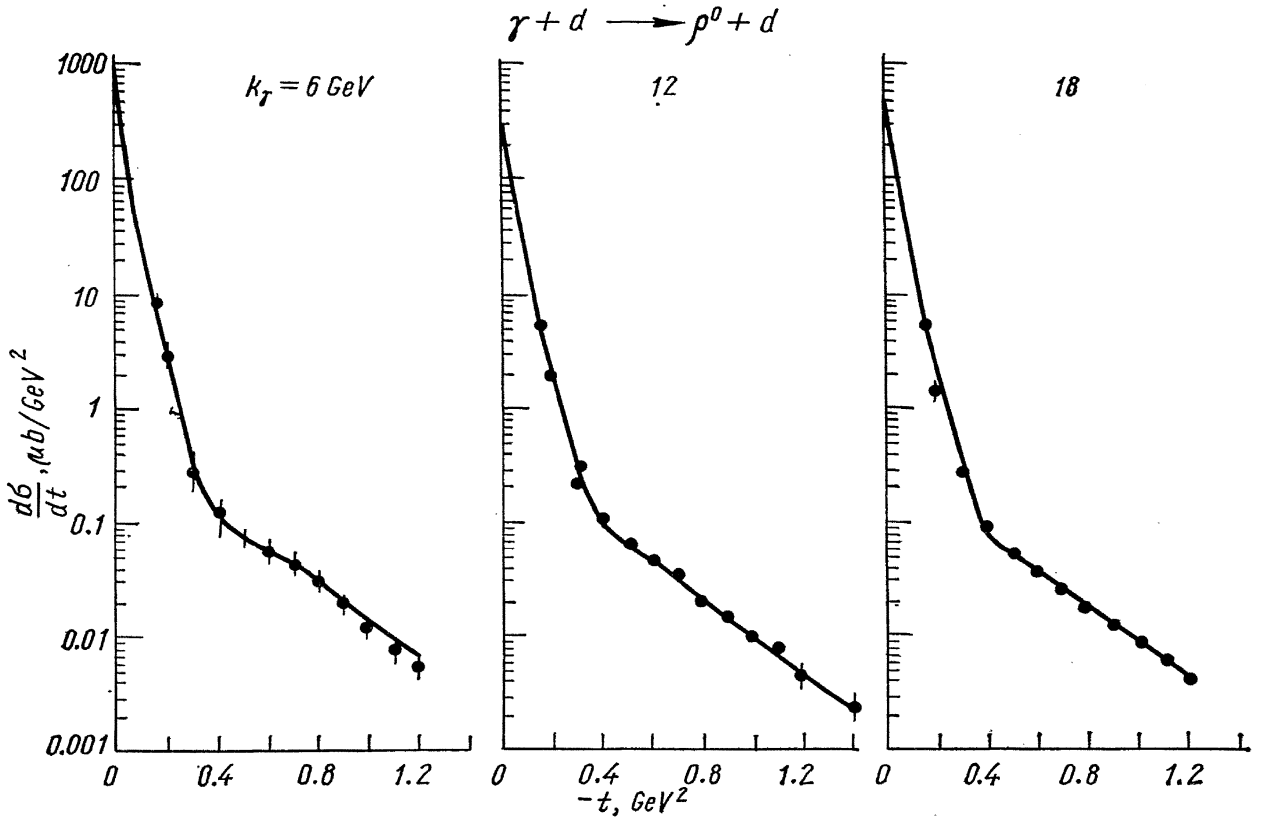

Fig. 22. The solid lines are obtained from Glauber theory calculations.

tion depends differently on $\sigma_{\rho N}$ in these two regions of momentum transfer, a measurement over a wide range of $|t|$ may determine $\sigma_{\rho N}$ and hence $\gamma_\rho^2/4\pi$ without being dependent of the problems involved in compex nuclei physics. Fig. 22 shows the results. The different slopes in the single scattering and double scattering region are nicely seen. The curves show fits, which have been done for each energy separately. In these fits the deuteron data were used only in the double scattering region from $|t| = 0.7\ GeV^2$ to $1.4\ GeV^2$. At $t = 0$ the proton data from ref. (1) were used. This avoids the use of the deuteron data at small t-values which have still relatively large uncertainties, as well as the data between $|t| = 0.3\ GeV^2$ and $0.6\ GeV^2$ where interference terms and deuteron D-state contributions are important. The fits describes the data very well in the whole momentum transfer range covered. The results on $\sigma_{\rho N}$ and $\gamma_\rho^2/4\pi$ are given in table 4 together with the $t = 0$ proton data of ref. (1). A discussion is contained in the next section.

Table 4

k [GeV]	$\frac{d\sigma}{dt}$ $(t = 0,\ A = 1)$ [$\mu\ b/GeV^2$]	$\gamma_\rho^2/4\pi$	$\sigma_{\rho N}$ [mb]
6	133±14	.66± .14	30.2±3.0
12	112±7	.70± .14	28.6±2.5
18	105±6	.71± .14	27.8±2.5

2.3.2. ρ^0 PHOTOPRODUCTION ON COMPLEX NUCLEI

In an optical model approach, following the theory of Koelbig and Margolis [71] the coherent diffractive amplitude for vector meson photoproduction off a nucleus can de written as

$$f_C = 2\pi f_0 \int_0^\infty b\,db \int_{-\infty}^\infty dz J_0(b\sqrt{|t_\perp|})\,\rho(b, z)\exp(iz\sqrt{|t_\parallel|}) \times$$

$$\times \exp\left(-\frac{\sigma_{VN}}{2}(1 - i\beta_V)\int_z^\infty \rho(b, z')\,dz'\right). \qquad (27)$$

This form relates the production amplitude f_C on a nucleus to the spin and isospin independent part (i. e. diffraction) of the forward photoproduction amplitude f_0 on a single nucleon. The integral over the impact parameter b for a nucleus with density ρ takes into account the reabsorption of the produced vector mesons with a total cross section σ_{VN}. The quantity β_V is the ratio of the real to the imaginary part of the forward vector-meson nucleon scattering amplitude. At the moment the largest amount of information exists for the ρ^0 meson. Measuring the A (nuclear mass) and t dependence of the coherent ρ^0 photoproduction cross section, an analysis in terms of equ. (27) allows to determine the total ρ-nucleon cross section $\sigma_{\rho N}$ and the radius of the nucleus, provided a certain model for the nuclear density distribution has been adopted. Furthermore the quantity β_ρ must be known. From the VDM assuming ρ dominance and the optical theorem one has then

$$\frac{d\sigma}{dt}(\gamma N \to \rho^0 N)|_{t=0} = |f_0|^2 = \frac{\alpha}{64\pi}\left(\frac{\gamma_\rho^2}{4\pi}\right)^{-1}\sigma_{\rho N}^2(1 + \beta_\rho^2) \qquad (28)$$

from which the $\gamma - \rho$ coupling constant $\gamma_\rho^2/4\pi$ can be determined. Between 1967 and 1969 three experiments on ρ^0 photoproduction on complex nuclei were performed at DESY [72], Cornell [73] and SLAC [74]. The results were largely inconsistent essentially because the procedure adopted by the groups to analyse the data were different and the fundamental role of β_ρ was not recognized.

This situation has improved considerably in the last year. Three new «second generation» experiments from DESY [75], Cornell [55] and from the Rochester group [76] working at Cornell have been contributed to this conference. Furthermore the SLAC data [74] have been reanalyzed [77]. The DESY — MIT group and the Cornell group used a two arm spectrometer to detect the $\pi^+\pi^-$ pairs. The Rochester and SLAC groups used a spark chamber set up, where the decay angular acceptance in the SLAC experiment was large enough to verify, that the ρ^0 mesons are indeed transverseley polarized.

In all experiments the coherent ρ^0 photoproduction cross section is now analyzed in terms of equs. (27) and (28) to extract the quantities $\sigma_{\rho N}$ and $\gamma_\rho^2/4\pi$. In this procedure the knowledge of the nuclear density distribution $\rho(r)$ and the ratio β_ρ enters. Each group has measured directly the nuclear radii. The DESY — MIT experiment allowed the most precise determination of the radii by measuring the diffraction slope for 13 elements ranging from beryllium ($A = 9$) to uranium ($A = 238$). After making a subtraction for incoherent production on lighter nuclei (Be — Cu) the data were compared with equ. (27). The model of Trefil [78] was used for the incoherent contribution. The best values for $R(A)$ in the Wood — Saxon form

$$\rho(r) = \frac{\rho_0}{1 + \exp\frac{r - R(A)}{s}} \tag{29}$$

with fixed $s = 0.545$ are shown in fig. 23. For Be, C and Al the presence of background causes larger errors. The Wood — Saxon radii fit the scaling law

$$R(A) = r_0 A^{1/3} \tag{30}$$

with $r_0 = (1.12 \pm 0.02)$ *fm*.

This value is larger but not inconsistent with $r_0 = 1.08$ *fm* as determined in electron scattering experiments [79]. In conclusion one can say, that for $A > 27$ the radii determined in all four ρ production experiments quoted above

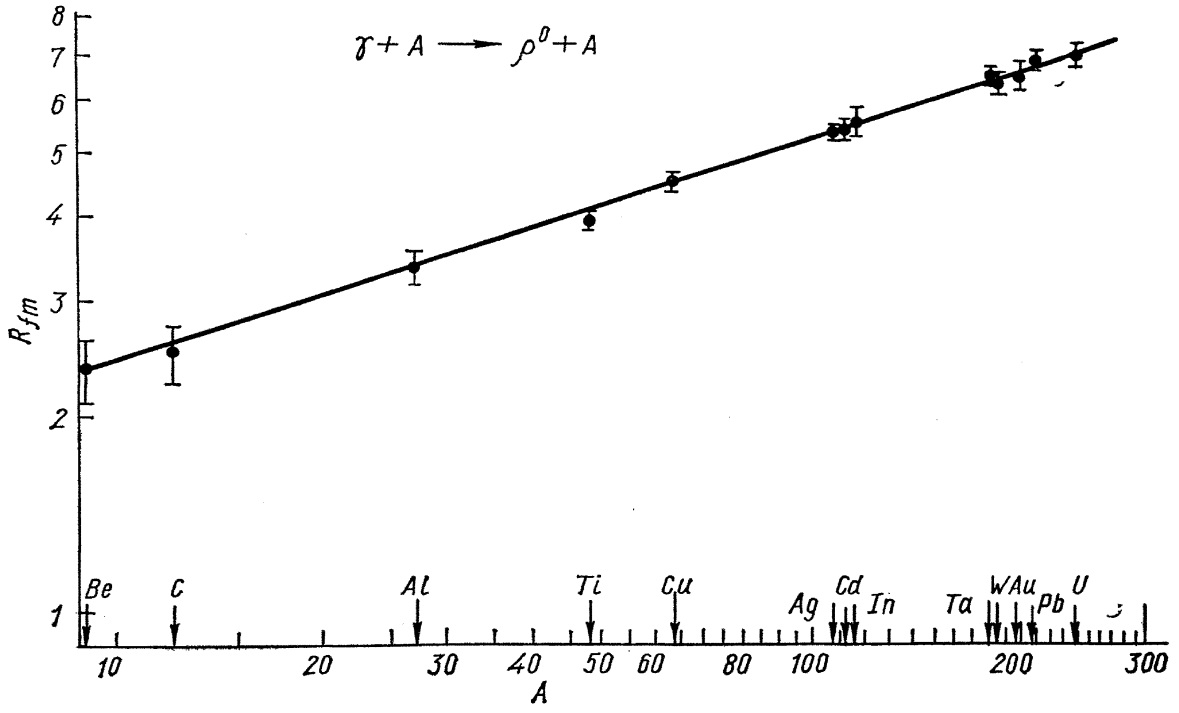

Fig. 23. Nuclear radii obtained from the measured $t_\perp$ dependence of the cross section (ref. [75]). The solid line represents a best fit to the form $R = r_0 A^{1/3}$.

are consistent. On the other hand for light nuclei each group uses different distributions and different radii.

Up to this year no direct information on β_ρ was available and a value of $\beta_\rho \sim -0.2$ at $k \sim 6$ *GeV* was estimated on the basis of the quark model prediction and the VDM

$$\beta_\rho = \beta_{\pi^0 N} \sim \beta_{\gamma N} \tag{31}$$

where $\beta_{\gamma N}$ was obtained from $\gamma - p$ total cross section measurements [80].

Recently this quantity has been directly measured by the DESY—MIT group and at Nina (see section 2.6) giving $\beta = -0.2 \pm 0.1$ for photon energies around 6 *GeV* in good agreement with the quark model prediction of equ. (31).

Table 5

Ref.	Energy [*GeV*]	$\sigma_{\rho N}$ [*mb*]	$\gamma_\rho^2/4\pi$	$\lvert f_0 \rvert^2 \left[\frac{\mu b}{GeV^2}\right]$	Remarks
DESY — MIT [75]	4.8—7.2	26.7 ± 2.0	$0.57 \pm 0{,}1$	118 ± 6	$\beta_\rho = -0.2$
	6.1	26.1 ± 0.9	0.58 ± 0.03	117 ± 10	$\beta_\rho = -0.27$
Cornell [55]	6.5	30.1 ± 1.5	0.74 ± 0.05	124 ± 15	$\beta_\rho = -0.27$
	8.8	26.8 ± 1.2	0.68 ± 0.04	105 ± 11	$\beta_\rho = -0.24$
Rochester [76]	8	29.2 ± 2.5	0.71 ± 0.12	117 ± 8	$\beta_\rho = -0.2$
SLAC (B — C) [77]	9	$28.8 \pm {}^{2.6}_{1.7}$	$0.85 \pm {}^{0.10}_{0.12}$	—	β_ρ ref. (80)
	6	30.2 ± 3.0	0.66 ± 0.14		
SLAC F [70]	12	28.6 ± 2.5	0.70 ± 0.14	—	table 4
	18	27.8 ± 2.5	0.71 ± 0.14		
Orsay [81]		—	0.50 ± 0.03	—	—

The last problem consists now in the separation of the coherently (diffractively) produced ρ^0 mesons from background in the mass and t-distributions.

The DESY — MIT group [75] has analyzed their data by fitting the experimental distributions to the form:

$$\frac{d\sigma}{d\Omega dm}(A, m, p, t_\perp) = \frac{1}{\pi} p^2 2mR(m)(\lvert f_c \rvert^2 + \lvert f_{\text{inc}} \rvert^2) + BG(A, m, p, t_\perp). \tag{32}$$

The first term represents the main contribution from ρ photoproduction: $\lvert f_c \rvert^2$ is the dominant coherent part (equ. 27) while $\lvert f_{\text{inc}} \rvert^2$ represents an incoherent production as calculated by Trefil [78]. The background function BG accounts for nonresonant production. For the ρ^0 mass distribution the three hypothesises discussed in section 2.1 have been investigated. All 3 assumption lead to consistent results.

The Rochester group [76] analyzed their data in a similar way. They fit the ρ^0 spectrum with the Ross — Stodolsky [58] and the Drell — Söding model allowing for an arbitray incoherent background. In the final analysis the Ross — Stodolsky model was used.

The Cornell group [55] analyzed their data on nuclei in the same way as their hydrogen data discussed in section 2.1 allowing for no arbitray background. The same way the SLAC group [77] reanalyzed their data.

I have summarized the results with respect to $\sigma_{\rho N}$ and $\gamma_\rho^2/4\pi$ in table 5 and fig. 24. Also included are the data of the SLAC deuteron experiment [70] discussed in section 2.3.1 and the colliding beam value of $\gamma_\rho^2/4\pi$ from Orsay [81]. In conclusion the total picture is still not very precise but within the quoted errors all data are consistent. The weighted average 0.65 for $\gamma_\rho^2/4\pi$ of

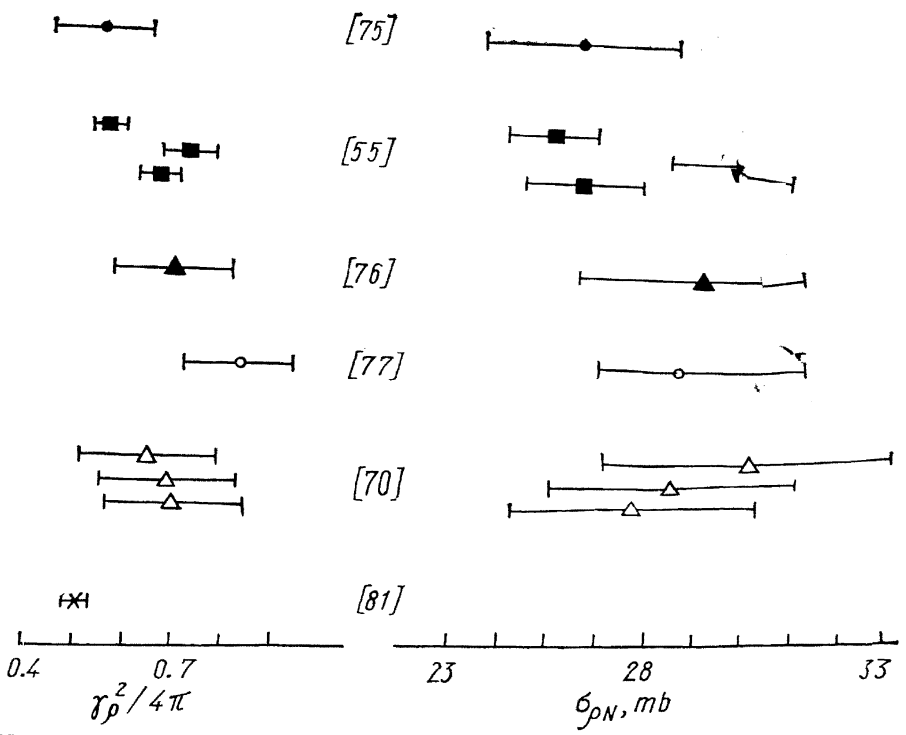

24.

all photoproduction experiments is somewhat higher than the Orsay storage ring value. The results on $\sigma_{\rho N}$ support the quark model prediction $\sigma_{\rho N} = 0.5\,(\sigma_{\pi^+ p} + \sigma_{\pi^- p}) \sim 28$ *mb* at energies around 6 *GeV* [60].

2.4. ω MESON PHOTOPRODUCTION

2.4.1. ω MESON PHOTOPRODUCTION FROM HYDROGEN AND DEUTERIUM

Two experiments on ω photoproduction on hydrogen have been contributed to this conference. The group at SLAC using the 82″ HBC have studied ω production on protons by linearly polarized photons at 2.8 and 4.7 *GeV* [82]. This is part of the programm of the SBT-collaboration, which

Table 6

$\gamma + p \to \omega + p$

	$k = 2.8$ *GeV*	$k = 4.7$ *GeV*
σ_{tot}	5.8 ± 0.5 *μb*	3.2 ± 0.3 *μb*
A $(0.02 < \lvert t\rvert < 0.4$ *GeV*$^2)$	34 ± 4 *μb/GeV*^{2}	25 ± 3 *μb/GeV*^{2}
B $(0.02 < \lvert t\rvert < 0.4$ *GeV*$^2)$	6.2 ± 0.7 *GeV*$^{-2}$	8.0 ± 0.8 *GeV*$^{-2}$
P_σ $(\lvert t\rvert < 1$ *GeV*$^2)$	-0.04 ± 0.13	0.19 ± 0.14
σ^+ $(\lvert t\rvert < 1$ *GeV*$^2)$	2.50 ± 0.37 *μb*	1.84 ± 0.28 *μb*
σ^- $(\lvert t\rvert < 1$ *GeV*$^2)$	2.70 ± 0.39 *μb*	1.25 ± 0.27 *μb*
A_+ $(0.02 < \lvert t\rvert < 0.4$ *GeV*$^2)$	13.1 ± 4.1 *μb/GeV*^{2}	15.2 ± 3.8 *μb/GeV*^{2}
B_+ $(0.02 < \lvert t\rvert < 0.4$ *GeV*$^2)$	5.5 ± 1.6 *GeV*$^{-2}$	7.5 ± 1.5 *GeV*$^{-2}$

includes the ρ^0 production mentioned earlier. The data are analyzed in terms of a zero constraint fit, the photon energy k being not constrained. Most of the multineutral events are removed by requiring the reconstructed photon energy to lie within the limits $2.4 < k < 3.3$ and $4.1 < k < 5.3$ for the central energies

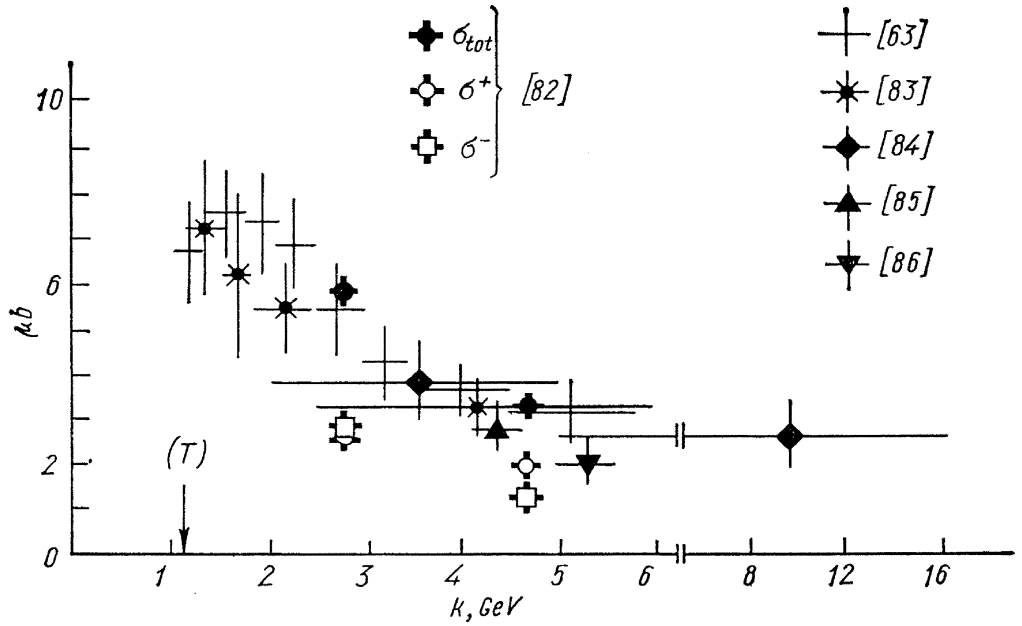

Fig. 25. $\gamma p \to \omega p$. (T) — threshold.

2.8 and 4.7 *GeV*, respectively. The $\pi^+\pi^-\pi^0$ mass distribution show spectacular ω peaks. The total ω production cross sections are given in table 6 and are shown in fig. 25 together with those of other experiments [63, 83—86]. The differential cross sections are shown in fig. 26 [82]. A fit of $d\sigma/dt$ for $0.02 < |t| < 0.4$ *GeV*^{2} to the form $A \exp(Bt)$ leads to values for A and B given in table 6.

The decay angular distributions of the ω meson are analyzed in the helicity frame. In **contrast** to ρ^0 photoproduction considerable helicity flip contributions are found. From the density matrix elements one can again, as in the case of the ρ^0, deduce the parity asymmetry P_σ, which measures the ratio

$$P_\sigma = \frac{\sigma^+ - \sigma^-}{\sigma^+ + \sigma^-} \tag{23}$$

of the cross section contributions from natural (σ^+) and unnatural (σ^-) parity exchange in the t-channel. In the high energy limit P_σ is given by

$$P_\sigma = 2X^1_{1-1} - X^1_{00}. \tag{24}$$

In table 6 the values of P_σ, σ^+ and σ^- are given for ω production for $|t| < 1.0$ *GeV*^{2}. The values of σ^+ and σ^- are also shown in fig. 25. Natural and unnatural parity exchange contribute in approximately equal amounts ($P_\sigma \sim 0$). The unnatural cross section σ^- decreases from 2.8 to 4.7 *GeV* by more than a factor of 2 whereas the natural cross section σ^+ does not change significantly. The natural differential cross section $d\sigma^+/dt$ for $0.02 < |t| < 0.4$ *GeV*^{2} is shown in fig. 26. A fit of $d\sigma^+/dt$ to the form $A_+ \exp(B_+ t)$ give the values A_+ and B_+ of table 6. The slope parameters B_+ are quite similar to those found in ρ^0 photoproduction.

The large unnatural parity exchange contribution (non diffractive) in ω photoproduction in comparison to ρ^0 photoproduction can be easily understood. *SU* (3) (including $\omega - \Phi$ mixing) predicts that the OPE contribution (unnatural parity) to $\gamma p \to \omega p$ is nine times larger than in $\gamma p \to \rho^0 p$ while the diffractive part (natural parity), assuming the Pomeron is an *SU* (3) singlet, is nine times larger in ρ^0 production than in ω production. Thus we have

$$\frac{\sigma_{\text{Diff}}(\rho^0)}{\sigma_{\text{Diff}}(\omega)} = \frac{9}{1}, \quad \frac{\sigma_{\text{OPE}}(\rho^0)}{\sigma_{\text{OPE}}(\omega)} = \frac{1}{9}. \tag{33}$$

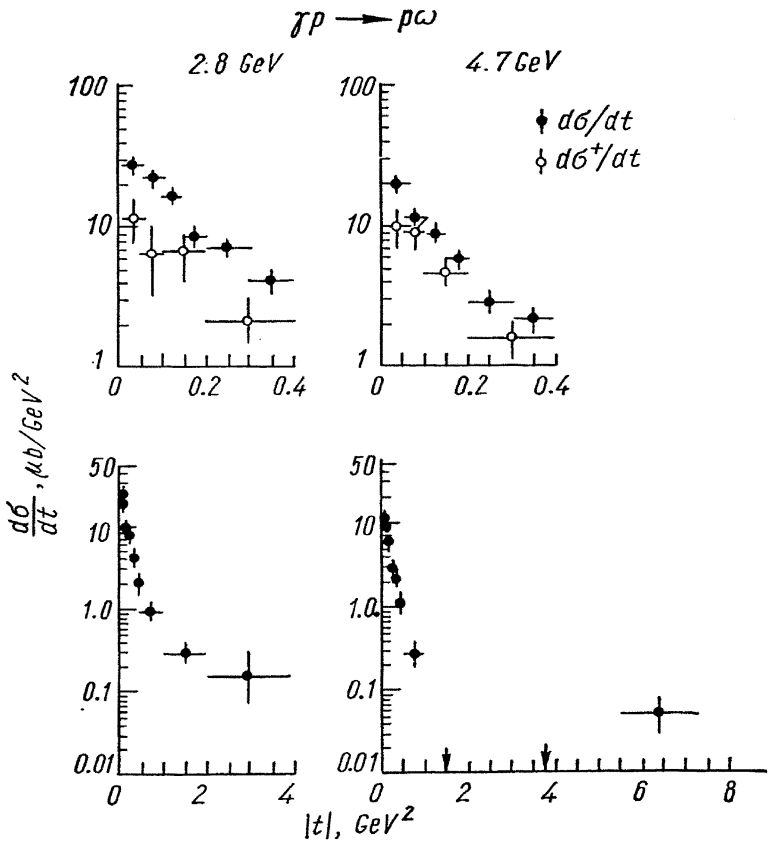

Fig. 26.

For example, if at a given energy 99% of the ρ^0 cross section is contributed by diffraction and 1% by OPE the ratio $\sigma_{OPE}(\omega)/\sigma_{Diff}(\omega)$ for ω photoproduction at the same energy will be 0.8 : 1. This is supported by the data of table 6. Since σ_{OPE} is proportional to s^{-2} (both for Reggeized and elementary π exchange) and σ_{Diff} is nearly constant the ratio $\sigma(\rho)/\sigma(\omega)$ should approach 9 for high energies. The comparison of the natural parity exchange cross sections for ω and ρ^0 photoproduction of ref. (64) (table 2) give for $|t| < 1.0\ GeV^2$ a ratio $\sigma_\rho^+/\sigma_\omega^+$ between 9 and 6 depending on the models used to determine the ρ^0 cross section. According to equ. 33 this ratio should be 9 for pure diffractive production. A considerable amount of A_2 exchange [87], which contributes to the natural parity part σ_ω^+ could however reduce the value of this ratio (the A_2 exchange contribution to σ_ρ^+ is expected to be small). Furthermore one can compare the contributions from unnatural parity exchange with the predictions of one-pion exchange. The OPE model predicts a decrease of the ω cross section σ_ω^- for $|t| < 1\ GeV^2$ by a factor 2.5 between 2.8 and 4.7 *GeV*. This ratio is practically independent of whether form factor or absorption corrections are used. Experimentally we have from table 6 a value of 2.2 ± 0.6 for this ratio in good agreement with the OPE prediction. Assuming that σ_ω^- is accounted for by OPE, a fit of $d\sigma/dt$ in the interval $0.02 < |t| < 0.4\ GeV^2$ to the form

$$d\sigma/dt = C \exp(Dt) + d\sigma_{OPE}/dt \qquad (34)$$

where the first term represents the natural parity contribution, yields $C = 12.1 \pm \pm 2.1\ \mu b/GeV^2$, $D = 5.6 \pm 1.2\ GeV^2$ and $\Gamma_{\omega\pi\gamma} = 0.98 \pm 0.10\ MeV$. The value of $\Gamma_{\omega\pi\gamma}$ is consistent with the value obtained from the width and branching ratio (88) and D is consistent with the slope for ρ^0 production (when analyzed using the Drell — Söding model, see fig. 16).

The Rochester group at Cornell has measured ω photoproduction [89] at 9 *GeV* on hydrogen and deuterium. The ω meson was detected through its dominant decay mode $\omega \to \pi^+\pi^-\pi^0$. The charged pions were measured in a wire spark chamber arrangement. Both decay photons of the neutral pion were converted in 1.5 radiation lengths of lead and the position of the converted photons is recorded by a second spark chamber and the energy by shower counters. This way the momenta of the three decay pions were measured, but there is no additional kinematical constraint left to distinguish between elastic and inelastic processes. They measure the sum of all differential cross sections of

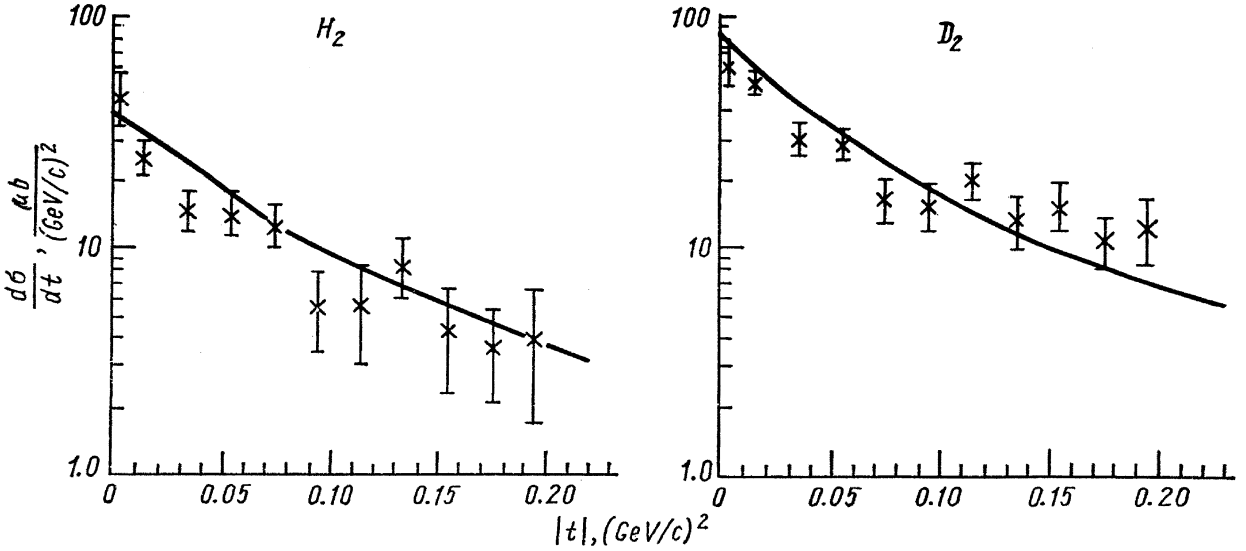

Fig. 27.

the type

$$\gamma + \begin{pmatrix} p \\ d \end{pmatrix} = \omega + \begin{pmatrix} N \\ 2N \end{pmatrix} + (k\pi); \quad k = 0, 1, 2, \ldots \tag{35}$$

Therefore the cross section will be dominated by the following processes

$$\gamma + \begin{pmatrix} p \\ d \end{pmatrix} = \omega + \begin{pmatrix} p \text{ or } N^* \\ p + n \text{ or } d \text{ or } N + N^*) \end{pmatrix} \tag{36}$$

where N^* is the 1236 *MeV* first $\pi - N$ resonance. Fig. 27 shows the measured angular distributions, averaged over the energy interval from 5 to 9 *GeV*.

The hydrogen elastic ω photoproduction cross section can be written in the high energy limit as

$$\frac{d\sigma}{dt}(\omega p) \simeq |T_0^+ + T_1^+|^2 + |T_0^- + T_1^-|^2 \tag{37}$$

where $T_0^{\pm}$ and $T_1^{\pm}$ are the amplitudes for isospin 0 and 1 natural (+) and unnatural (—) parity exchange in the t channel. $|T_0^+|^2$ is taken as

$$|T_0^+|^2 = |T_{00}^+|^2 e^{Bt} \tag{38}$$

where $|T_{00}^+|^2 = (9.6 \pm 1.2)\ \mu b/GeV^2$ is determined from ω photoproduction on complex nuclei by the same group (see section 2. 4. 2) and B is taken from ρ^0 photoproduction in hydrogen. The π exchange contributes to I_1^- and is calculated using the Bennecke — Dürr model [90]; the same model is used to calculate $d\sigma/dt$ (ωN^* 1236). For photoproduction in deuterium an impulse approximation calculation (including the assumption of closure) is used. Allowing further for an A_2 contribution to T_1^+ and an arbitrary normalization of $d\sigma/dt$ (ωN^*) in the fits, the curves in fig. 27 have been obtained. As a result the A_2 contribution is consistent with zero and the OPE calculation for the process $\gamma N \to \omega N^*$ (1236) somewhat overestimates the measured cross section.

2. 4. 2. ω PHOTOPRODUCTION ON COMPLEX NUCLEI

The results of two experiments of ω photoproduction on complex nuclei from the Rochester group [91] using the Cornell synchrotron and our Bonn — Pisa group [92] working at DESY have been contributed to this conference. The Rochester group has measured this process at $k = 6.8$ *GeV* on

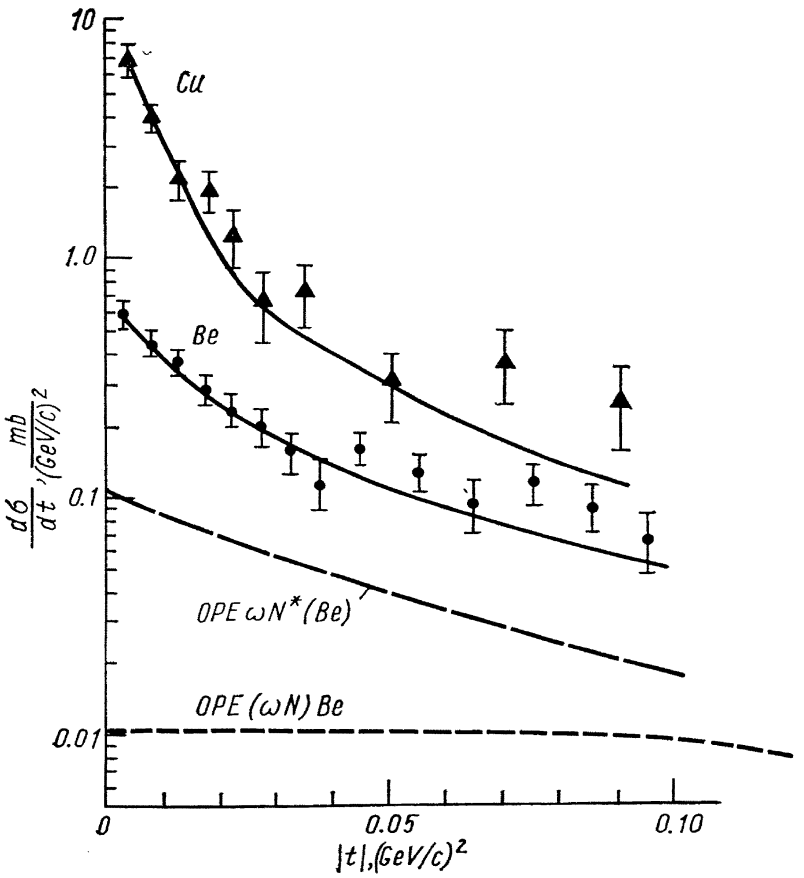

Fig. 28.

Be, C, Al, Cu and Pb targets. The ω mesons were detected by their $\pi^+\pi^-\pi^0$ decay mode with the same experimental set up as used for the hydrogen and deuterium runs described in the previous section. The differential cross sections $d\sigma/dt$ for Be and Cu are shown in fig. 28 [91]. They show a clear diffraction-type forward peak, but there is also a very substantial nondiffractive background, as to be expected from the discussion in section 2. 4. 1. The contribution of inelastic and incoherent events was calculated using the following expression:

$$\frac{d\sigma}{dt}^{\text{OPE}} = A_{\text{eff}} \left| \frac{d\sigma}{dt}(\omega N^*) + \right.$$
$$\left. + \quad (1 - G(t)) \frac{d\sigma}{dt}(\omega N) \right|. \tag{39}$$

Here A_{eff} is the effective number of nucleons contributing to incoherent photoproduction; its value was taken from large angle ρ^0 [93] and π^+ [94] photoproduction. The differential cross sections have been calculated by Wolf [90] using an OPE model. $G(t)$ is a correction factor and takes into account the suppression of incoherent processes at small t [95]. The long and short dashed lines in fig. 28 indicate the relative importance of the inelastic and incoherent contribution to $\frac{d\sigma}{dt}^{\text{OPE}}$. The solid lines in fig. 28 are obtained by fitting

$$\frac{d\sigma}{dt}(\omega A) = \frac{d\sigma}{dt}^{\text{Diff}}(\omega A) + \frac{d\sigma}{dt}^{\text{OPE}} = \frac{1}{\eta(A)} \cdot \frac{d\sigma}{dt}(\rho A) + \frac{d\sigma}{dt}^{\text{OPE}} \tag{40}$$

where the OPE cross section is taken from equ. (39). $\left(\frac{d\sigma}{dt}\right)_{\rho A}$ is the ρ^0 photo production cross section as measured by the same group (76) and $\eta(A)$ is a fitting parameter which gives the ratio between diffractive ρ^0 and ω photoproduction cross sections. The diffractive coherent cross section obtained from the fits according to equ. (40) are analyzed in terms of equ. (27) and (28) with ρ^0 replaced by ω. Adopting the same nuclear density distribution as in the case of the ρ^0 [76] and $\beta_\omega = \beta_\rho = -0.2$ the results obtained are given in table 7.

In the Bonn — Pisa experiment (92) the ω was observed via its $\pi^0\gamma$ decay, detecting the direct photon and the forward emitted photon of the π^0 disintegration in an arrangement of 8 total absorbing Cerenkov counters. The branching ratio for the $\omega \to \pi^0 + \gamma$ decay $\frac{\Gamma(\omega \to \pi^0 + \gamma)}{\Gamma(\omega \to \text{all})} = 9.4\%$ was taken from ref. [88]. The experiment was performed at a mean photon energy of 5.7 *GeV* on C, Al, Zn, Ag, Ta, and Pb targets. The resulting angular distributions are shown in fig. 29. The diffraction type forward peak and the incoherent background is clearly seen.

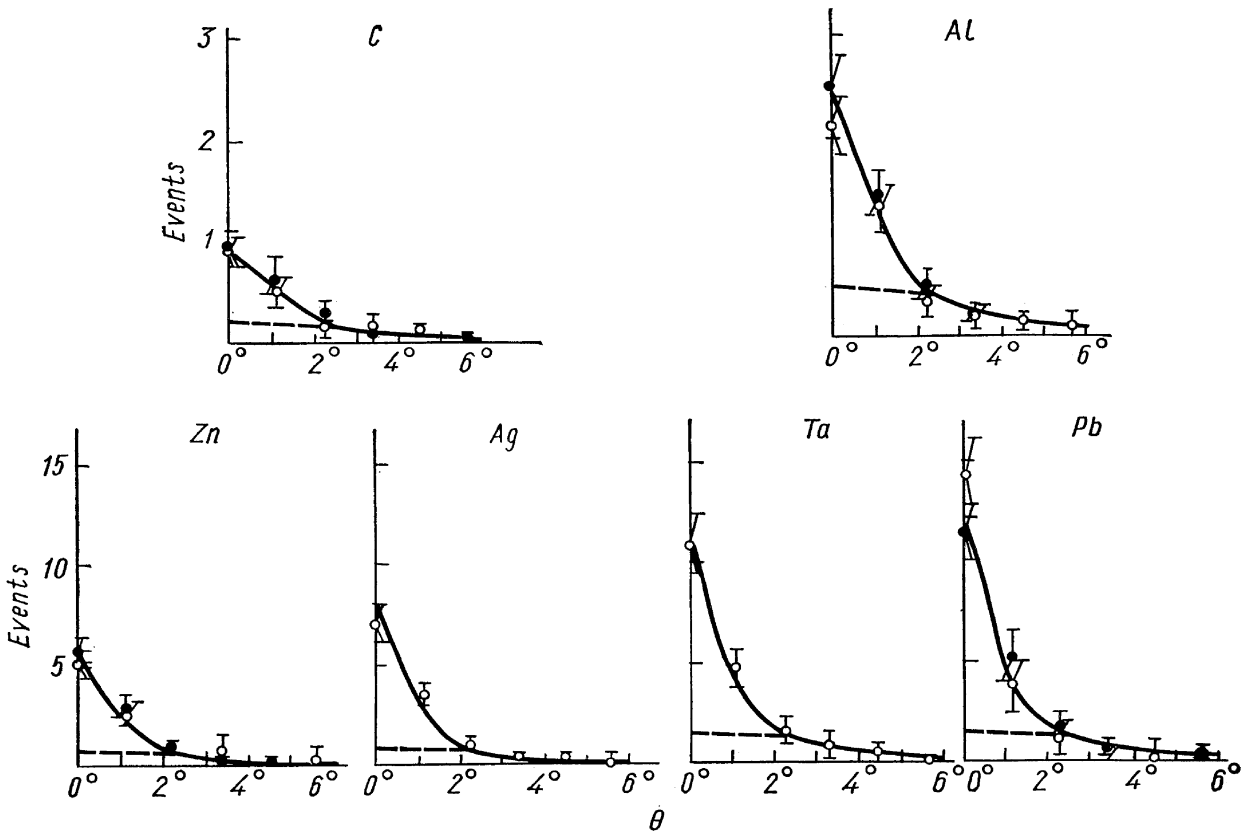

Fig. 29. The full lines are the best fit curves calculated according to model 4. The incoherent production at small angles is also shown as dotted lines.

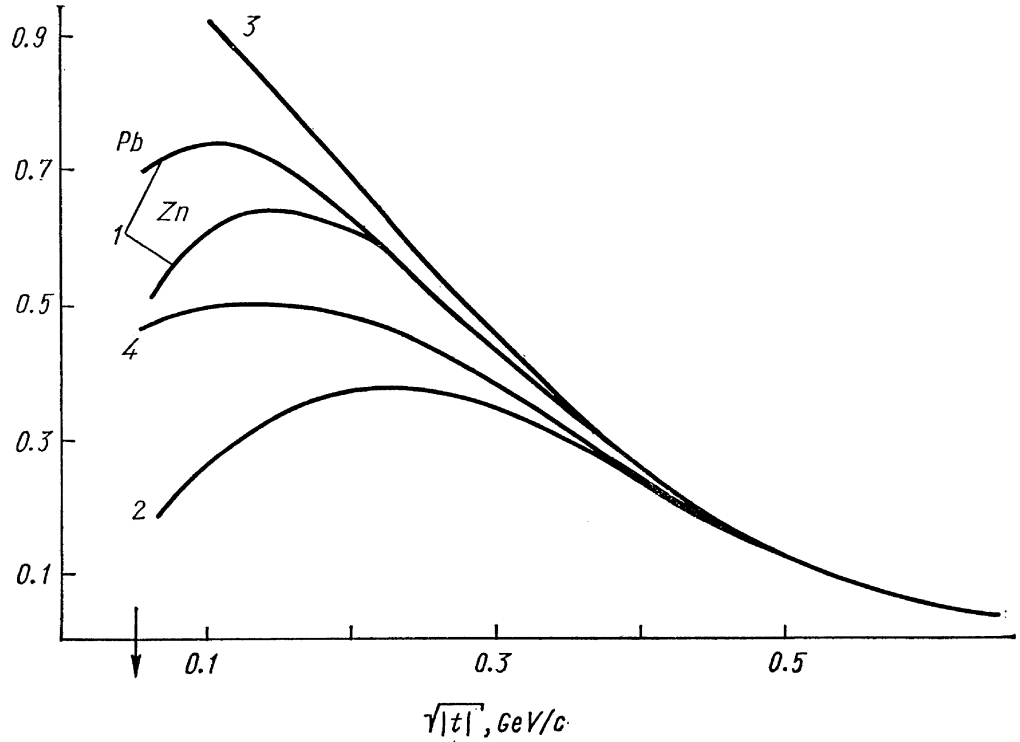

Fig. 30. *1* — «CLOSUR» (J. S. Trefil), ref. [78]; *2* — $[1 - G(t)]e^{8t}$, ref. [96]; *3* — $e^{8t}(\gamma N \to \omega N^*$; no suppression); *4* — $Z_{\text{eff}}(\pi^{\pm})e^{8t}$, ref. [94].

We analyzed our data similar to equ. (40), assuming in addition to the diffractive contribution an incoherent contribution of the form

$$\frac{d\sigma}{dt}^{\text{inc}} = N_{\text{inc}}(A, t, \sigma_\omega)\frac{d\sigma}{dt}(\omega N). \tag{41}$$

This incoherent contribution is measured at large angles, but unfortunately one cannot rely on an unambigous theory of its t-dependence under the coherent peak. We therefore tried four models for this background, which are summarized in fig. 30. Model 2 and 3 give the extreme possibilities. The normalization of the incoherent cross section $d\sigma/dt$ (ωN) has been determined by fitting the large angle data of each angular distribution separately. After the subtraction of the incoherent con-

Table 7

Ref.	Energy [GeV]	$\sigma_{\omega N}$ [mb]	$\gamma_\omega^2/4\pi$	$\lvert f_0\rvert^2 \left[\frac{\mu b}{GeV^2}\right]$	Remarks
Rochester [91]	6.8	33.5 ± 5.5	9.5 ± 2.1	11.4 ± 1.9	$\beta_\omega = -0.2$
Bonn — Pisa [92]	5.7	$30.0\pm^{7.0}_{6.0}$	5.8 ± 1.3	15.1 ± 3.1	$\beta_\omega = -0.2$ (no $\rho^0 \to \pi^0\gamma$)
SLAC [82]	4.7	—	4.6 ± 1.4	15.2 ± 3.8 (A_+ from table 6)	$\sigma_{\omega N} = 27$ mb
Orsay [81]			3.7 ± 0.7		

tribution according to the four models, an overall fit to the corrresponding sets of the coherent data has been applied in terms of equs. (27) and (28) to determine $\sigma_{\omega N}$ and $\gamma_\omega^2/4\pi$. For the nuclear density distributions the Wood — Saxon form has been adopted with a radius as determined by the DESY—MIT group [75]. The ratio β^ω of the real to the imaginary part of the forward $\omega - N$ scattering cross section was fixed at values $\beta_\omega = 0$, -0.1, -0.2, -0.3, -0.4 and -0.5. Within the errors all four models gave consistent results. As an illustration in fig. 31 the results of $\sigma_{\omega N}$ and $\gamma_\omega^2/4\pi$ are plotted as function of β_ω, using model 4 for the subtraction of the incoherent background. The plot shows the strong dependence of both quantities on β_ω. For a value $\beta_\omega = -0.2$ (which is suggested by the quark model

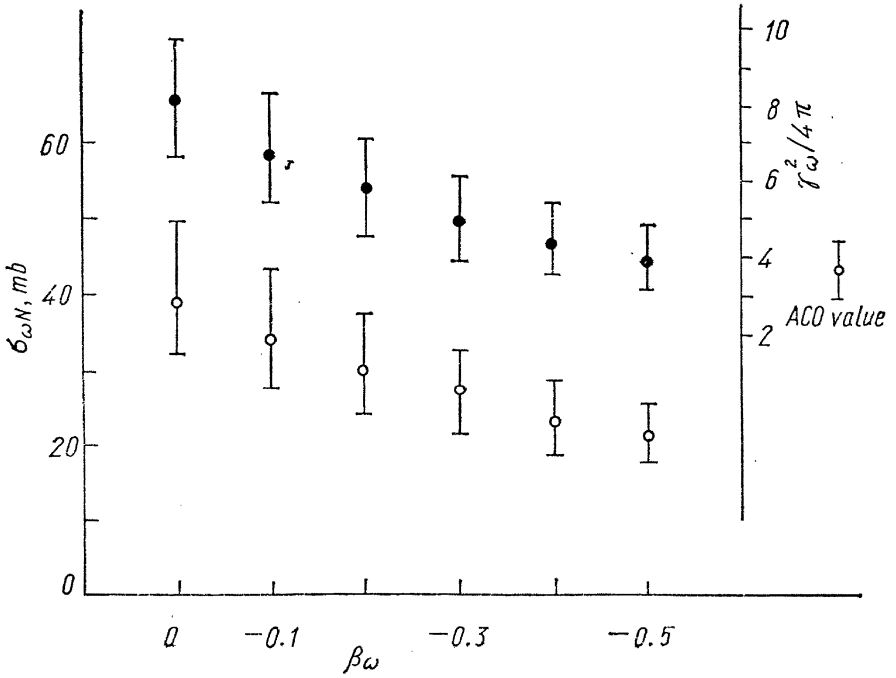

Fig. 31.

prediction $\beta_\rho = \beta_\omega$) the results are summarized in table 7. Also included are the SLAC [82] hydrogen data and the Orsay storage ring value on $\gamma_\omega^2/4\pi$ [81]. The data on $\sigma_{\omega N}$ are not very precise, however within the errors they are consistent with $\sigma_{\rho N}$ from table 5 in agreement with the quark model prediction [60]. The situation with respect to $\gamma_\omega^2/4\pi$ is even worse. The value of the Rochester group is quite high. The results of our group (an additional error of $\pm 13\%$ introduced by the branching ratio [88] is not included in the error quoted in table 7) and the SLAC group are higher than the storage ring value bat statistically not inconsistent. This seems to indicate the same fact as in the case of the ρ meson, where $\gamma_\rho^2/4\pi$ as obtained from photoproduction experiments is higher than the storage ring result. The ratio $\gamma_\rho^2/\gamma_\omega^2$ as obtained from the photoproduction experiments (table 5 and 7) is consistent with the *SU* (3) prediction $\gamma_\rho^2/\gamma_\omega^2 = 1/9$. The Bonn — Pisa value of $|f_0|^2$, which is the diffractive part of the forward ω photoproduction cross section on single nucleons agrees nicely with the natural parity contribution of the ω cross section as measured by the SLAC group. This is consistent with a vanishing A_2 t-channel exchange contribution [89]. In view of the more difficult experimental situation compared to ρ^0 photoproduction on complex nuclei no too strong conclusions should be drawn from these first results on ω photoproduction on complex nuclei. Clearly further experiments are required with better statistics and resolution so that one can begin to study systematic effects in detail.

2.5. Φ MESON PHOTOPRODUCTION

Preliminary results on Φ meson photoproduction from hydrogen and carbon using a polarized photon beam have been contributed by a Cornell group [97]. The asymmetry Σ (see equ. 24) has been measured at an average photon energy of $k = 5.4$ *GeV*. The production from carbon is mainly diffractive resulting in $\Sigma_C = 1.02 \pm 0.05$. The hydrogen asymmetry is $\Sigma_{H_2} = 0.60 \pm 0.2$, indicating an appreciable nondiffractive contribution. These values have to be regarded as rather preliminary, since theoretical shapes tor the coherent photon spectra have been used in the analysis. For a summary of previous Φ photoproduction experiments using unpolarized photons see refs. [53] and [139].

2.6. INTERFERENCE EFFECTS IN ρ^0 AND ω MESON PHOTOPRODUCTION PROCESSES

2.6.1. DETERMINATION OF THE PHOTOPRODUCTION PHASE OF ρ^0 MESONS

The analysis of the recent experiments on photoproduction of ρ^0 mesons from complex nuclei (see section 2.3) shows that in order for the vector dominance model to hold the ρ^0 nucleon amplitude in the *GeV* region must not be purely diffractive but should contain a substantial real part. Independently the quark models of several authors [60] predict the equality of the ρ^0 nucleon amplitude and the π nucleon scattering amplitude. For the ratio β of the real to the imaginary parts of these amplitudes this leads to

$$\beta_p = \beta_{\pi^0 N} \tag{42}$$

where the amplitude for π^0 nucleon scattering is related to the $\pi^\pm$ nucleon scattering amplitudes by isospin invariance:

$$T(\pi^0 N) = \frac{1}{2}(T(\pi^+ N) + T(\pi^- N)). \tag{43}$$

For energies around 5 *GeV* this leads to $\beta_\rho \sim -0.2$ [98].

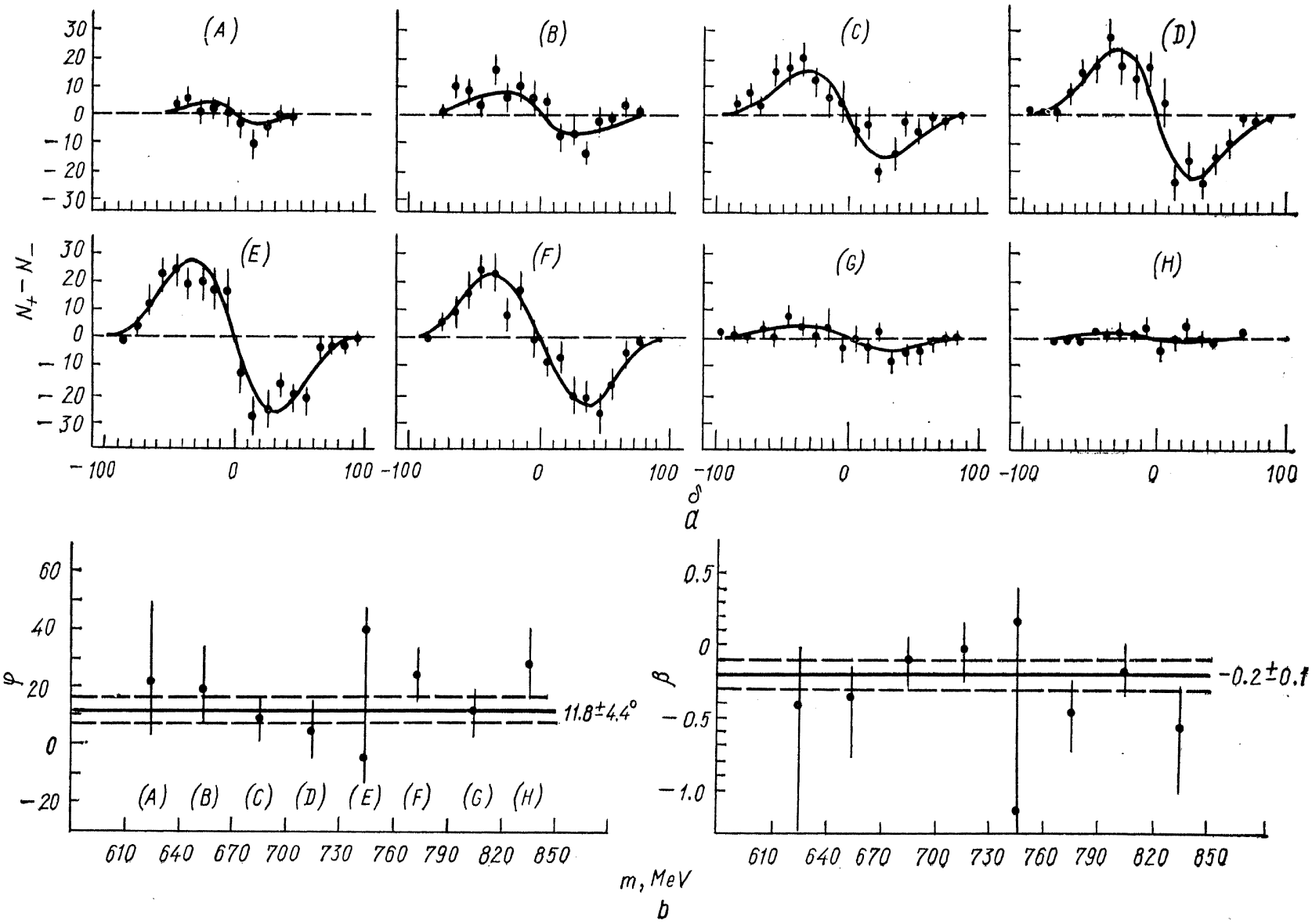

Fig. 32. The curves are fits with $\Phi_\rho^{Be} = 11.8^0$.

The results of three experiments have been contributed to this conference in which the quantity β_ρ is directly measured. The DESY — MIT group [99] and a group [100] at Nina have studied electron-positron pair production in the invariant mass region around the ρ^0 mass on beryllium for photon energies between 4.1 and 6.1 *GeV* [99] and on carbon at a mean energy of 3.5 *GeV* [100], respectively. The main contributions to this channel come from wide angle electron pair production (Bethe — Heitler) and from diffractive ρ^0 photoproduction followed by the $\rho^0 \to e^+e^-$ decay (Compton). The interference between these two terms depends on the phase of the ρ^0 photoproduction amplitude since the Bethe — Heitler amplitude is real. This interference term σ_i is antisymmetric with respect to

Table 8

ρ^0 Meson Photoproduction Phase

Ref.		k [*GeV*]	Target (A)	Φ_ρ^A	β_ρ
DESY — MIT [99]	Photoproduct. (e^+e^-),	4.1—6.1	Be	$11.8° \pm 4.4°$	-0.2 ± 0.1
Nina [100]	Photoproduct. (e^+e^-)	3.5	C	$19° \pm {}^{8.5°}_{7.5°}$	—
CEA [101]	Electroproduct. $(\mu^+\mu^-)$	5	C	$16° \pm 22°$	—

the exchange of the electron and positron four-momenta p_- and p_+. Thus the effect of the interference term is to produce an asymmetric distribution of experimental events as a function of variables antisymmetric in p_+ and p_- as for instance the transverse momentum of the pair $\delta = p_R\theta_R - p_L\theta_L$, where R (L) refers to the right (left) arm of the spectrometer. Denoting by the subscripts «+» and «—» the sign of the charge of the lepton passing through the right arm of the spectrometer the quantities $N_+(\delta, m)$ and $N_-(\delta, m)$ represent then the number of events with mass m and pair transverse momentum δ.

The results of the DESY — MIT experiment [99] on the difference $N_+(\delta, m) - N_-(\delta, m)$, which is proportional to σ_i, is shown in fig. 32*a* as a function of δ for different mass bins. The asymmetric structure of the interference term is nicely seen.

The direct comparison of the asymmetric data with σ_i to extract the phase is complicated because of the difficulties inherent in the analysis of ρ^0 photoproduction data (i. e. ρ^0 line shape, m_ρ, Γ_ρ, forward differential cross section, slope, coupling constant $\gamma_\rho^2/4\pi$). To reduce the dependence on these parameters the two quantities

$$\frac{\sigma_i(\delta, m)}{\sqrt{\sigma_{BH}(m)\,\sigma_C(m)}}$$

and

$$\frac{N_+(\delta, m) - N_-(\delta, m)}{\sqrt{N_{BH}(m) \cdot N_C(m)}} \tag{44}$$

have been compared in the DESY — MIT experiment. $N_{BH}(m)$ is the calculated BH mass spectrum corresponding to σ_{BH}, and $N_C(m)$ is the number of experimental events attributed to the diffraction Compton process. The resulting phase (fig. 32*b*) for ρ^0 photoproduction on beryllium is $\Phi_\rho^{Be} = 11.8° \pm 4.4°$. Using the Margolis scattering theory [71] this phase angle Φ_ρ^{Be} can be related to the phase for ρ^0 nucleon scattering or to the ratio β_ρ of the real to the imaginary part of the

ρ^0 nucleon scattering amplitude. From the value of Φ_ρ^{Be} one obtains $\beta_\rho = -0.2 \pm \pm 0.1$ (fig. 32*b*).

The result of the Nina experiment for the ρ^0 photoproduction phase on carbon at 3.5 *GeV* is $\Phi_\rho^C = 19° \pm {}^{8.5°}_{7.5°}$. At CEA an experiment on electroproduction of μ-pairs on carbon using the 5 *GeV* external electron beam has been performed [101]. The result on the ρ^0 phase is $16° \pm 22°$. The results of the three experiments are summarized in table 8. The values of the phase Φ are quite similar; however they cannot directly compared with each other because of different experimental conditions. Only the DESY — MIT group gave a value for β_ρ in good agreement with the quark model prediction, showing that the real part of the ρ^0 nucleon scattering amplitude is quite small in accordance with a dominant diffraction-type mechanism.

2.6.2. DETERMINATION OF THE PHOTOPRODUCTION PHASE OF THE ω MESON

In a similar experiment the Nina group [100] also obtained a value for the ω meson photoproduction phase on carbon at 3.5 *GeV*. They obtained $\Phi_\omega^C = 128° \pm 30°$, which is roughly 90° larger than the corresponding result for ρ^0 photoproduction (table 8). However, because of the different production mechanisms involved in ω and ρ^0 photoproduction especially from light nuclei, it is hard to draw a direct conclusion for β_ω from the comparison of Φ_ω^C and Φ_ρ^C.

2.6.3. ρ-ω INTERFERENCE EFFECTS

The Orsay storage ring group [102] have presented evidence that the excitation curve for the $\pi^+\pi^-$ final state shows some structure, which can be understood as an interference of the amplitudes connected with the graphs shown in fig. 33*a*. The right graph contains the *G*-parity violating decay $\omega \to \to \pi^+\pi^-$. This decay is possible assuming that the physical particles ω and ρ are both superpositions of pure isospin $I = 0$ and $I = 1$ states. There is also evidence for ρ — ω interference in strong interactions. These results have been recently summarized by Coyne [103]. The photoproduction of ρ^0 and ω mesons and the subsequent decay of both vector mesons into either e^+e^--pairs or $\pi^+\pi^-$-pairs should show up similar interference effects and provide a useful tool to measure the relative phase of the ρ^0 and ω meson production amplitudes.

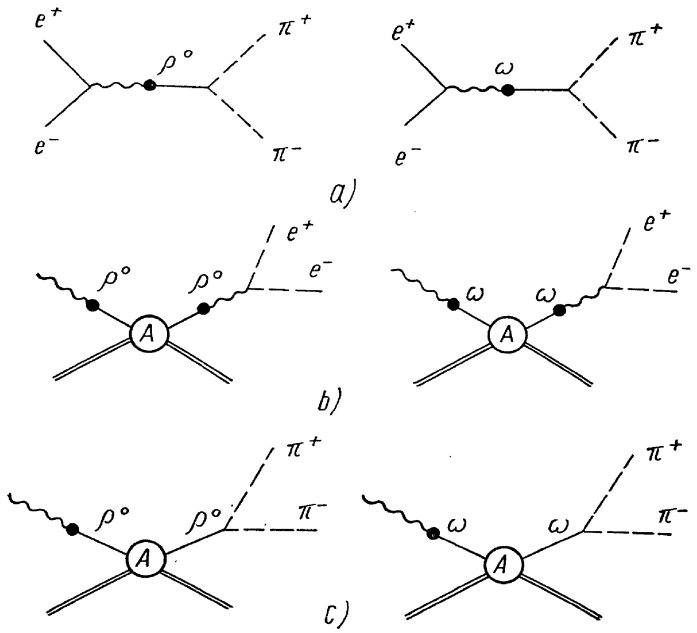

Fig. 33.

Let me first describe the experiments detecting the e^+e^- final state. The DESY — MIT group [104] has measured (ρ, ω) photoproduction on beryllium at 5.1 *GeV* and the Nina group [105] on carbon at 3.5 *GeV*, using two arm spectrometers in both experiments.

To the observed reaction

$$\gamma + A \to A + (\rho^0, \omega) \qquad (45)$$
$$\qquad\qquad\quad \downarrow \to e^+e^-$$

five diagrams contribute near the mass region $m_{ee} \sim m_\rho \sim m_\omega$: the two Bethe—Heitler diagrams, the two Compton diagrams shown in fig. 33*b* and a fifth diagram, which represents the e^+e^--contribution from vector mesons produced via OPE or incoherent production [90, 76, 78]. The contribution to the e^+e^- yield from coherent ρ^0 and ω production is given by the amplitude [106]

$$T_v = \frac{em_v^2}{2\gamma_v} \times$$

$$\times \frac{1}{m_v^2} T_{vA \to vA} \frac{1}{m_v^2 - m^2 - im_v\Gamma_v} \times$$

$$\times \frac{em_v^2}{2\gamma_v} \cdot \frac{1}{-m^2} T_{\gamma \to e^+e^-} \qquad (46)$$

leading to

$$|T|^2 = |T_\rho + T_\omega|^2 =$$

$$= \frac{\alpha^2\pi^2}{\gamma_\rho^4} |T_{\rho A \to \rho A}|^2 \frac{m_\rho^4}{m^4} \times$$

$$\times \left| \frac{1}{m_\rho^2 - m^2 - im_\rho\Gamma_\rho} + \right.$$

$$\left. + \frac{\gamma_\rho^2 m_\omega^2}{\gamma_\omega^2 m_\rho^2} \cdot \frac{|R| e^{i\Phi_{ee}}}{m_\omega^2 - m^2 - im_\omega\Gamma_\omega} \right|. \qquad (47)$$

The Nina group did not include the propagator for the vector meson when coupled to real photons leading to a factor m_ω^4/m_ρ^4 in front of $|R|$ and an overall factor m_ρ^8/m^4 in equ. (47) instead of m_ω^2/m_ρ^2 and m_ρ^4/m^4, respectively. In equ. (47) we have set for the coherent (diffractive) ρ and ω scattering amplitudes on nuclei

$$\frac{T(\omega A \to \omega A)}{T(\rho A \to \rho A)} = |R| e^{i\Phi_A} \qquad (48)$$

where Φ_A is the relative $\rho - \omega$ scattering phase on nuclei. The overall phase Φ_{ee} can be written as [107]

$$\Phi_{ee} = \Phi_A + 2(\alpha_\omega - \alpha_\rho) \qquad (49)$$

where α_ω and α_ρ are additional phases to take account of the induced $\rho - \omega$ mixing at each photon vertex.

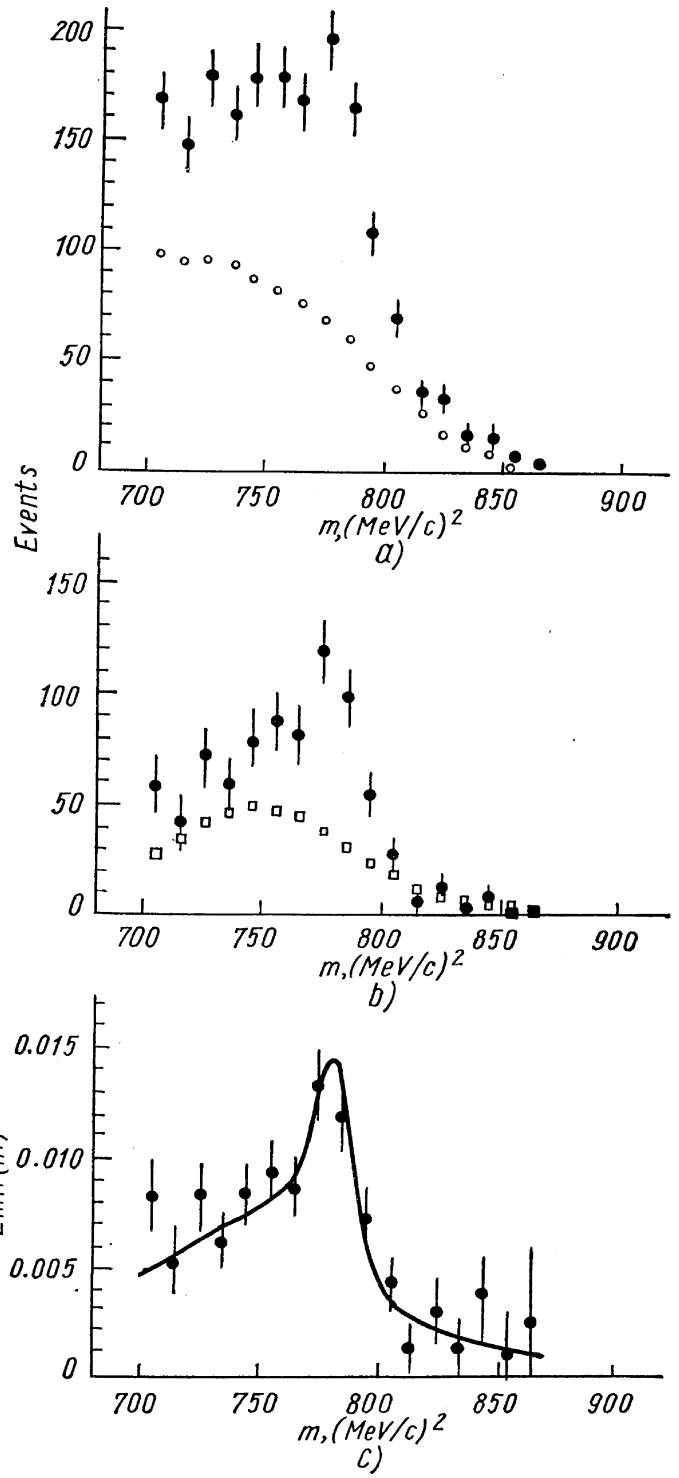

Fig. 34. e^+e^- yields from (ρ, ω) photoproduction on beryllium from ref. [104]. *a*) The open circles are the calculated *BN* contribution; *b*) The black dots are the event distribution attributed to the Compton terms. The squares are the contributions from $\rho \to e^+e^-$ alone.

In the analysis the calculated Bethe—Heitler contributions have been subtracted from the measured yields (fig. 34*a*, *b*). Fig. 34*c* shows the DESY — MIT results and fig. 35 those from Nina [105]. Both mass distributions exhibit a clear

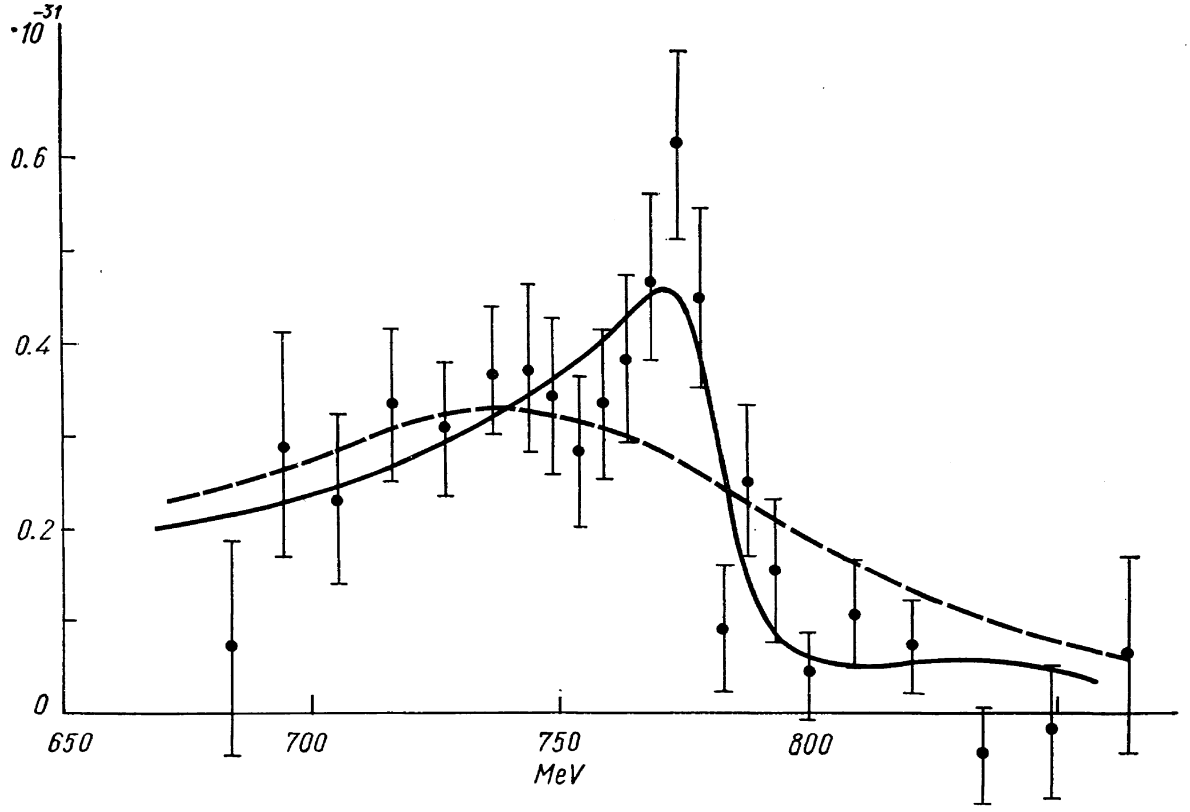

Fig. 35. $\frac{d^6\sigma}{dp_+ dp_- d\Omega_+ d\Omega_-}$ [$cm^2/(GeV/c)^2 sr^2$ · nucleon · EQ] versus $m_{e^+e^-}$. The solid line is the best fit assuming (ρ — ω) interference according to equ. (47). The dashed line gives the $\rho \to e^+e^-$ contribution alone.

interference effect showing up in an enhancement at the ω mass and follow the general features expected from equ. (47) (solid curves in fig. 34*c* and 35). After subtraction of the contribution due to incoherent ω production in the DESY — MIT experiment, the yields have been fitted to equ. 47 with the free parameters $\varepsilon = \frac{\gamma_\omega^2}{|R|\gamma_\rho^2}$ and Φ_{ee}. (For a more detailed comparison of both analyses see E. Gabathuler

Table 9

ρ — ω Interference (e^+e^- Final State)

Ref.	k [GeV]	Target (A)	Φ_{ee}	ε	$\gamma_\omega^2/\gamma_\rho^2$
DESY — MIT [104]	5.1	Be	$41° \pm 20$	$9.4 \pm \frac{2.6}{1.6}$	$9.4 \pm \frac{2.6}{1.6}$
Nina [105]	3.5	C	$100° \pm \frac{38°}{30°}$	$7.0 \pm \frac{2.1}{1.5}$	$7.0 \pm \frac{2.1}{1.5}$

[108]). The results are summarized in table 9. The errors quoted come mainly from uncertainties due to the ρ-line shape, absolute normalization and uncertainties in the parameters Γ_ω, Γ_ρ, m_ω etc. The sensitivity of the fit parameters to the values of the different input parameters have been checked, leading for instance to a change of $\Delta\Phi_{ee} = 7°$ for an 1 *MeV* change of m_ω in the DESY experiment. The difference in the phases Φ_{ee} of the two experiment is most likely due to statistics or differences in energy, target and the input parameters (for instance m_ω). Assuming $|R| = 1$ as predicted by the quark model [60] and the Margolis scattering (71) theory the results on ε lead to values of $\gamma_\omega^2/\gamma_\rho^2$ which are consistent with the *SU* (3) prediction giving 9 for this ratio.

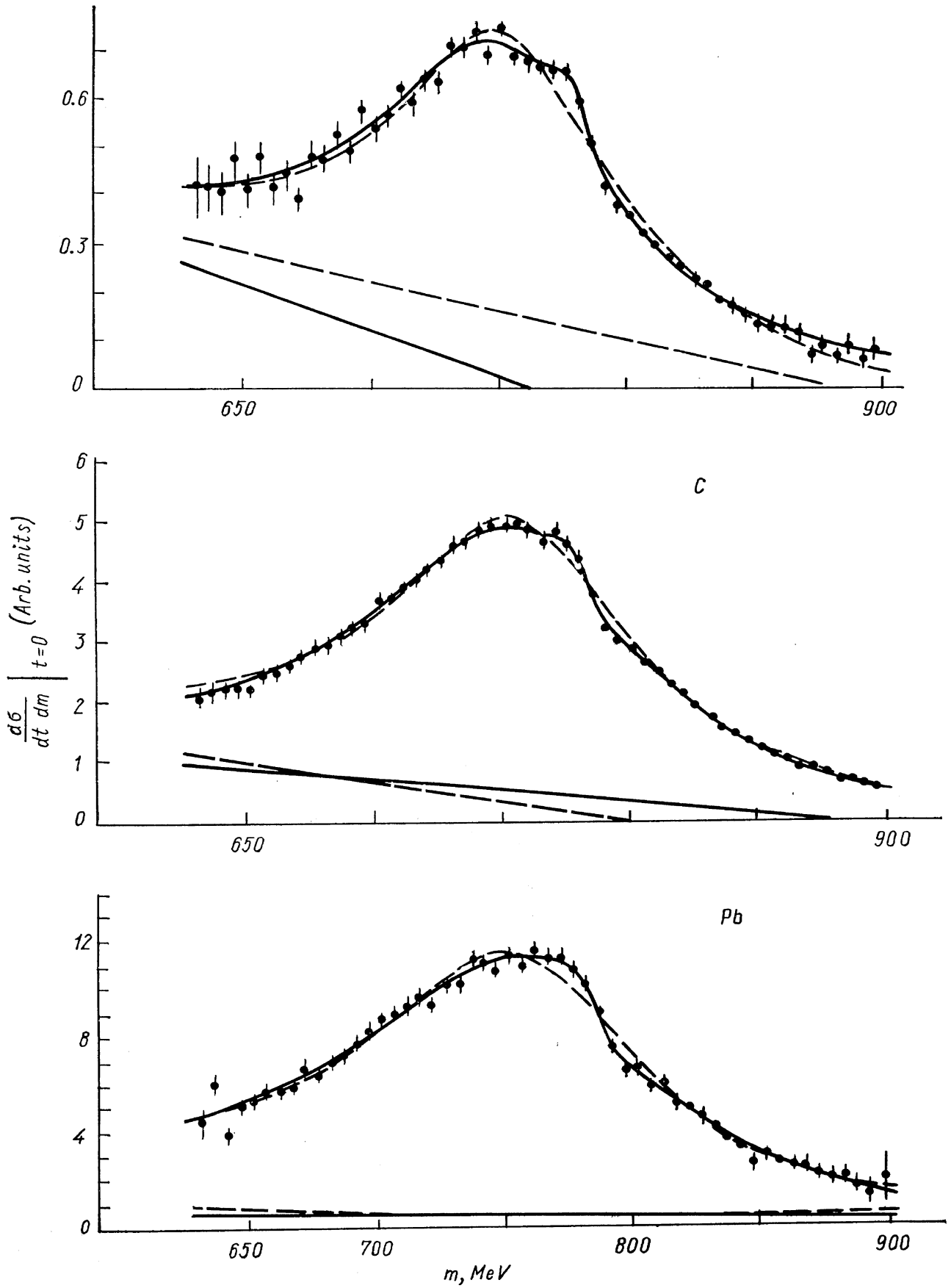

Fig. 36. The solid lines are the best fits according to equ. (52). The dashed lines show the contribution from $\rho \to \pi^+\pi^-$ alone. The background is also indicated.

Furthermore the quark model together with the Margolis theory predicts the relative ρ — ω nuclei scattering phase Φ_A to be zero. Under this assumption the prediction of ref. [107] for α_ρ and α_ω gives from equ. (49)

$$\Phi_{ee} = 2 \cdot (\alpha_\omega - \alpha_\rho) = 22^\circ \pm 8^\circ \tag{50}$$

not in contradiction with the DESY — MIT result. With the same experimental set up the DESY — MIT group [109] has investigated the reaction

$$\gamma + A \to \pi^+ + \pi^- + A \tag{51}$$

for a maximum bremsstrahlung energy of 7.4 *GeV* on H_2, carbon and lead. The invariant masses of the pion pairs covered the region of the ρ^0, ω and Φ mesons. Preliminary results have been contributed for measurements on carbon in the $\rho-\omega$ mass region. The Nina group [105] measured reaction (51) in the ρ — ω mass region using a photon beam of a maximum energy of 4.6 *GeV* and a carbon target. An interference between the ρ^0 and ω meson production amplitudes in the $\pi^+\pi^-$ final state in reaction (51) is possible due to the *G* parity violating decay mode $\omega \to \pi^+\pi^-$. Because this decay is a second order process the effect is expected to be small and difficult to observe. Figs. 36 and 37 show the DESY — MIT [109] and Nina [105] pion pair mass spectra $\left.\frac{d\sigma}{dtdm}\right|_{t=0}$. The effect of a ρ — ω interference in the $\pi^+\pi^-$ mode is clearly evident in all four graphs. These spectra have been fit with the following phenomenological formula

$$\left.\frac{d\sigma}{dtdm}\right|_{t=0} = \left.\frac{d\sigma}{dt}\right|_{t=0} \frac{2m}{\pi} m_\rho \Gamma_\rho \left(\frac{m_\rho}{m}\right)^n \left| D_\rho + \xi e^{i\Phi_{\pi\pi}} D_\omega + N \right|^2 + BG \tag{52}$$

which is a relativistic *P*-wave Breit — Wigner [57] with mass dependent widths and

$$D_{\rho,\omega} = (m^2_{\rho,\omega} - m^2 - i m_{\rho,\omega}\Gamma_{\rho,\omega})^{-1}. \tag{53}$$

The BW mass distribution is modified to fit the ρ line shape in the following way:

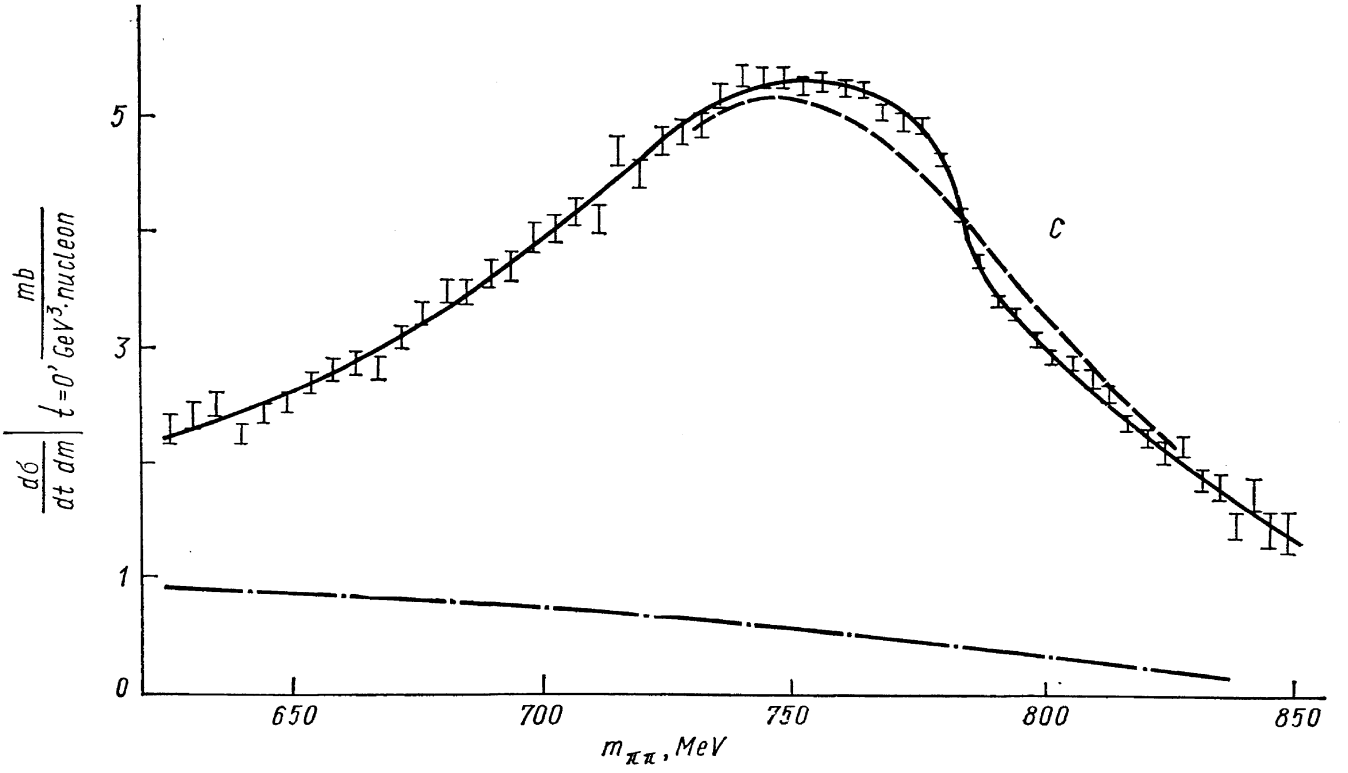

Fig. 37. The solid line is the best fit according to equ. (52). The dashed line shows the same fit with no ω contribution. The chain line shows the incoherent background.

DESY — MIT:

1a) Ross — Stodosky factor [58]

$$n = 4 \text{ and } N = 0$$

1b) Drell — Söding interference [59] $n = 0$ and $N = 1 = c \cdot (m_\rho^2 - m^2) / / (m_\rho^2 - m^2 - i m_\rho \Gamma_\rho)$.

This mechanism assumes an interference between coherently produced non resonant pion pairs (Drell-term) and pions from $(\rho, \omega) \to 2\pi$.

Nina:

2) $n = 4$, $N =$ Drell — Söding type coherent background.

BG is a polynomial background function in m. The quantity ξ is given by

$$\xi = \left(\frac{m_\omega}{m_\rho}\right)^{n/2} \cdot \frac{\gamma_\rho}{\gamma_\omega} \left| \frac{T_{\omega A \to \omega A}}{T_{\rho A \to \rho A}} \right| \left[\frac{\Gamma_{\omega \to 2\pi}}{\Gamma_{\rho \to 2\pi}} \cdot \frac{m_\omega}{m_\rho} \right]^{1/2} \tag{54}$$

where $\Gamma_{\omega \to 2\pi}$ is the width of the $\omega \to 2\pi$ decay. The relative phase $\Phi_{\pi\pi}$ of the ρ and ω two pion final state can be expressed as [107]

$$\Phi_{\pi\pi} = \Phi_A + \alpha + (\alpha_\omega - \alpha_\rho) \tag{55}$$

where Φ_A again is the relative phase of the hadronic amplitudes. α is the relative phase of the 2π decay amplitudes and α_ω and α_ρ are again corrections due to ρ — ω mixing as in equ. (49).

The preliminary results of the DESY — MIT experiment on carbon and the Nina results obtained by fitting the experimental data with equ. (52) are given in table 10. The solid lines in fig. 36 and 37 show the fits in good agreement with

Table 10

ρ — ω Interference ($\pi^+\pi^-$ Final State)

	DESY — MIT [109] (1a)	DESY — MIT [109] (1b)	Nina [105] (2)
$\left(\frac{d\sigma}{dt}\right)^{A=1}_{t=0}$	108 ± 1.0 $\mu b/GeV^2$	116.0 ± 1.0 $\mu b/GeV^2$	good agreement
m_ρ	768.4 ± 0.8 *MeV*	769.9 ± 0.9 *MeV*	767 ± 1.9 *MeV*
Γ_ρ	142.7 ± 2.0 *MeV*	152.6 ± 1.9 *MeV*	146.1 ± 2.9 *MeV*
m_ω	784.6 ± 1.0 *MeV*	786.3 ± 0.9 *MeV*	783 ± 1.6 *MeV*
ξ	$(1.08 \pm 0.07) \cdot 10^{-2}$	$(1.01 \pm 0.06) \cdot 10^{-2}$	$(0.97 \pm 0.08) \cdot 10^{-2}$
$\Phi_{\pi\pi}$	$80.8° \pm 9.0°$	$98.5° \pm 6°$	$104° \pm 5.1°$
$\Gamma_{\omega \to 2\pi}$	—	—	$0.091 \pm^{0.031}_{0.025}$
B			$0.80\% \pm^{0.28\%}_{0.22\%}$

the data. It was not possible to get reasonable fits without including ρ — ω interference terms. The fit results of both experiments in table 10 agree remarkably well within the errors.

The phase $\Phi_{\pi\pi}$ can be compared with theoretical predictions. Assuming again according to the quark model that the hadronic phase Φ_A is zero, equ. (55) leads to

$$\Phi_{\pi\pi} = \alpha + (\alpha_\omega - \alpha_\rho) \sim 112° \pm 10° \tag{56}$$

with the numerical prediction of ref. (107). This number is in excellent agreement with both the DESY—MIT and Nina result. In storage rings the same quantity

$$\Phi_{\pi\pi}^{ST} = \alpha + (\alpha_\omega - \alpha_\rho) \tag{57}$$

independent of the hadronic phase is measured. The Orsay result [110] $\Phi_{\pi\pi}^{SI} = 164° \pm 28°$ does not agree very good with the prediction of equ. (56). From this

however a definite conclusion should not be drawn at the moment; clearly more accurate storage ring experiments are needed. Assuming again the quark model prediction $T_{\omega A\to\omega A} = T_{\rho A\to\rho A}$ equ. (54) allows to determine $\Gamma_{\omega\to 2\pi}$ from the fit results given in table 10. Only the Nina group give a numerical value for $\Gamma_{\omega\to 2\pi}$ and the branching ratio $B = \Gamma_{\omega\to 2\pi}/\Gamma_{\omega\to 3\pi}$. However since all parameters entering equ. (54) agree nicely, the DESY—MIT group would come to similar results. The value of B is in agreement with a theoretical prediction $B = 1.5\%$.

In conclusion I like to say that the results of the experiments on the ρ phase (table 8), the DESY—MIT result on $\rho - \omega$ interference in the e^+e^- final state (table 9) and the results on $\rho - \omega$ interference in the $\pi^+\pi^-$ final state (table 10) are consistent with the quark model prediction $T(\rho N) = T(\omega N) = I(\pi^0 n)$, which leads to $\beta_\rho = \beta_\omega \sim -0.2$ around 6 *GeV*. The phases measured are in agreement with results from $\rho - \omega$ mixing theories [107]. The Nina result on the $\omega - BH$ phase, discussed in section 2.6.2, together with the value for the phase Φ_{ee} from Nina (table 9) may indicate however that things might be more complicated; to study this in more detail better experiments on electron positron pair photoproduction are required.

2.7. TOTAL PHOTOPRODUCTION CROSS SECTIONS

2.7.1. TOTAL PHOTOPRODUCTION CROSS SECTION ON HYDROGEN AND DEUTERIUM

Several recent experiments using bubble chambers [111—113] inelastic electron [114] and muon [115] scattering techniques gave for the first time results on the total photoproduction cross section on protons $\sigma_{\gamma p}$ from threshold up to 18 *GeV*. This quantity is of considerable fundamental interest. Via the optical theorem it is connected with the spin independent forward Compton scattering amplitude $f_1(k)$ by [120]

$$\mathrm{Im}\, f_{1(\gamma\gamma)}(0^\circ) = \frac{k}{4\pi}\,\sigma_{\gamma p} \tag{58}$$

thus allowing a comparison between $\sigma_{\gamma p}$ and the measured differential cross section for high energy Compton scattering from protons (see section 2.8). Furthermore $\sigma_{\gamma p}$ can be compared with several other quite fundamental quantities as the total vector meson nucleon cross sections $\sigma_{\rho N}$, $\sigma_{\omega N}$ and $\sigma_{\Phi N}$ via the vector dominance model (see section 2.9).

The final results of two new experiments using counter techniques and a tagged photon beam have been contributed to this conference. The Santa Barbara group at SLAC [116, 117] ($\Delta k/k$ of tagged beam $\sim \pm 2.5\%$) measured the total photoproduction cross section on hydrogen and deuterium for photon energies between 4 and 17 *GeV* while the DESY group [118] (Δk of tagged beam ± 50 *MeV*) covered the energy range from 1.5 to 6.6 *GeV*. Both groups derived from these data the total cross section $\sigma_{\gamma n}$ on neutrons by

$$\sigma_{\gamma n} = \sigma_{\gamma D} - \sigma_{\gamma p} + GC \tag{59}$$

where GC is the Glauber correction for the shadowing of one nucleon by the other in deuterium [121]. This corrections amounts up to $\sim 5\ \mu b$ at the highest energies measured.

The great problem of these experiments is to avoid counting electron pairs as hadronic final states. A background contribution from electromagnetic processes would result in a different A (mass-number) as well as energy dependence of the cross sections in comparison to those as obtained from pure had-

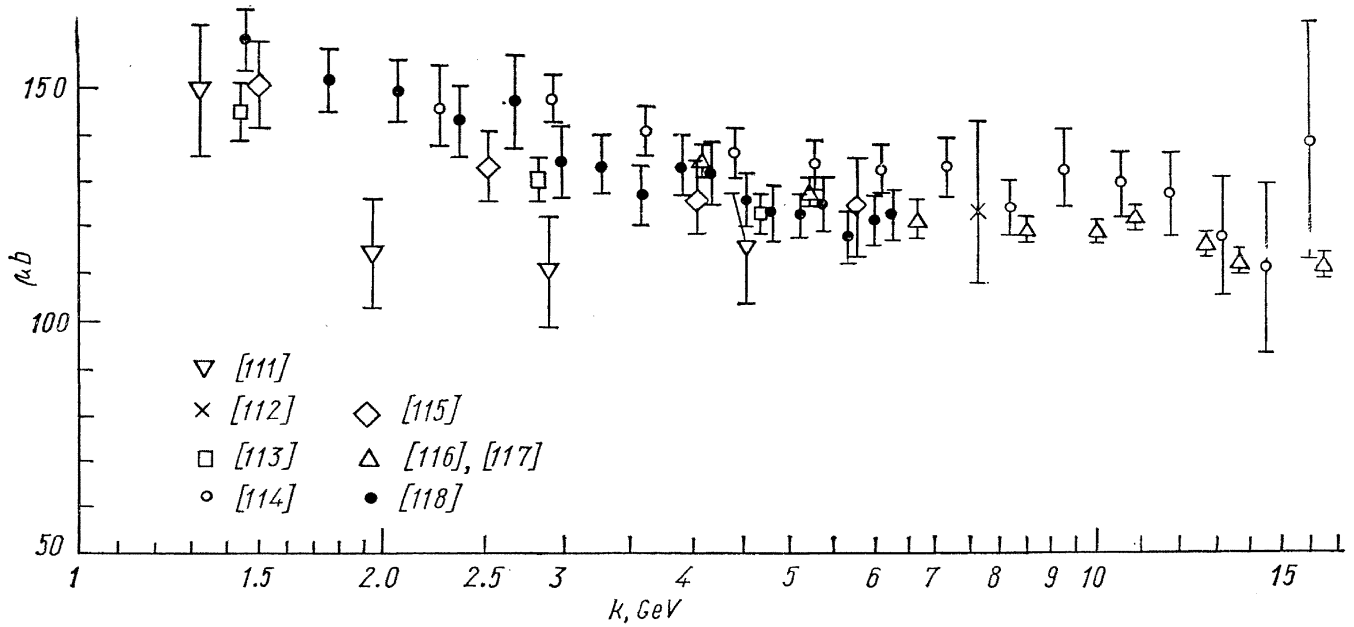

Fig. 38.

ronic final states. To overcome these difficulties both groups took advantage of the small opening angles of high energy pair and Compton scattering events as compared with the larger angles of hadronic events. Fig. 38 shows the results on $\sigma_{\gamma p}$ of all experiments mentioned above. Considering the completely different methods applied the argeement is quite good, although the values from ref. [111] at 2 and 3 *GeV* are rather low and the data from $e - p$ scattering [114] seem to be systematically higher by $\sim 8\%$ than those of other experiments. Since the systematic errors are not shown this is however not unreasonable. Fig. 39 shows the results on $\sigma_{\gamma n}$ obtained according to equ. (59) from the deuterium and hydrogen results of refs. [117] and [118]. The neutron cross sections are systematically lower than the proton data. The differences $\Delta_{pn} = \sigma_{\gamma p} - \sigma_{\gamma n}$ are shown in the lower graph.

The similarity in the shapes of the photoabsorption cross sections and strong interaction total cross sections, such as those from pion nucleon scattering,

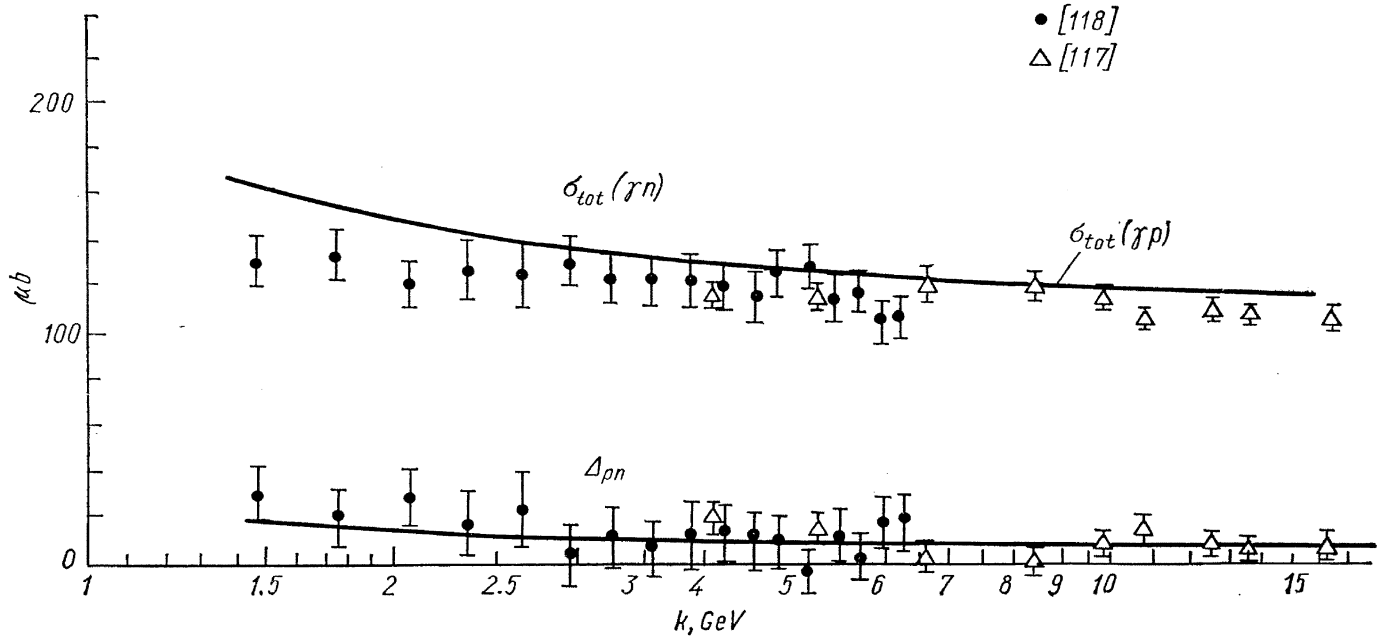

Fig. 39. The solid lines are fits to equ. (61).

suggests a parametrization in terms of a simple Regge pole model

$$\sigma_{\gamma N}(k) = \sum_i c_i k^{\alpha_i(0)-1} \tag{60}$$

where $k = (s - M_N^2)/2M_N$ is the photon laboratory energy and M_N the nucleon mass. α_i (0) is the $t = 0$ intercept of the contributing trajectories. In the high energy limit the leading trajectories with charge conjugation $\eta_c = +1$ and isospin 0 and 1 are the Pomeron P ($\alpha_P(0)$ defined to be unity) and the f ($J^P = 2^+$) and A_2 ($J^P = 2^+$) both of which have $\alpha(0) \sim 0.5$ as observed in high energy hadron-hadron collisions. Thus the data are fit to the simple form

$$\sigma_{\gamma N}(k) = \sigma_{0N} + a_N k^{-1/2} \tag{61}$$

where the Pomeron contributes to σ_{0N} and the f and A_2 trajectories to a_N. N is the proton or neutron. A fit to the data of refs. [112, 113, 117, 118] according to equ. (61) yields [119]

$$\begin{aligned} \sigma_{\gamma p}(k) &= (98.1 \pm 2.6) + (65.2 \pm 6.6)\, k^{-1/2}\ |\mu b|, \\ \sigma_{\gamma n}(k) &= (95.6 \pm 5.7) + (48.3 \pm 15.4)\, k^{-1/2}\ |\mu b|. \end{aligned} \tag{62}$$

The curve according to $\sigma_{\gamma p}$ is shown as solid line in fig. 39. For the difference of the proton and neutron cross sections we obtain from (62)

$$\Delta_{pn}(k) = (2.5 \pm 6.3) + (16.9 \pm 16.8)\, k^{-1/2} \tag{63}$$

which is also shown in fig. 39 describing the data very well. For $k = 6$ *GeV* this gives a difference of Δ_{pn} (6 *GeV*) $= (9.4 \pm 13.2)$ μb. This might indicate a non negligible $I = 1$ exchange contribution (the A_2 meson). However we

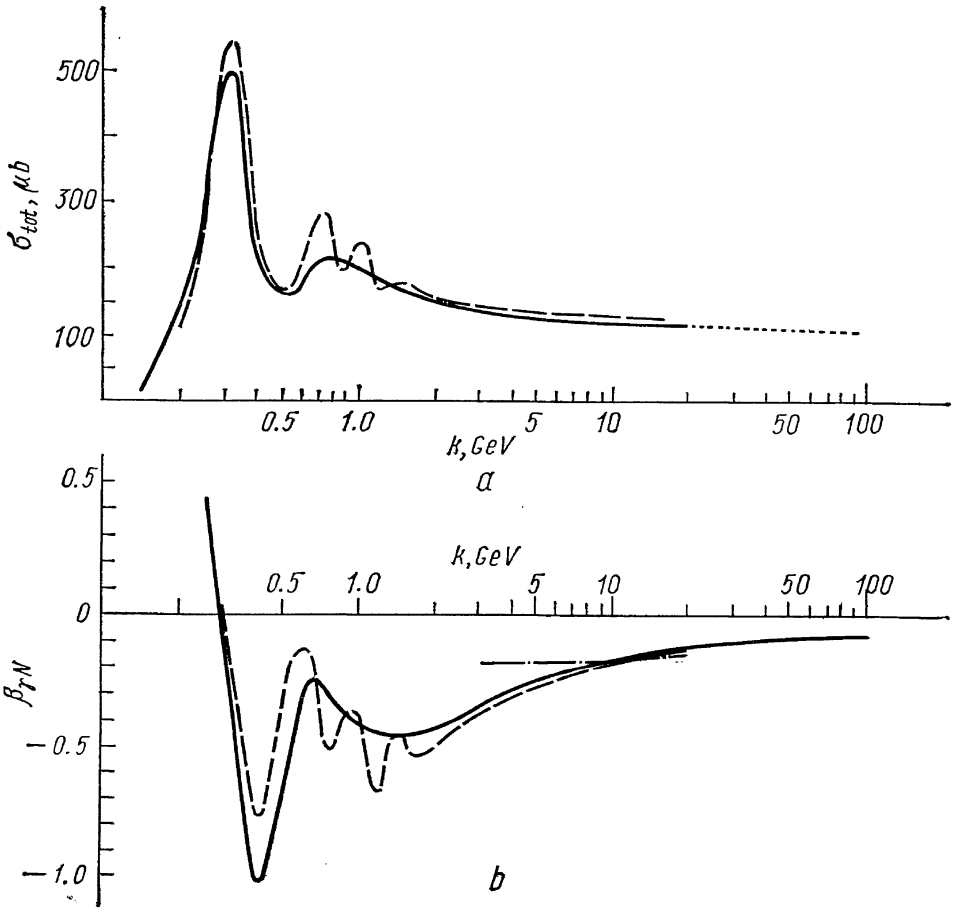

Fig. 40.

have seen, that similar indications of $I = 1$ exchange in forward diffraction type cross sections (ρ^0 photoproduction on D_2, section 2.3.1 and ω photoproduction, section 2.4.1 and 2.4.2) are questionable; the results are consistent with zero $I = 1$ isospin exchange. With regards to the errors in equ. (63) conclusions on the infinite energy behaviour of the total photon nucleon cross sections should be regarded carefully.

The data for $\sigma_{\gamma p}$ can be used to calculate the real part of the spin independent forward Compton amplitude $\mathrm{Re}\, f_1(k)$ from a dispersion relation. As input below 1.5 *GeV* the DESY group [118] used the sum of the total cross sections for $\gamma p \to p\pi^0$, $\pi^+ n$, $\pi^+\pi^-$, ηp which certainly gives a lower limit. Above 16 *GeV* an extrapolation proportional to $\sigma_{\pi^0 p} = {}^1/_2(\sigma_{\pi^+ p} + \sigma_{\pi^- p})$ was used [98]. The solid line in fig. 40*a* shows the smoothed cross section used to evaluate the dispersion integral; the dashed line gives the cross section according to the data of ref. [114] alone. Fig. 40*b* shows the results on $\beta_{\gamma N}$, the ratio of the real to the imaginary part of the forward Compton amplitude $f_1(k)$. These results are in very good agreement with recent calculations of ref. [120]. For comparison in fig. 40*b* also the quantity $\beta_{\pi^0 N} = \mathrm{Re}\, f(\pi^0 p)/\mathrm{Im}\, f(\pi^0 p)$ is shown as dashed dotted line calculated from $\sigma_{\pi^0 p} = {}^1/_2(\sigma_{\pi^+ p} + \sigma_{\pi^- p})$ [122]. Vector dominance and the quark model predict approximately $\beta_{\gamma N} \sim \beta_\rho = \beta_{\pi^0 N}$. For energies above 5 *GeV* $\beta_{\gamma N} \sim \sim \beta_{\pi^0 N}$ seems to be well satisfied.

2.7.2. TOTAL PHOTOPRODUCTION CROSS SECTION ON NUCLEI

The last section showed that the total cross section for photoproduction of hadrons on protons and neutrons is $\sigma_{\gamma N} \sim 120\ \mu b$ for energies of a few *GeV*. This corresponds to a photon mean free path of ~ 700 *fm* in nuclear matter, very long compared to a nuclear diameter of a few *fm*. Thus one would expect the total cross section for photoproduction of hadrons on nuclei to be proportional to the number A of nucleons. Neglecting the small difference of the cross sections on protons and neutrons this would mean

$$\sigma_{\gamma A} = A\sigma_{\gamma N}. \tag{64}$$

In the framework of the VDM the photons interact mainly via the ρ^0 mesons, which has a mean free path of only a few *fm*. Consequently the surface nucleons would shadow the rest. For complete shadowing the cross section would be proportional to the nuclear area. At high energies Stodolsky [123] predicted the A dependence of $\sigma_{\gamma A}$ to be the same as for $\sigma_{\rho A}$, which should be similar to that of $\sigma_{\pi A} \sim A^{0.75}$.

Later detailed calculations [124] showed, that at energies of a few *GeV* the total cross sections $\sigma_{\gamma A}$ should have an A dependence somewhere between the extreme values mentioned. In addition to the previously published results [125, 126] the final results of the DESY counter experiment [127] and the results of a new muon scattering experiment at SLAC [128] have been contributed to this conference.

The DESY results [127] for $\sigma_{\gamma A}$ at a mean photon energy of 5.4 *GeV*, averaged over an interval of ± 0.5 *GeV* on Be, C, Al, Ti, Cu, Ag and Au and the data of ref. [128] on C and Cu together with the other recent data are shown in fig. 41. Plotted is the quantity

$$A_{\mathrm{eff}}/A \equiv \sigma_{\gamma A}/(A \cdot \sigma_{\gamma N}) \tag{65}$$

versus the mass number A, where $\sigma_{\gamma N}$ is the mean value of the cross sections on protons and neutrons (section 2.7.1). The quoted errors do not include systematic errors. The agreement between the results of the two counter experiments refs. [126] and [127] and the muon scattering experiment [128] for C is very

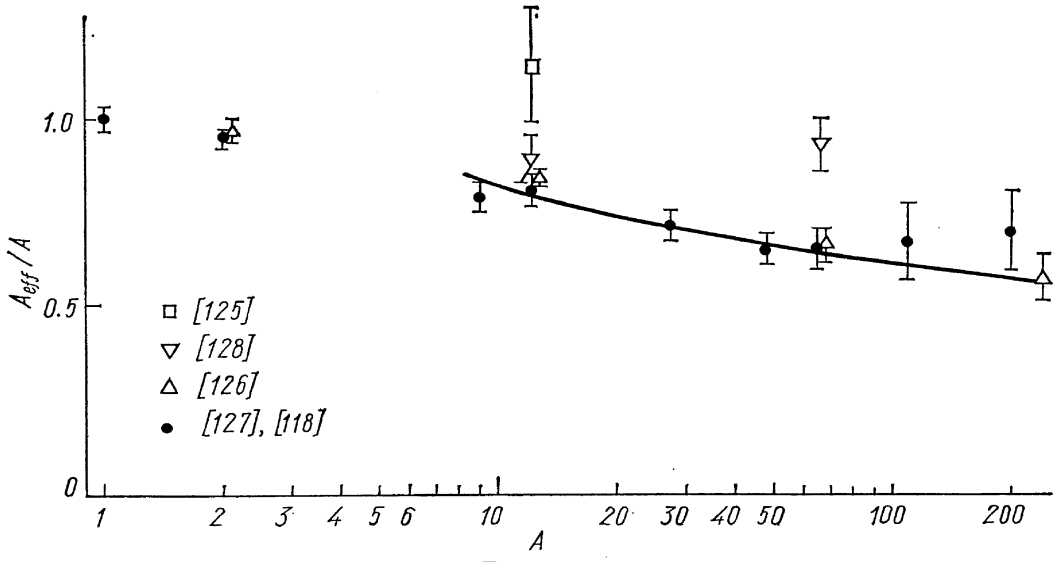

Fig. 41.

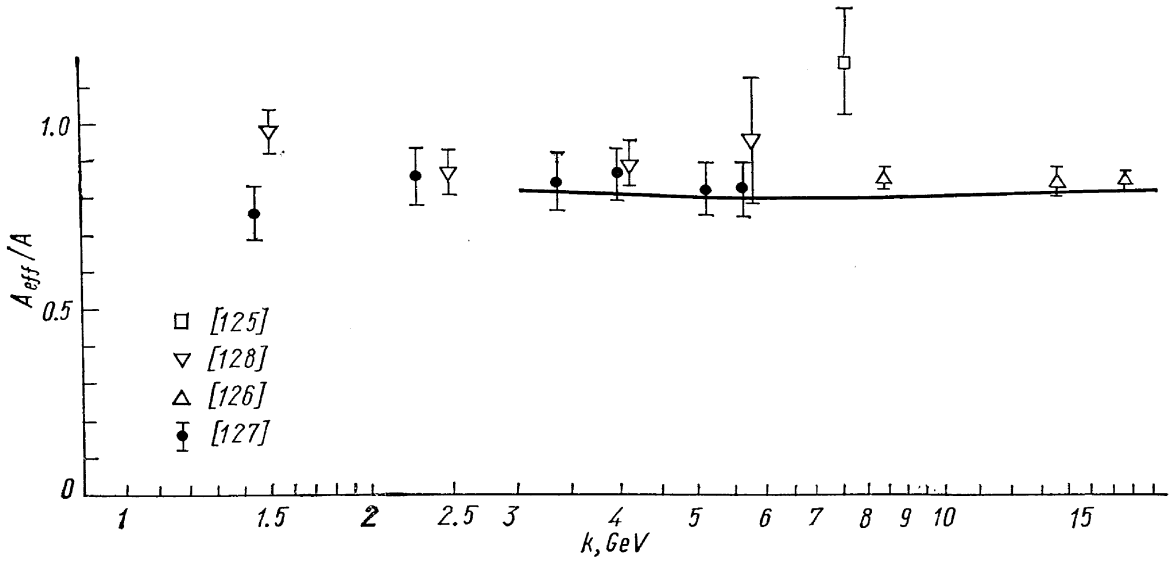

Fig. 42. The solid line is the VDM prediction of ref. [129].

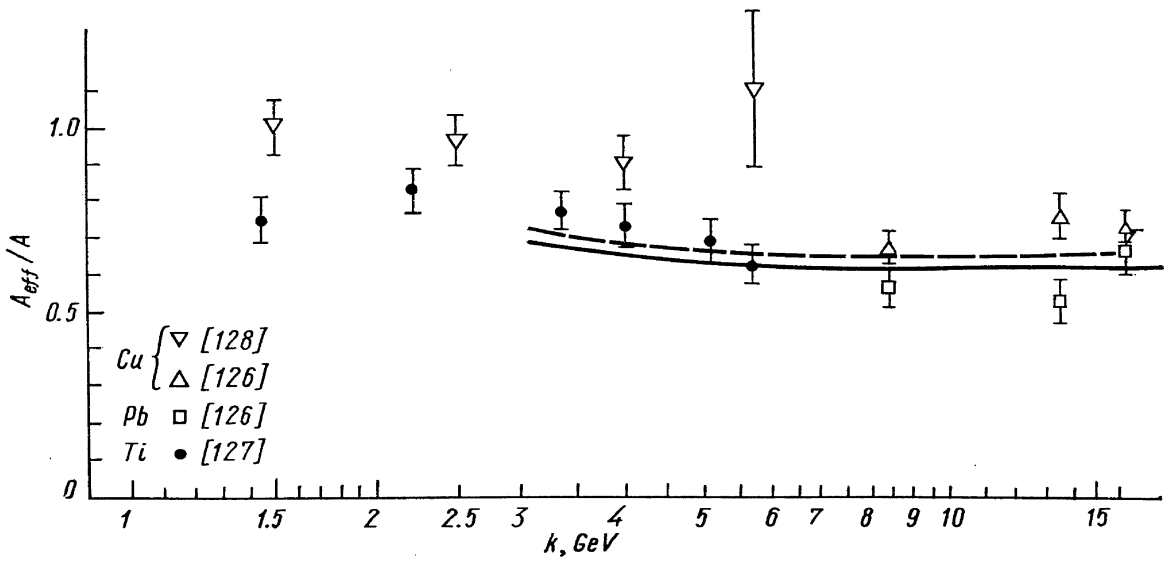

Fig. 43. The solid and dashed lines are the VDM predictions for Cu and Ti respectively.

satisfactory. A fit of the A dependence of the data of refs. [126] and [127] to the form

$$A_{\text{eff}} = \frac{\sigma_{\gamma A}}{\sigma_{\gamma N}} = A^x \tag{66}$$

yields $x = 0.914 \pm 0.005$ [119]. The solid line in fig. 41 is the theoretical prediction of *v.* Bochmann, Margolis and Tang [129]. They calculate the forward amplitude for Compton scattering on nuclei, which is related to the total cross section by the optical theorem, on the basis of the Glauber multiple scattering theory. As input the following quantities have been used

$$k = 5.5 \ GeV$$
$$\sigma_{\rho N} = \sigma_{\omega N} = 26 \ mb \quad \text{(table 5 and 7)}$$
$$\sigma_{\Phi N} = 12 \ mb \ [130]$$
$$\beta_v = -0.25 \ [119]$$
$$r_0 = 1.1 \ fm.$$

These parameters give $A_{\text{eff}} \sim A^{0.9}$ in good agreement with the data.

The energy dependence of A_{eff}/A is shown in Fig. 42 for carbon and in Fig. 43 for Ti, Cu and Pb. For carbon all data agree nicely and show practically no dependence on the energy between 1.5 and 15 *GeV*. This is fully reproduced by the prediction of ref. (129), taking the energy dependence of $\sigma_{\rho N}$ equal to that of $\sigma_{\pi^0 p}$. The data and the theoretical predictions for Ti and Cu in fig. 43 seem to indicate a slightly stronger energy dependence. This smooth energy behaviour justifies the study of the A dependence in Fig. 41 for data at different energies.

In conclusion one can say that the small shadowing effect (A dependence) and the energy dependence of $\sigma_{\gamma A}$ can be fully reproduced on the basis of the VDM and the Glauber theory [129] with the inputs mentioned above.

2.8. HIGH ENERGY COMPTON SCATTERING FROM PROTONS

The Compton scattering process $\gamma + p \rightarrow \gamma + p$ is interesting as one of the fundamental reactions involving photons and nucleons. At high energies it is expected to be predominantly diffractive at low t values but possibly to become nondiffractive at larger momentum transfers. This behaviour is predicted from the vector dominance model, where the Compton cross section is directly related to the measured cross sections for photoproduction of vector mesons (see section 2.9). Maybe of even more fundamental interest is the comparison of the forward Compton cross section at $t = 0$ with the total photoproduction cross section $\sigma_{\gamma p}$ discussed in the last section via the optical theorem.

Previous to this conference data were available only up to incident photon energies of 1.5 *GeV* (for a summary of these references see ref. [132]). To this conference new results of two very nice experiments from SLAC [132] and DESY [133] have been contributed. The results of a third experiment done at CEA have been reported by M. Deutsch [134].

The SLAC group [132] has measured the Compton process for mean photon energies of 5.5, 8.5, 11.5 and 17 *GeV* in the momentum transfer range $|t|$ from 0.06 to 1.1 GeV^2. For large t values ($|t| > 0.6 \ GeV^2$) they used a conventional liquid hydrogen target while for smaller momentum transfers a high pressure gas target was used [2]. The DESY group [133] investigated the reaction at a

mean photon energy of 6 *GeV* ($5 < k < 7$ *GeV*) in the $|t|$ range from 0.06 to 0.6 GeV^2.

In both experiments the scattered photon and the recoil proton was observed in coincidence. In the SLAC experiment the photons have been detected in a lead-lucite sandwich shower counter. The apertures were defined by movable lead slits. The proton momentum and angle was measured in the SLAC 1.6 *GeV/c* spectrometer. In the DESY experiment the photon angles θ_γ and φ_γ were measured by means of two crossed counter hodoscope behind a 1 *cm* lead converter, the energy of the photon being determined in nine lead glass shower counters. The recoil protons were detected with a wire spark chamber range telescope.

The recoil proton and the incoming photon defind the plane of elastic scattering. Photoproduced π^0 mesons, which were the main source of background in the experiments, decay into two photons with a typical half opening angle (m_π/E_π). Since the angular resolution of the photon detectors was small compared with this decay cone the separation of Compton scattered events and (γp) coincidences from π^0 photoproduction could be achieved by requiring coplanarity for the outgoing photon and the scattering plane defined above.

Fig. 44*a* shows a (γp) coincidence peak of the SLAC experiment [132]. Plotted is the coincidence yield versus missing mass for the photon detector in and out of the Compton scattering plane. The contribution from π^0 photoproduction out of the plane is small as expected. Fig. 44b shows the result of subtracting the out-of-plane yield from the in-plane yield. The resultant curve is the experimental Compton yield. The DESY group determined their Compton yield in an analogous way by measuring a coplanarity distribution of the differences of the proton and scattered photon azimuthal angles. For subtraction the π^0 background was determined by fitting the coplanarity distribution on both sides of the Compton peak.

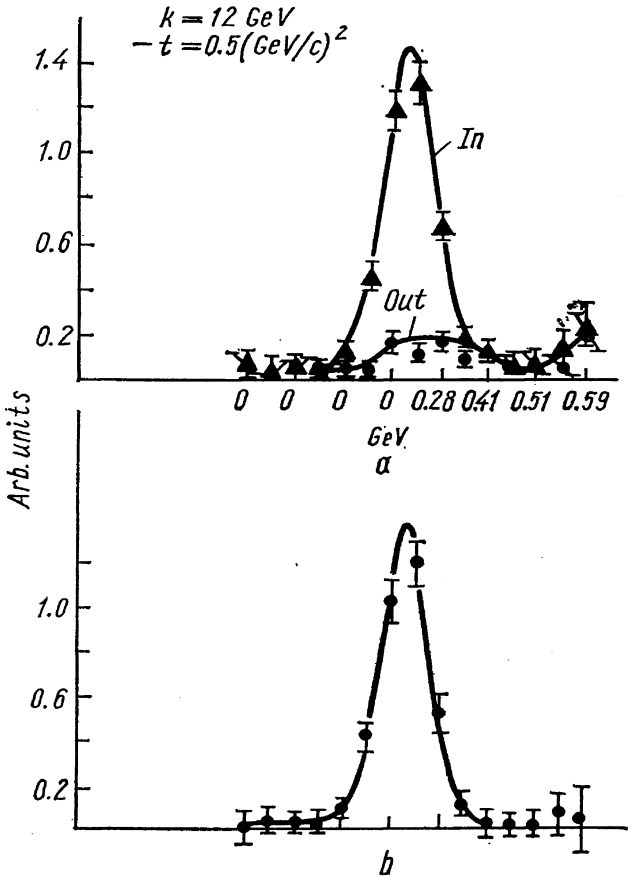

Fig. 44.

The results of both experiments are shown in Fig. 45 [132] and 46. The data include statistical and systematical errors besides an overall normalization error of $\sim 5\%$ in the SLAC and of $\sim 7\%$ in the DESY experiment. The t distributions show the predominantly diffractive character of the Compton process. Fig. 46 demonstrates the good agreement between both experiments at energies around 6 *GeV*.

For a momentum transfer range $0.06 < |t| < 0.40$ GeV^2 the DESY data have been fitted to the form $d\sigma/dt = A \exp(Bt)$. The results are $A = (0.79 \pm 0.05)\,\mu b/GeV^2$ and $B = (6.7 \pm 0.3)$ GeV^{-2}. Since the data deviate significantly from this curve for $|t| > 0.4$ GeV^2 a fit to the form

$$\frac{d\sigma}{dt} = a \cdot \exp(bt + ct^2) \qquad (67)$$

has been performed for all the DESY data.

In the momentum transfer range $|t| < 0.6$ GeV^2 also the SLAC group ob-

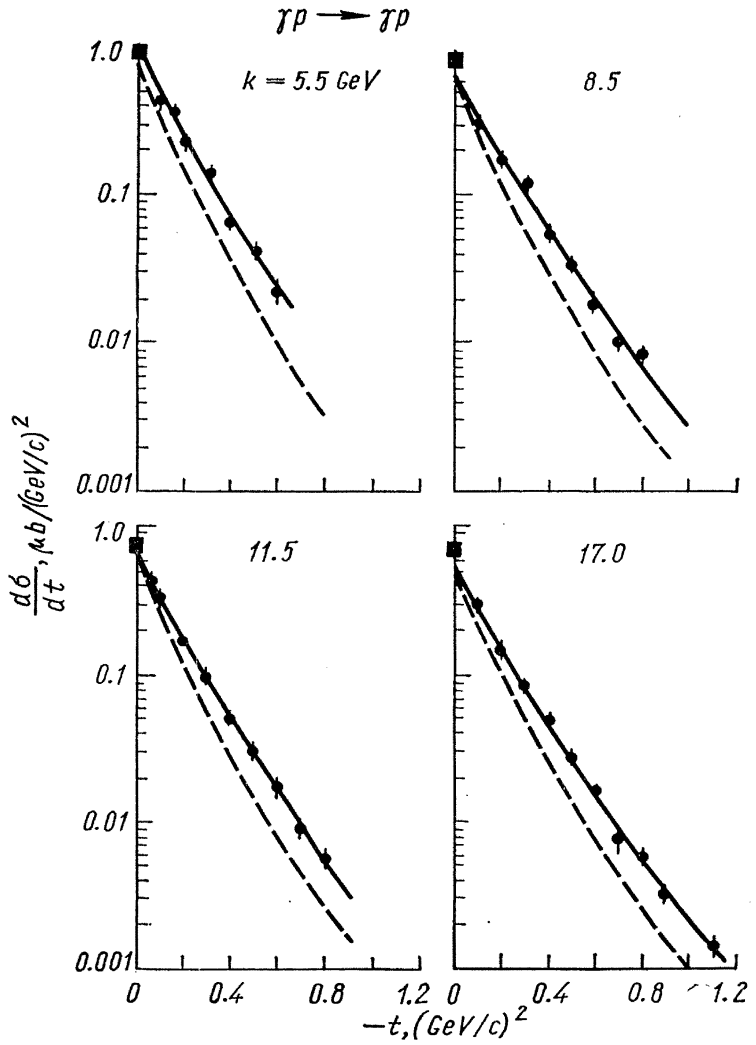

Fig. 45. The black dots are the Compton data. The black squares at $t = 0$ are the optical points calculated including the real part of $f_1(k)$ from ref. [80]. The solid lines are the results of a fit of the form $a \exp(bt + ct^2)$. The dashed lines are VDM predictions (see section 2.9).

tained a good fit to the data at all energies with a single exponential with a slope of approximately $B \sim 6\ GeV^{-2}$. The curves shown in Fig. 45 have been obtained by fitting the SLAC data to the form of equ. (67). The fit parameters of both experiments are given in table 11. The slopes b are compatible with those found in ρ^0 photoproduction (see fig. 16 and section 2.9).

Table 11

$$\gamma + p \to \gamma + p;\ \frac{d\sigma}{dt} = a \cdot \exp(bt + ct^2)$$

	$\bar{k} = 6$ GeV [133]	$\bar{k} = 5.5$ GeV [132]	$\bar{k} = 8.5$ GeV [132]	$\bar{k} = 11.5$ GeV [132]	$\bar{k} = 17$ GeV [132]
a [$\mu b\ GeV^{-2}$]	0.93±0.08	0.88±0.15	0.6±0.1	0.63±0.06	0.55±0.05
b [GeV^{-2}]	8.4 ±0.7	6.9 ±1.3	6.2±0.8	6.5 ±0.6	0.66±0.4
c [GeV^{-4}]	3.8 ±1.1	1.3 ±1.9	0.7±0.9	0.8 ±0.7	1.1±0.4

To compare the results of the Compton experiments with the total photoproduction cross section $\sigma_{\gamma p}$, we use the forward ($t = 0$) amplitude for Compton scattering as given by [135]:

$$f(k) = f_1(k)(\vec{\varepsilon}_f \cdot \vec{\varepsilon}_i) + i f_2(k)\,\vec{\sigma}(\vec{\varepsilon}_f \times \vec{\varepsilon}_i) \qquad (68)$$

where k is the incoming photon energy and $\vec{\varepsilon}$ and $\vec{\varepsilon}_f$ are the polarization vectors of the incoming and outgoing photon. $\vec{\sigma}$ is the Pauli spin matrix for the recoil

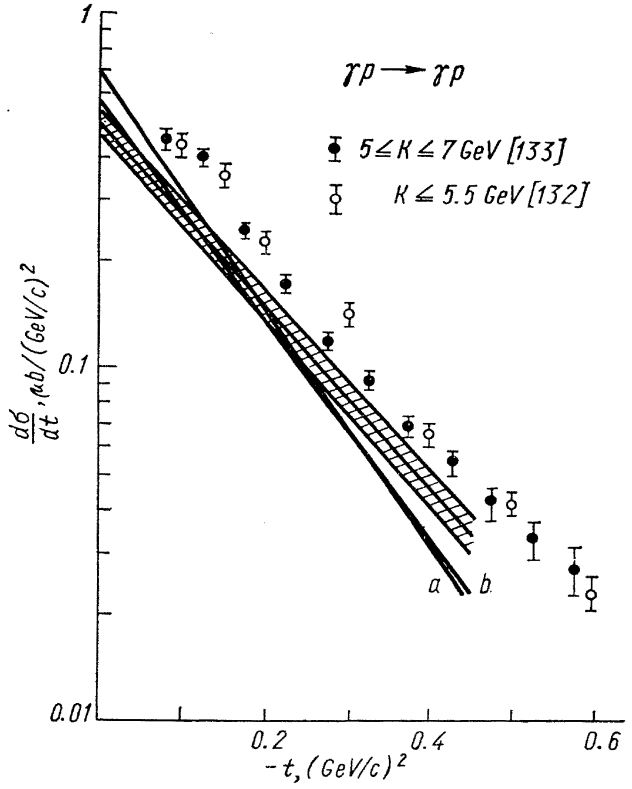

Fig. 46. The dashed area gives the VDM prediction according to equ. (80) using for the ρ^0 photoproduction cross section the data from ref. [64] analyzed with the Drell — Söding model. The solid lines give predictions for different ρ^0 cross sections (SLAC [64] (*b*) and DESY [63] (*a*)).

nucleon. Using the optical theorem $\mathrm{Im}\, f_1(k) = (k/4\pi)\,\sigma_{\gamma p}(k)$ one derives the forward cross section

$$\left.\frac{d\sigma}{dt}\right|_{t=0}(k) = \frac{1}{16\pi}\,\sigma^2_{\gamma p}(k)\,(1+\beta^2_{\gamma p}(k)) + |f_2(k)|^2 \qquad (69)$$

with $\beta_{\gamma p}(k) = \mathrm{Re}\ f_1(k)/\mathrm{Im}\ f_1(k)$ and $\mathrm{Re}\ f_1(k)$ given by a disperion relation. Neglecting $f_2(k)$ (in the case of pure diffraction scattering $f_2(k)$ is zero) equ. (69) permits to calculate $\frac{d\sigma}{dt}(t=0)$ for Compton scattering (optical point) from the measured total cross sections $\sigma_{\gamma p}(k)$.

Inserting in equ. (69) $\sigma_{\gamma p} = (122 \pm \pm 5)\ \mu b$ and $\beta_{\gamma p} = -0.23$ [118] the DESY group obtained a value $(0.80 \pm \pm 0.07)\ \mu b/GeV^2$ for the forward cross section. This value is in fair agreement with the $t = 0$ intercepts A and a of both exponential fits to the DESY data. The SLAC group evaluated equ. (69) with the total cross sections $\sigma_{\gamma p}(k)$ of ref. [117] and the real part of $f_1(k)$ as computed by Damashek and Gilman [120]. The results are shown as squares in fig. 45. The $t = 0$ intercepts of the exponential fits to the SLAC data are in fair agreement with these optical points, although on the average they are somewhat lower.

The results of both high energy Compton experiments together with the data on total photoproduction cross sections allowed for the first time a test of equ. (69). The results are consistent with $f_2(k)$ being equal to zero.

2.9. VECTOR DOMINANCE MODEL COMPARISONS

The starting point for all vector dominance model (VDM) relations is the assumption that the electromagnetic current $j_\mu(x)$ can be written as a sum of the vector meson fields [136]:

$$j_\mu(x) = -\left(\frac{m^2_\rho}{2\gamma_\rho}\,\rho_\mu(x) + \frac{m^2_\omega}{2\gamma_\omega}\,\omega_\mu(x) + \frac{m^2_\Phi}{2\gamma_\Phi}\,\Phi_\mu(x)\right) \qquad (70)$$

where m_v is the mass of the three known vector mesons ($J^P = 1^-$, see section 2.10.) and γ_v is the photon-vector meson coupling constant. The extensive literature existing on the applications of equ. (70) is summarized in the review papers given under ref. [137]. The ratio of the coupling constants γ_v is obtained from pure *SU* (3) with ideal ω — Φ mixing as

$$\gamma_\rho : \gamma_\omega : \gamma_\Phi = 1 : 3 : -\frac{3}{\sqrt{2}} \qquad (71)$$

which leads to

$$\frac{1}{\gamma^2_\rho} : \frac{1}{\gamma^2_\omega} : \frac{1}{\gamma^2_\Phi} = 9 : 1 : 2. \qquad (72)$$

Modifications due to symmetry breaking change this ratios (for a summary of modifications see ref. [81]).

We will consider the following relations between the amplitudes of vector meson photoproduction $T_{\gamma v}$, vector meson — vector meson scattering $T_{v'v}$ and Compton scattering $T_{\gamma\gamma}$:

$$T_{\gamma v}(t) = \left(\frac{\alpha}{4}\right)^{1/2} \sum_{v'} \left(\frac{\gamma_v^2}{4\pi}\right)^{-1/2} T_{v'v}(t) \tag{73a}$$

and

$$T_{\gamma\gamma}(t) = \left(\frac{\alpha}{4}\right)^{1/2} \sum_{v} \left(\frac{\gamma_v^2}{4\pi}\right)^{-1/2} T_{\gamma v}(t). \tag{74}$$

In deriving these relations the assumption has been made that the scattering is the same for all helicity states. Neglecting contributions of the type $V'p \to \to Vp$ in equ. (73a) we obtain

$$T_{\gamma v}(t) = \left(\frac{\alpha}{4}\right)^{1/2} \left(\frac{\gamma_v^2}{4\pi}\right)^{-1/2} T_{vv}(t) \tag{73}$$

which describes obviously only the diffractive part of vector meson photoproduction.

From equ. (73) we obtain

$$\frac{d\sigma}{dt}(t)_{\gamma v} = \frac{\alpha}{4}\left(\frac{\gamma_v^2}{4\pi}\right)^{-1} \frac{d\sigma}{dt}(t)_{vv} \tag{75}$$

and together with the optical theorem

$$\left.\frac{d\sigma}{dt}\right|_{t=0\,\gamma v} = \frac{\alpha}{64\pi}\left(\frac{\gamma_v^2}{4\pi}\right)^{-1} \sigma_{vN}^2 (1 + \beta_v^2) \tag{76}$$

where σ_{vN} is the total vector meson nucleon scattering cross section and $\beta_v = \mathrm{Re}\, T_{vv}/\mathrm{Im}\, T_{vv}$. With the predictions of the quark model [60, 138]

$$\sigma_{\rho p} = \sigma_{\omega p} = \frac{1}{2}(\sigma_{\pi^+ p} + \sigma_{\pi^- p}) \sim 28\ mb \quad \text{at} \sim 5\ GeV$$

and (77)

$$\sigma_{\Phi p} = \sigma_{K^+ p} + \sigma_{K^- p} - \sigma_{\pi^+ p} \sim 12\ mb \quad \text{at } 5\ GeV$$

which are in agreement with the measured total cross sections on complex nuclei (table 5 and 7 and ref. [130]) one obtains for the **diffractive** part of forward vector meson photoproduction from equs. (76), (72) and (77) (neglecting β_v which is of the order of 4%)

$$\left.\frac{d\sigma}{dt}\right|_{t=0\gamma\rho^0} : \left.\frac{d\sigma}{dt}\right|_{t=0\gamma\omega} : \left.\frac{d\sigma}{dt}\right|_{t=0\gamma\Phi} = 9:1:0.4. \tag{78}$$

At 4.7 *GeV* one finds experimentally with $\left.\frac{d\sigma}{dt}\right|_{t=0_{\gamma\Phi}} = (3 \pm 1)\ \mu b/GeV^2$ as quoted by E. Lohrmann (139) the ratios

$$9 : (1.2 \pm 0.35) : (0.25 \pm 0.09)$$

and

$$9 : (1.7 \pm 0.45) : (0.34 \pm 0.11)$$

where for the ρ^0 cross sections the extreme values (Ross — Stodolsky and Drell—Söding) of table 2 and for the ω cross section only the natural parity exchange contribution of table 6 has been used. The experimental data are compatible with the prediction equ. (78). We can further use equ. (76) to determine $\gamma_v^2/4\pi$. Adopting for the total cross sections the values of equ. (77) values for $\gamma_\rho^2/4\pi$

and $\gamma_\omega^2/4\pi$ are given in table 12 for various forward ρ^0 photoproduction cross sections and the natural parity part of the ω cross section [82]. The results obtained on $\gamma_\rho^2/4\pi$ reflect the uncertainties inherent in the forward ρ^0 photoproduction cross sections. The values calculated from the SLAC cross sections [64] are somewhat high, however not in disagreement with those obtained from ρ^0 photoproduction on complex nuclei (table 5). The DESY—MIT [56] value agrees with the Orsay result [81]. $\gamma_\omega^2/4\pi$ is compatible with the Bonn — Pisa ω photoproduction and the Orsay storage ring results (table 7).

Table 12

Determination of $\gamma_v^2/4\pi$ using equ. (77) (β_v^2 is neglected)

k [GeV]	$\frac{d\sigma}{dt}\Big\|_{t=0\,\gamma\rho}$ [$\mu b/GeV^2$]	$\gamma_\rho^2/4\pi$
4.7	110±8 (ref. 64)	0.65±0,05
4.7	80±5 (ref. 64)	0.89±0.07
4.7	139±5 (ref. 56)	0.51±0.04
Orsay [81]		0.50±0.03

k	$\frac{d\sigma}{dt}\Big\|_{t=0\,\gamma\omega}$ [$\mu b/GeV^2$]	$\gamma_\omega^2/4\pi$
4.7	15.2±3.8 (ref. 82)	4,6±1.2
Orsay [18]		3.7±0.7

The most direct test of VDM is provided by the following relation, which is obtained from equ. (74) via the optical theorem

$$\sigma_{\gamma p} = (4\pi\alpha)^{1/2} \sum_v \left[\left(\frac{\gamma_v^2}{4\pi} \right)^{-1} \times \right.$$

$$\left. \times \frac{d\sigma}{dt}\Big|_{t=0\gamma v} (1+\beta_v^2) \right]^{1/2}. \quad (79)$$

Here the diffractive part of the forward cross sections for $\gamma p \to \to Vp$ have to be inserted. Since on the r. h. s. of equ. (79) the by far largest contribution comes from the ρ^0, equ. (79) can be used to determine $\gamma_\rho^2/4\pi$. The inputs and the results are given in table 13. Also here the results in the evaluation of $\gamma_\rho^2/4\pi$ reflect the uncertainties in the ρ^0 cross sections. However all photoproduction data give values for $\gamma_\rho^2/4\pi$ which are smaller than the storage ring value [81].

A similar conclusion is reached by comparing the Compton scattering results with vector meson photoproduction data. Assuming maximum interference between the vector meson amplitudes one obtains from equ. (74)

$$\frac{d\sigma}{dt}(t)_{\gamma v} = \frac{\alpha}{4} \left[\sum_v \left(\frac{\frac{d\sigma}{dt}(t)_{\gamma v}}{\gamma_v^2/4\pi} \right)^{1/2} \right]^2. \quad (80)$$

In evaluating equ. (80) the SLAC [132] and the DESY [133] group used the Orsay storage ring [81] values for the coupling constants. The SLAC group took the ρ^0 and Φ photoproduction data from their earlier measurements (1) and put $\frac{d\sigma}{dt}_{\gamma\omega} = \frac{1}{9} \times$ $\times \frac{d\sigma}{dt}_{\gamma\rho}$. The results are shown in fig. 45 as dashed lines. They are systematically lower and the slope is steeper. The DESY group used different ρ^0 photoproduction data as indicated in fig. 46. All predictions for the Compton scattering cross section are too low. However using the data of the SLAC — HBC — group [64] analyzed with the Drell — Söding model gives the right slope. Agreement in the momentum transfer range $0.1 < |t| < 0.25$ GeV^2 can be achieved by taking $\gamma_\rho^2/4\pi$ equal to ~ 0.3. This is consistent with the low values on $\gamma_\rho^2/4\pi$ of table 13 obtained from the comparison with the total cross section data. From these results one

may conclude, that the photon is not completely described by the three vector mesons ρ^0, ω and Φ but couple also to other states. The next section is concerned with the search of possible further high mass vector mesons.

Combining equs. (73) and (74) a VDM relation between the total cross sections can be obtained as follows

$$\sigma_{\gamma p} = \frac{\alpha}{4} \sum_v \left(\frac{\gamma_v^2}{4\pi} \right)^{-1} \sigma_{vN}. \tag{81}$$

Table 13

Determination of $\gamma_\rho^2/4\pi$ using equ. (79)

Input: $k = 4.7$ *GeV*

$$\left.\frac{d\sigma}{dt}\right|^{\text{Diff}}_{t=0\gamma\omega} = 15.2 \pm 3.8 \ \mu b/GeV^2 \text{ (table 6)}$$

$$\left.\frac{d\sigma}{dt}\right|^{\text{Diff}}_{t=0\gamma\Phi} = 3 \pm 1 \ \mu b/GeV^2 \text{ (ref. 139)}$$

$\gamma_\omega^2/4\pi = 3.7 \pm 0.7$, $\gamma_\Phi^2/4\pi = 2.9 \pm 0.22$ (ref. 81)

equ. (79) then leads to (neglecting β_v^2; 2—5% effect)

$$\gamma_\rho^2/4\pi = \frac{36.6 \cdot \left.\frac{d\sigma}{dt}\right|_{t=0\gamma\rho}}{(\sigma_{\gamma\rho} - 18.4 \pm 2.7)^2}$$

with $\frac{d\sigma}{dt}$ in units $\mu b/GeV^2$ and $\sigma_{\gamma p}$ in μb.

$\left.\frac{d\sigma}{dt}\right\|_{t=0\gamma\rho}$ [$\mu b/GeV^2$]	$\sigma_{\gamma p}$ [μb]	$\gamma_\rho^2/4\pi$
110 ± 8 (ref. 64)	128 ± 6 (equ. 62)	0.33 ± 0.04
102 ± 8 (ref. 64)	128 ± 6	0.30 ± 0.04
80 ± 5 (ref. 64)	128 ± 6	0.24 ± 0.03
139 ± 7 (ref. 56)	128 ± 6	0.42 ± 0.04

Inserting the Orsay storage ring values for the coupling constants and the values of equ. (78) for the total vector meson cross sections one obtains

$$\sigma_{\gamma p} = 123 \pm 8 \mu b$$

for energies around 5 *GeV* in excellent agreement with the measured photon total cross sections. This might show that one should be carefull to draw too strong conclusions about the validity or non validity of the vector dominance model by looking at certain reactions only.

2.10. HEAVY VECTOR MESONS

There are many experiments which have searched for additional vector mesons beyond the mass of the ρ^0, ω and Φ mesons. These experiments have been reviewed in the talks of Prof. Silverman [53] and more recently by Davier [140].

Two experiments looking at photoproduction of pion pairs from the DESY—MIT group [141] and a SLAC group [142] have been contributed to this conference. The DESY data was obtained with a 7.4 *GeV* bremsstrahlung beam from carbon covering the invariant mass region $0.6 < m_{\pi\pi} < 1.8$ *GeV*. The SLAC group

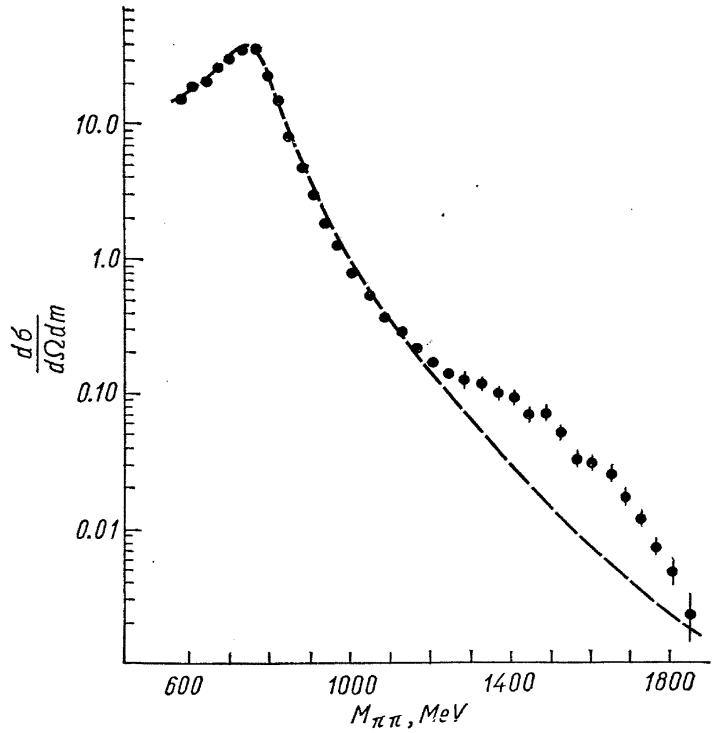

Fig. 47. The curve is the best eye fit.

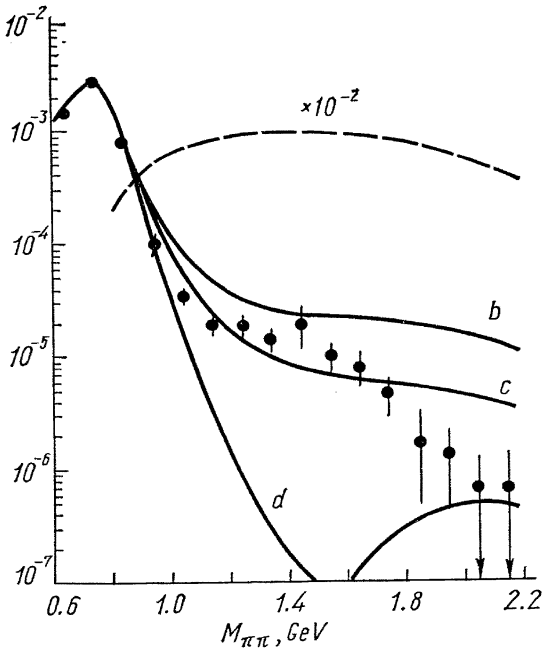

Fig. 48. $\pi\pi$ mass-spectrum (weighted events/0.1 BeV/c^2/monitor) for $|t - t_{min}| < 0.046$ GeV^2, $|\cos\theta_{\pi\pi}| < 0.6$ and $E_{\pi\pi} > 14.0$ GeV. The dashed curve is the calculated acceptance.

measured $\pi\pi$ mass distributions in the range $0.9 < m_{\pi\pi} < 2.2$ GeV using a 16 GeV bremsstrahlung beam and a beryllium target. Fig. 47 [141] shows the $d\sigma/(d\Omega dm)$ averaged over the spectrometer acceptance at very small momentum transfers. A broad enhancement in the mass region $1.3 < m < 1.8$ GeV is seen.

Fig. 48 shows the SLAC results [142] also showing a broad shoulder around 1.5 GeV. The solid lines b, c, and d correspond to different assumptions for the ρ width. None of these models is able to describe the data. From both experiments one can conclude that the observed mass-spectra do not exhibit a clear narrow resonance. The data show up a broad enhancement in the mass region around 1.5 GeV.

From CEA [143] an experiment on muon pair production from carbon using the 6 GeV CEA bremsstrahlung beam has been reported. This experiment covers the invariant mass region $0.93 < m_{\eta\eta} < 1.77$ GeV. These kinds of experiments, i. e. detecting muon pairs, are particularly interesting since $\mu^+\mu^-$ is an allowed decay mode for all vector mesons. The measured mass-spectrum is consistent with QED and shows no evidence for new vector mesons.

Preliminary results of a second experiment at CEA [144] using a missing mass technique together with a tagged photon beam have been reported by M. J. Tannenbaum. The ρ and ω mesons are clearly seen. The analysis is in-progress.

In the DESY streamer chamber [145] photoproduction of $\pi^+\pi^-$ and $2\pi^+2\pi^-$ systems on carbon between 4.3 and 6.3 GeV has been investigated. From the momentum transfer distributions it appears, that for both final states coherent as well as incoherent production on the nucleus is observed. The $\pi^+\pi^-$ channel is dominated by the ρ^0. The 4π mass distribution shows a broad shoulder between invariant masses from 1.2 to 2.4 GeV. If the 4π system observed has the quantum number $J^P = 1^-$ then one would expect to see it also in e^+e^- annihilation. Indications for this have been indeed found at the Frascati storage ring [146].

In conclusion no sharp narrow resonances with quantum numbers $J^P = 1^-$ have been seen yet with masses ranging up to roughly 2 *GeV*.

I like to thank the discussion leaders Prof. G. Vartapetyan and Prof. S.C.C.Ting. The help of the scientific secretaries Drs. P. Baranov, E. Leikin, V. Zamiralov and M. Khvastunov is greatly acknowledged. Many discussions with Profs. P. L. Braccini, W. Braunschweig, H. Fischer, E. Gabathuler, H. Meyer, W. Paul and H. Rollnik have been of much help.

DISCUSSION

T i n g:

We at DESY have also measured $\varphi \to 2\pi$, and the branching ratio seems to be much smaller than $\omega \to 2\pi$. I wonder if anyone can suggest how to analyze these data?

T e r - M a r t i r o s y a n:

May we say that at present all the data on the photoproduction of π^0, ρ^0 are in agreement with the Regge pole + cut theory? Some time ago marked discrepancies were indicated.

S c h o p p e r:

1) The strong interaction nuclear radii as deduced from ρ photoproduction agree very well with radii obtained from *n*-nuclei total cross sections if the correlation parameter entering the analysis is put equal to zero.

2) The similarity between photoproduction reactions and corresponding hadronic reactions is qualitative, but the detailed mechanism might be quite different. For example π^0 photoproduction and *np* charge exchange both show the very sharp forward peak. However, it seems that the data presented at this conference cannot be explained by the same model.

C r i e g e e:

I disagree with the speaker's statement that the comparison of Compton scattering and ρ photoproduction is not conclusive with respect to vector dominance. The main difficulty does not come from the data, but from difficulties of the interpretation of rho photoproduction. These difficulties are particularly bad at $t = 0$. However, at $t \sim -0.2$ the interference between the diffractive production and the Drell effect is small, and there is a clear-cut 30% discrepancy between the VDM-prediction in the sense that $\gamma_\rho^2/4\pi$ would have to be ≈ 0.35 ($\pm$ 0.05). In this *t*-range the ρ^0 data can not manage to give agreement with VDM.

D e u t s c h:

The MIT — CEA Compton data cover a range from $-t = 0.14$ to $-t = 0.41$ at 3.2 *GeV* and a wider range at lower energies. Since the signal to noise was somewhat better than in the DESY data, the extrapolation was comparable.

B e r t o c c h i:

I would like to make two comments on the coherent photoproduction on deuterium at large *t*. In my opinion, this experiment contains more information than that is contained in the analysis performed by the authors of the experiment as I understand it.

The first remark concerns the slope of the double scattering region. The good fit shown in the slide was obtained by assuming the slope of the ρ*N* angular distribution to be the same as that of ρ photoproduction on nucleons.

In fact, the slope of the double scattering region can be considered as a sensitive way of measuring the slope of the ρ*N* differential cross section (as discussed in a paper by Caneschi and myself in Nuovo Cimento (1967)). The fact that the agreement obtained using slope (ρ*N*) = slope (photoproduction) ≈ 6 $(GeV/c)^{-2}$ means that in fact they are almost equal. One could extract the slope, with its error, analyzing the slope of the double scattering region.

The second remark concerns the absolute value of the cross section in the double scattering region. An experience with coherent πd scattering at large $|t|$ tells us that, in the energy region

where spin effects are important, as in πN scattering around 1 *GeV*, by neglecting spin effects the prediction can be wrong by more than a factor 5.

The fact that assuming $\sigma_{\rho N} \sim 28$ *mb* gives a good fit means therefore very likely that helicity flip is negligible for $|t| \sim 0.3 \div 0.4$ $(GeV/c)^2$, not only in ρ photoproduction, but also in ρN elastic scattering.

T a l m a n:

I can comment only on the first point made in the question. The point in question is the good fit between our theory and data at large t (0.6 to 1.4 $(GeV/c)^2$). If one wishes, one can interpret the measurements in this region as a measurement of the angular distribution of ρ^0-nucleon scattering. The result, as Bertocchi pointed out, is excellent agreement with the ρ^0 photoproduction angular distribution. I would like to add that this also gives excellent agreement with the quark model prediction for $\rho^{\bar{0}}$ scattering, as described in previous publications of the Ritson group.

S a l v i n i:

In the experiment $\gamma + C \to 4\pi + C$ that you mentioned last, the comparison is made with one of the Frascati experiments. The comparison is very good: this is one indication perhaps that the multiple production observed at Frascati is not due to the decay of η', as could be suggested by the Brodsky — Kinoshita ($e^+ + e^- \to e^+ + e^- + \eta'$) effect. So far my question is:

how sure they are, with the streamer chamber experiment, that in the reaction $\gamma + C \to C + 4\pi$ there are 4 charged pions, and nothing else?

M e y e r:

In the coherent 4π events observed in the streamer chamber:

there are no additional π produced;

they are most probably π;

the final state is mostly $\rho\pi\pi$.

B i n g h a m:

I have 2 comments: first — you said the bubble chamber total hadronic cross section values are low. Our values (SLAC — Berkeley — Tufts 82″ HBC Laser Beam) at 2.8 and 4.7 *GeV* are in good agreement with subsequent Santa Barbara, DESY, SLAC, etc. results.

Secondly — we also have observed an indication of $\rho\omega$ interference in $\gamma p \to p\pi^+\pi^-$ (i. e. from hydrogen, not Be or C), at 2.8 and 4.8 *GeV*. Our values for the magnitude ($f \cos\beta = 2.6 \pm 1.0$ *MeV*) and phase ($\beta \sim -9°$ relative to the ρ decay phase at M_ω) are in good agreement with the DESY and Nina results.

K h a r i t o n o v:

We have started to study photoproduction of charged ρ-mesons on hydrogen and complex nuclei. We now have some preliminary results for carbon and (more preliminary) for aluminum. The results show $\sim 2\mu b$ per nucleus for each with 4 *GeV* γ's. Within the limits of statistics ($\sim 10 \div 15\%$ for C, $15 \div 25\%$ for Al), the cross sections for C and for Al are the same, and there may be a difference for ρ^+ and for ρ^-, being $\sim 30\%$ lower for ρ^+ which may indicate the presence of an isovector part of the photoproduction amplitude. There are also some data on angular and t-distributions. The results on ρ-charged photoproduction may throw some light concerning Ross — Stodolsky and Söding — Kramer — Uretsky models of the ρ-meson-mass-spectrum shape. Our work is in progress.

G e r a s i m o v:

I would like to ask a question and to make a short comment.

The Notre Dame University Group suggested previously that some admixture of the pion-pion d-wave in the reaction $\pi N \to 2\pi N$ may be present, and than when it is taken into account it improves the VDM prediction for the pion production by linearly polarized photons. Now, as we heard from the report the SLAC Group claimes no evidence for the d-wave. So, how definite and unambiguous is their conclusion? Do they apply the same type of data analysis as the Notre Dame Group did?

It appears rather striking that the VDM fails in this particular type of reaction and nevertheless describes properly some other features of the unpolarized cross section: the forward peak, the slope of the differential cross section, dip in the $\gamma p \to \pi^0 p$, etc.

A. S. Goldhaber:

Is there a discrepancy still between DESY and Daresbury data on e^+e^- photoproduction in nuclei as far as the relative phase of ρ and ω production is concerned?

Comment: there is not a serious descrepancy between simple theory and the Orsay data on $\rho\omega$ interference. This has been pointed out by many people, including Sachs and Willemson.

The discrepancy is between one and two standard deviations depending on how small effects are estimated. One reason many people have thought it was larger is that the sign convention for the phase used in the Orsay paper is opposite to the usual sign.

Gabathuler:

The phase of the overall ρ and ω two pion final states, as measured at Daresbury and DESY, are in agreement. However if you take the phase of the production amplitudes as given by the electron pair experiments, then allowing for second order mass mixing terms, the results will be different for the phase of the $\omega \to 2\pi$ since the measured phases in the electron pair experiments are different.

Caldwell:

In agreement with Griegee, I do not think the disagreement of proton Compton scattering and total cross sections with vector meson dominance should be swept under the rug. Both the comparison of the proton total cross section and proton forward ρ photoproduction, as well as the A-dependence of the total cross section give low values for the $\gamma\rho$ coupling constant. You showed the DESY A-dependence, along with a few old Santa Barbara points, but if one uses the much more extensive complex-nuclei data we submitted to this conference, this disagreement is clearly demonstrated.

Meyer:

The coupling constant $\gamma_\rho^2/4\pi$ just cancels in analysing $\sigma_{tot}\ (\gamma A)$.

Roos:

This is in answer to a question by Ting earlier in this session. There is a reason why the $\varphi \to 2\pi$ decay should be much less important than the $\omega \to 2\pi$ decay, namely the near degeneracy between the ω and ρ masses. This makes ω and φ quite different. In fact, the reason for seeing an $\omega \to 2\pi$ decay in the first place is that the mass degeneracy enhances it, as pointed out by Glashow in 1962 in the first paper on interference.

Ting:

I would like to point out that the different results in $\rho\omega$ interference in e^+e^- final states from my group at DESY and the Daresbury group may most likely be due to a systematic error in one of the experiments.

H. Lynch:

Remark in answer to question on need of D-wave for ρ data, We divided the data into a 20×20 matrix for θ and Φ and calculated chi-squared of fit for each value of θ with respect to Φ distribution; likewise for each Φ with respect to θ. The confidence levels are reasonable for $-0.8 < \cos\theta < 0.8$ and $0 \leqslant \Phi \leqslant 2\pi$.

Sakurai:

I also have a comment on the slide showing comparison between the Frascati cross section and the mass distribution seen in the DESY streamer chamber experiment. First, it is not so clear to me whether we should compare the mass distribution with the colliding beam cross section or with s times the colliding beam cross section. There is a factor of seven already.

Second, it is not conclusively established that the four pion bump seen in the DESY experiment is produced coherently or diffractively.

I also have a general remark. One should not take too seriously a 30% discrepancy in the ρ meson coupling constant. After all, the Goldberger — Treiman relation is off by 15 to 20% (in the squared coupling constant), and there the extrapolation distance is shorter by more than an order of magnitude.

1. R. L. Anderson et al., Phys. Rev. **1D**, 27 (70).
2. R. L. Anderson et al., paper 8a—1 and SLAC — PUB 770, (Aug. 1970).
3. J. R. Johnson; SLAC Report 124 (Sept. 1970).
4. W. Braunschweig et al., paper 8a—18 and PL, **33B**, 236 (1970).
5. K. Lübelsmeyer; Proceedings of the International Symposium on Electron and Photon Interactions at High Energies, Liverpool (1969).
6. See Ref. (88).
7. C. Bemporad et al., PL **25B**, 380 (1967).
8. A. Capella, J. Tran Thanh Van; L. N. C. **1**, 321 (1969).
9. J. Tran Thanh Van; L. N. C. **3**, 678 (1970).
10. A. P. Contogouris, J. P. Lebrun; Nuovo Cim. **64A**, 627 (1969).
11. A. P. Contogouris, J. P. Lebrun, G. von Bochmann; Nucl. Phys. **B13**, 246 (1969).
12. J. Froyland; Nucl. Phys. **B11**, 204 (1969).
13. F. Henyey et al., PRL, **21**, 946 (1968).
14. G. Kane, F. Henyey, D. R. Richards, M. Ross, G. Williamson; Michigan Univ., Preprint (1970).
15. M. Collocci; L. N. C. **4**, 53 (1967).
16. M. Braunschweig et al., Nucl. Phys. **B20**, 191 (1970).
17. A. Dar, T. L. Watts, V. F. Weisskopf; P. L. **30B**, 264 (1969).
18. P. Sonderegger et al., PL **20**, 75 (1966).
19. M. A. Wahlig et al., PRL, **13**, 103 (1964).
20. O. Guisan et al., P. L. **18**, 200 (1965).
21. F. Bulos et al., paper 8a—19.
22. B. Richter; Proceedings of the 14th International Conference on High Energy Physics, Vienna (1968).
23. C. F. Cho, J. J. Sakurai; Preprint University of California, L. A. and University of Chicago.
24. P. P. Johnson et al., PR, **176**, 1651 (1968).
25. N. N. Biswas et al., Phys. Rev. **D1**, 2705 (1968).
26. C. C. Morehouse et al., paper 8a—3; SLAC — PUB 778, UCRL 19492; P. R. L. **25**, 835 (1970).
27. J. D. Jackson, C. Quigg; UCRL 19410 (March 1970).
28. K. Ekstrand et al., paper 8a—22 and CLNS — 124 (Aug. 1970).
29. R. A. Alvarez et al., R. R. **1D**, 1946 (1970).
30. R. L. Anderson et al., P. R. L. **21**, 479 (1968).
R. L. Anderson et al., P. R. L. **23**, 721 (1969).
31. V. Barger and P. Weiler; Nucl. Phys. **B20**, 615 (1970).
32. Aachen — Berlin — Bonn — Hamburg — Heidelberg — München Collaboration, P. L. **23**, 707 (1966) and P. R. **175**, 1669 (1968).
33. Cambridge Bubble Chamber Group; P. R. **163**, 1510 (1967).
34. A. M. Boyarski et al., P. R. L. **22**, 148 (1969).
35. P. Stichel, M. Scholz; Nuovo Cim. **34**, 1381 (1964).
36. SLAC — Berkeley — Tufts Collaboration, paper 8a—2 and SLAC — PUB 766 (June 1970); P. R. L. **25**, 1223 (1970).
37. J. J. Murray, P. Klein, SLAC — TN — 67—19;
C. K. Sinclair et al., IEEE Trans. on Nucl. Sci. **16**, 1065 (1969).
38. G. von Holtey, Bonn Univ. Preprint PI 1—123 (1971).
39. H. Fischer, Bonn Univ. Preprint PI 1—122 (1970).
40. A. Bleckmann et al., paper 8a—5 and Bonn Univ. Preprint PI 1—92 (1970).
41. D. Décamp et al., paper 8a—6 and L. A. L. 1236 (July 1970).
42. S. G. Tonapetyan et al., paper 8a—16.
43. M. Beneventano et al., paper 8a—7.
44. P. Blüm et al., paper 8a—10 and Bonn Univ. Preprint PI 1—105 (1970).
45. Yu. P. Antufyev et al., paper 8a—9.
46. G. Bologna et al., paper 8a—23 and LNF —70/39 (1970).
47. V. M. Kuznetsov et al., paper 8a—14.
48. E. Hilger et al., paper 8a—11 and Bonn Univ. Preprint PI 1—103 (1970).
49. G. Fischer et al., paper 8a—13 and Bonn Univ. Preprint PI 1—101 (1970).
50. G. Fischer et al., paper 8a—12 and Bonn Univ. Preprint PI 1—100 (1970).
51. T. Fujii et al., paper 8a—15.
52. C. A. Heusch et al., paper 8a—20 and CALT—68—275.
53. A. Silverman; Proceedings of the International Symposium on Electron and Photon Interactions at High Energies, Liverpool (1969).
54a. Proceedings of the Daresbury Study Weekend, Daresbury (June 1970).

54b. D. W. G. L. Leith; Scottish Summer school in Physics (July 1970).
55. G. McClellan et al., paper 8b—8.
56. H. Alvensleben et al., paper 8b—9 and P. R. L. **23**, 1058 (1969).
57. J. D. Jackson; Nuovo Cim. **34**, 1644 (1964).
58. M. Ross, L. Stodolsky; Phys. Rev. **149**, 1172 (1966).
59. P. Söding; P. L. **19**, 702 (1965).
60. B. Margolis; Nucl. Phys. **B6**, 687 (1968).
61. M. N. Focacci, G. Giacomelli; CERN — Report 66—18.
62. F. Bulos, W. Busza, R. Giese, E. E. Kluge, R. R. Larsen, D. W. G. S. Leith, B. Richter, S. H. Williams, M. J. Beniston; Paper to this conference.
63. German HBC Collaboration ABBHHM; Phys. Rev. **175**, 1669 (1968).
64. H. H. Bingham et al., paper 8b—3 and P. R. L. **24**, 995 (1970) and P. R. L. **24**, 960 (1970).
65. L. Criegee et al., paper 8b—5 and DESY 70/19 (May 1970). P. R. L. **25**, 1306 (1970).
66. G. Diambrini — Palazzi et al., paper 8b—6, P. R. L. **25**, 478 (1970).
67. G. Wolf; private communication.
68. K. Schilling, P. Seyboth, G. Wolf; SLAC — PUB 683 (Dez. 1969); Nucl. Phys. **B15**, 397 (1970).
69. D. Schildknecht, B. Schrempp; DESY 70/8 (1970).
70. R. L. Anderson et al., paper 8b—12.
71. K. S. Koelbig, B. Margolis; Nucl. Phys. **B6**, 85 (1968).
72. J. G. Asbury et al., P. R. L. **19**, 865 (1967) and P. R. L. **20**, 227 (1968).
73. G. Mc. Clellan et al., P. R. L. **22**, 377 (1969).
74. F. Bulos et al., P. R. L. **22**, 490 (1969).
75. H. Alvensleben et al., paper 8b—11 and P. R. L. **24**, 786 (1970), P. R. L. **24**, 792 (1970) and Nucl. Phys. **B18**, 333 (1970).
76. H. J. Behrend, F. Lobkowicz, E. H. Thorndike, A. A. Wehmann; P. R. L. **24**, 336 (1970).
77. F. Bulos, W. Busza, R. Giese, E. E. Kluge, R. R. Larsen, D. W. G. S. Leith, B. Richter, S. H. Williams, A. Stetz, V. Perez-Mendez, M. J. Beniston; Paper to this conference.
78. J. S. Trefil; Nucl. Phys. **B11**, 330 (1969).
79. H. R. Collard, L. R. B. Elton, R. Hofstädter in «Landolt — Börnstein tables I», Vol. 2.
80. M. Damshek, F. J. Gilman; SLAC — PUP —697 (1969).
81. J. E. Augustin et al., P. L. **28B**, 503 (1969) and quoted by J. Perez-y-Jorba in the Proceedings of the 4th Symposium on Photon and Electron Interaction at High Energies, Liverpool (1969).
82. J. Ballam et al., paper 8b—4 and SLAC — PUB —729 (1970); P. R. L. **24**, 1364 (1970).
83. Cambridge Bubble chamber group; Phys. Rev. **155**, 1468 (1967).
84. M. Davier et al., P. L. **28B**, 619 (1969).
85. Y. Eisenberg et al., P. R. L. **22**, 669 (1969).
86. J. Ballam et al., P. L. **30B**, 421 (1969).
87. H. Harari; Proceedings of the 4th International Symposium on Electron and Photon Interactions at High Energies, Liverpool (1969).
88. Review of Particle Data; P. L. **33B**, 1 (1970).
89. H. J. Behrend et al., paper 8a—14.
90. J. Bennecke, H. P. Dürr; Nuovo Cim. **56**, 269 (1969); G. Wolf; Phys. Rev. **182**, 1538 (1969).
91. H. J. Behrend et al., paper 8b—15 and P. R. L. **24**, 1246 (1970).
92. P. L. Braccini et al., paper 8b—16 and Nucl. Phys. **B24**, 173 (1970).
93. G. McClellan et al., P. R. L. **23**, 554 (1969).
94. A. M. Boyarski et al., P. R. L. **23**, 1343 (1969).
95. G. V. Bochmann, B. Margolis, L. C. Tang; P. L. **30B**, 254 (1969).
96. C. A. Engelbrecht; Phys. Rev. **133**, B988 (1964).
97. G. Diambrini — Palazzi et al., paper 8b—7.
98. See ref. (61).
99. H. Alvensleben et al., paper 8b—10 and DESY 70/39 (1970).
100. P. J. Biggs, D. W. Braben, R. W. Clift, E. Gabathuler, G. L. Griffith, R. E. Rand; Paper to this conference.
101. D. R. Earles, P. Chase, W. Faissler, M. Gettner, G. Glass, G. Lutz, P. Rothwell, K. Moy, H. v. Briesen, E. v. Goeler, R. Weinstein; Paper to this conference.
102. J. E. Augustin et al., Nuovo Cim. Lett. **2**, 214 (1969).
103. D. G. Coyne; UCRL — 19450 (1970).
104. H. Alvensleben et al., paper 8b—1 and DESY 70/40 (1970).

105. P. J. Biggs, R. W. Clift, E. Gabathuler, P. Kitching, R. E. Rand; Paper to this conference and quoted in E. Gabathuler DNPL/P 41.
106. R. G. Parsons, R. Weinstein; P. R. L. **20**, 1314 (1968);
M. Davier; P. L. **27B**, 27 (1968);
H. R. Quinn, T. F. Walsh; DESY 70/13 (1970).
107. M. Gourdin, F. M. Renard, L. Stodolsky; P. L. **30B**, 347 (1969);
M. Gourdin in Proceedings of the Daresbury Study Weekend No. 1 (June 1970).
108. E. Gabathuler in Proceedings of the Daresbury Study Weekend No. 1 (June 1970).
109. H. Alvensleben et al., paper 8b—25.
110. J. Perez-y-Jorba in Proceedings of the Daresbury Study Weekend No. 1 (June 1970).
111. German HBC Collaboration ABBHHM; P. L. **27B**, 474 (1968).
112. J. Ballam et al., P. R. L. **21**, 1544 (1968).
113. J. Ballam et al., P. R. L. **23**, 498 (1969).
114. E. D. Bloom et al.; SLAC — PUP — 653 (1969).
115. M. L. Perl et al., P. R. L. **23**, 1191 (1969).
116. D. O. Caldwell et al., P. R. L. **25**, 609 (1970).
117. W. P. Hesse et al., paper 8b—17 and P. R. L. **25**, 613 (1970).
118. H. Meyer at al., DESY 70/17 (1970) and P. L. **33B**, 189 (1970).
119. B. Noraska; Thesis, DESY F1—70/3 (1970).
120. See ref. (80).
121. S. J. Brodsky, J. Pumplin; P. R. **182**, 1794 (1969).
122. K. J. Foley et al., P. R. L. **19**, 193 (1967).
123. L. Stodolsky; P. R. L. **18**, 135 (1967).
124. a) G. J. Brodsky, J. Pumplin; P. R. **182**, 1794 (1969);
b) K. Gottfried, D. R. Yennie; P. R. **182**, 1995 (1969);
c) B. Margolis, C. L. Tang; Nucl. Phys. **B10**, 329 (1969);
d) M. Nauenberg; P. R. L. **22**, 556 (1969).
125. C. M. Hoffman et al., P. R. L. **22**, 659 (1969).
126. D. O. Caldwell et al., P. R. L. **23**, 1256 (1969).
127. V. Heynen, H. Meyer, B. Naroska, D. Notz; quoted by H. Meyer at this conference and DESY 71/5 (1971).
128. W. L. Lakin et al., paper to this conference.
129. G. v. Bochmann, B. Margolis, C. L. Tang; P. R. L. **24**, 483 (1970).
130. McClellan et al.; Cornell CLNS — 69 and 70 (1969).
131. H. Genzel et al., paper 8b—21 and Bonn Univ. Preprint PI 1—104 (1970).
132. R. L. Anderson et al., paper 8b—19 and P. R. L. **25**, 1218 (1970).
133. G. Buschhorn et al., paper 8b—20 and P. L. **33B**, 241 (1970).
134. Results quoted by M. Deutsch at this conference.
135. M. Gell-Mann, M. C. Goldberger, W. Thirring; P. R. **95**, 1612 (1954).
136. J. J. Sakurai; Ann. Phys. **11**, 1 (1960);
M. Gell-Mann, F. Zachariasen; P. R. **124**, 953 (1961);
Y. Nambu, J. J. Sakurai; P. R. L. **8**, 79 (1962);
M. Gell-Mann, D. Sharp, W. G. Wagner; P. R. L. **8**, 261 (1962).
137. H. Joos; Proceedings of the International Conference on Elementary Particles, Heidelberg (1967);
J. J. Sakurai; Proceedings of the International Symposium on Electron and Photon Interactions ot High Energies, Liverpool (1969).
138. M. Krammer: DESY — Report 70/53 (1970).
139. E. Lohrmann; Review talk at the Lund International Conf. (1969).
140. M. Davier; Talk presented at the 5th Rencontre de Moriond, Meribel (1970).
141. H. Alvensleben et al., paper 8b—24 and DESY 70/61 (1970).
142. F. Bulos et al., paper 8b—13 and SLAC — PUB — 751 (1970).
143. D. R. Earles, W. L. Faissler, M. Gettner, G. Lutz, K. M. Moy, Y. W. Tang, H. v. Briesen, E. v. Goeler, R. Weinstein; Paper to this conf. and P. R. L. **25**, 1213 (1970).
144. G. Gladdin, J. J. Russel, M. J. Tannenbaum, G. Thomson, G. Weiss; paper to this conf.
145. P. Dittmann et al., paper 8b—23.
146. Frascati — Roma — Padova Collaboration; paper to this conference and LNF—70/38 (1970).